OPTIMIZED GROUND PENETRATING RADAR METHODS CAN ACCOUNT FOR LANDSCAPE VARIANCE IN PROPERTIES INFORMING SOIL CARBON DISTRIBUTION IN BOREAL FOREST HILLSLOPES

By

© ZACHARY W. GATES

A Thesis submitted to the School of Graduate Studies

In partial fulfillment of the requirements of the degree of

Master of Science

MEMORIAL UNIVERSITY

Department of Earth Sciences

St. John's Campus

Memorial University of Newfoundland

Dec 2022

St. John's Newfoundland

Optimized ground penetrating radar methods can account for landscape variance in properties informing soil carbon distribution in boreal forest hillslopes

by

Zachary W. Gates

Advisors: Dr. Susan Ziegler, Dr. Lakshman Galagedara

Committee members: Dr. Sharon Deemer

Abstract.

This thesis entailed developing optimized ground penetrating radar (GPR) methods for estimating soil horizon thickness and bulk density to determine soil carbon (C) distribution across forest hillslopes. A review of forest GPR studies was conducted to synthesize optimized system settings, survey parameters, and data processing steps. Recommended GPR survey settings (> 500 MHz antenna frequency, > 32 stacks, 5 cm sampling interval) and data processing tools were compiled for forest soil surveys and demonstrated to improve the interpretability of specific soil targets (ex. soil horizon boundaries, rock, and root content) in forest soil radargrams. Physical soil sampling and GPR surveying methods were conducted across a boreal forest hillslope in Pynn's Brook, Newfoundland to collect small (1 m^2 soil pits) and large (80 m GPR survey lines) spatial scale soil horizon thickness and bulk density estimates. This allowed for comparisons between physical soil sampling and GPR estimates of soil horizon thickness, soil bulk density and resulting soil C distribution calculated using soil C stocks. Furthermore, large spatial scale GPR surveying revealed landscape trends in soil bulk density, such as increasing density downslope and high

variability across the slope, which informs our understanding of forest soil C distribution and its landscape controls.

Keywords: Boreal Forest, Bulk density, Ground Penetrating Radar, Horizon thickness, Soil Carbon

General Summary.

Physical soil sampling methods result in high variability and neglect landscape influence for soil property and carbon (C) distribution measurements. Deeper, large-scale spatial soil data is required for forest soil investigations to accurately represent the totals and variability of soil content and C distribution, as well as identify the impacts of landscape-level processes on sitewide measurements. This thesis proposes that optimized ground penetrating radar (GPR) methods are a solution to obtaining high-resolution, large-scale, spatial forest soil property data. The appropriate background is provided on the methodology of forest GPR surveying for soil horizon thickness and bulk density estimates which are used to calculate soil C stocks. Furthermore, GPR's capabilities to investigate soil C distribution across large-scale forest sites are demonstrated along a boreal forest hillslope in Pynn's Brook, Newfoundland through comparative testing between optimized GPR and physical soil sampling methods.

Acknowledgements.

The research I have conducted and the experience I have gained through this project would not be possible without the immense support provided by my supervisor Dr. Susan Ziegler. I want to thank her for the guidance she provided throughout my academic journey and for allowing me the freedom and independence to pursue a very interesting study and gain a wealth of knowledge in a variety of fields from biology to geophysics. I would also like to thank my co-supervisor Dr. Lakshman Galagedara for his help during field work and data collection, including allowing us the use of his ground penetrating radar equipment for this study. His experience in conducting and processing geophysical surveys from difficult agricultural and boreal ecosystems was invaluable in the development and execution of this study.

I would also like to thank the B-BERG research group members for their help and input on the research conducted in this study, and the financial contributions and support from the Memorial University of Newfoundland, NSERC Discovery Grants Program (SPG#479224-15, RGPIN-2018-05383) and Canada Research Chairs program, the Newfoundland and Labrador Department of Fisheries, Forestry and Agriculture, and Atlantic Forestry Centre in Corner Brook, NL. I would also like to thank Maria Lear and Memorial University of Newfoundland's Department of Archeology for letting us borrow additional ground penetrating radar equipment for this study.

Lastly, I want to thank my father Rocky Gates and my late mother Myra Walsh Gates for giving me the support through this research and writing that only parents can.

Thank you to everybody who has helped me throughout this academic journey!

Zachary W. X. Gates

Table of Contents

Abstract.	ii
Keywords.	iii
General Summary.	iii
Acknowledgements.	iv
Table of contents.	v
List of Tables.	ix
List of Figures.	x
List of Abbreviations.	xii
Chapter 1 – Introduction and overview.	1
1.1. Introduction.	2
1.2. Rationale and goals of this research.	6
1.3. Thesis organization.	11
1.4. The potential of expanding the scale of forest soil carbon investigations with ground penetrating radar.	12
References.	14
Chapter 2 - Optimized ground penetrating radar methods for soil property estimates informing forest soil carbon distribution.	19
Abstract.	20

2.1. Introduction. 21

2.1.1. The potential for identifying landscape trends in forest soil properties via ground penetrating radar. 23

2.2. The challenges of utilizing ground penetrating radar to estimate forest soil thickness and soil bulk density. 25

2.3. Successful applications of ground penetrating radar methods for measurements of forest soil horizon thickness and soil bulk density. 28

2.4. Optimized landscape-scale ground penetrating radar methods for forest soil horizon thickness and soil bulk density. 31

2.4.1. Optimized ground penetrating radar system settings for measuring forest soil horizon thickness and soil bulk density. 36

2.4.2. Optimized data processing steps for ground penetrating radar measurements of forest soil horizon thickness. 41

2.4.3. Optimized data processing steps for ground penetrating radar measurements of forest soil bulk density. 44

2.5. Combing spatial datasets with ground penetrating radar holds potential for large-scale assessment of forest soil properties and controls. 48

2.6. Conclusions 52

References. 54

Co-author Statement 64

Appendix 65

Chapter 3 - Ground penetrating radar estimates of soil horizon thickness and soil bulk density inform boreal forest hillslope carbon distribution. 89

Abstract. 90

3.1. Introduction. 91

3.1.1. Ground penetrating radar methods can better inform forest soil property estimates with spatial scale and depth compared to physical soil sampling. 92

3.2. Materials and methods. 96

3.2.1. Site description. 96

3.2.2. Physical soil sampling methods and ground penetrating radar surveying schemes. 101

3.2.3. Physical soil sampling methods. 103

3.2.4. Ground penetrating radar surveying methods and settings. 106

3.2.5. Ground penetrating radar data processing for soil horizon thickness. 111

3.2.6. Ground penetrating radar data processing for soil bulk density. 112

3.2.7. Data handling and analyses. 113

3.3. Results. 115

3.3.1. Ground penetrating radar estimates of horizon thickness are similar to physical soil sampling methods but were greater downslope. 116

3.3.2. Ground penetrating radar estimates of soil bulk density are lower than physical soil sampling results. 117

3.3.3. Lower estimates of soil bulk density resulted in lower soil carbon stocks via ground penetrating radar. 119

3.3.4. Hillslope scale ground penetrating radar reveals landscape influences on soil horizon thickness, bulk density, and soil carbon distribution. 119

3.4. Discussion. 122

3.4.1. Ground penetrating radar reveals soil horizons at depth with potential to evaluate hillslope trends relevant to hydrogeomorphology. 122

3.4.2. Ground penetrating radar identified trends in soil bulk density consistent with hillslope transport and erosion. 122

3.4.3. Ground penetrating radar can reliably investigate soil heterogeneity and landscape trends impacting soil carbon distribution. 124

3.5. Conclusions. 126

References. 128

Co-author statement. 135

Appendix. 136

Chapter 4 – Conclusions. 172

4.1. Goals and achievements of this study. 173

4.2. Ground penetrating radar optimization recommendations for forest soil property investigations. 175

4.3. Large scale ground penetrating radar methods for measuring soil horizon thickness and bulk density allow for assessment of landscape trends. 175

References. 178

List of Tables

Table 2.1. A compilation of forest GPR soil studies with listed soil property targets. 29

Table 2.2. Recommended data processing steps for obtaining forest measurements of soil horizon thickness and soil bulk density using ground penetrating radar (GPR). 51

Table 3.1. Mineral soil properties obtained from soil sampling at the Pynn's Brook site for soil horizon classification by the Canadian System of Soil Classification (CSSC). 99

List of Figures

Figure 2.1. The path of a transmitted electromagnetic (EM) signal from a ground penetrating radar (GPR) system and the reflectors and sources of attenuation that the signal will encounter. 26

Figure 2.2. Horizon thickness radargram data collected from a forest hillslope in Pynn's Brook Experimental Watershed Area, western Newfoundland, Canada 32

Figure 2.3. Soil bulk density radargram data collected from a forest hillslope in Pynn's Brook Experimental Watershed Area, western Newfoundland, Canada 35

Figure 2.4. Radargram data collected along a 1 m line in a boreal forest in Newfoundland, Canada processed for soil horizon thickness estimates at small, soil pit and large, hillslope scales. 42

Figure 2.5. Radargram data collected along a 1 m line in a boreal forest in Newfoundland, Canada processed for soil bulk density estimates at small, soil pit and large, hillslope scales. 46

Figure 3.1. Physical soil sampling methods and ground penetrating radar (GPR) surveying grid schemes overlain on an air photo of the Pynn's Brook Experimental Forest Area (PBEWA). 95

Figure 3.2. Large scale, topography corrected, processed radargram interpretations 107

for measuring soil horizon thickness from a GPR survey.

Figure 3.3. Large scale, topography corrected, processed radargram interpretations 110

for measuring soil horizon thickness from a GPR survey.

Figure 3.4. Soil horizon thickness, bulk density, and C by weight for each mineral 117

soil horizon from the upslope (top panels) and downslope (lower panels) sites in the

Pynn's Brook boreal forest hillslope site.

Figure 3.5. GPR spatial averages from continuous radargram data collected from the 121

6 survey lines for soil horizon thickness (a), and soil bulk density (b) across the

Pynn's Brook boreal forest hillslope.

Abbreviations

AGC	-	Automatic Gain Control
APP	-	Assisted Pick Processing
C	-	Carbon
CMP	-	Common Mid-Point
C:N	-	Carbon: Nitrogen Ratio
CO_2	-	Carbon Dioxide
F	-	Frequency
F-K	-	Frequency – Wavelength
gdw	-	Grams Dry Weight
GPR	-	Ground Penetrating Radar
GPS	-	Global Positioning System
LiDAR	-	Light detection and ranging
MHz	-	Megahertz
PBEWA	-	Pynn's Brook Experimental Watershed Area
Pg C	-	Peta Grams Carbon
POM	-	Particulate Organic Matter
RMSE	-	Root Mean Square Error
SEC	-	Spherical and Exponential Compensation
SOC	-	Soil Organic Carbon
S/N	-	Signal to Noise Ratio
TWTT	-	Two-Way Travel Time
V_{gw}	-	Ground Wave Velocity
WARR	-	Wide-Angle Reflection-Refraction
WL	-	Wavelength

CHAPTER 1

Introduction and Overview

1.1 Introduction.

On a global scale, soils store a minimum of double and a maximum of quadruple the amount of carbon (C) that is stored as carbon-dioxide (CO_2) in the atmosphere (Scharlemann et al., 2014; Sothe et al., 2022). Current estimates state that Earth's soils contain around 1500-2400 Pg C while atmospheric C totals are close to 600 Pg C (Scharlemann et al., 2014). Additionally, about 450 Pg C is stored globally in live biomass vegetation, so global soil C represents a larger reservoir than atmospheric and vegetative C combined (Sothe et al., 2022). Forests across the planet store a significant portion of this total soil C reservoir, with up to a third of global soil C (800 Pg C) stored in these environments (Scharlemann et al., 2014; Sothe et al., 2022).

Soil C storage is particularly high in Canadian forests (IPCC, 2013; Scharlemann et al., 2014; Sothe et al., 2022)**.** Canadian forest and peatland soils contain more than a third of global forest soil C (306 ± 147 Pg C), of which about one third is derived from forested peatland areas (Sothe et al., 2022). Additionally, forest soils may store large quantities of soil C variably across large spatial scales and at depths up to 1 – 3 m (Jobbagy & Jackson, 2000). For example, recent modelling of Canadian soil C storage estimate 384 ± 200 Pg C within the top meter of soil, demonstrating a 90% confidence intervals value of uncertainty over 50% (Sothe et al., 2022). Furthermore, estimates of Canadian forest soil C up to 1 m deep represent an increase of almost 5 times that of values reported for only the top 30 cm, demonstrating substantial soil C storage with depth in these landscapes (Jandl et al., 2014; Sothe et al., 2022). As such, high resolution, deep, large scale global forest soil C investigations are required for accurate estimates of total soil C and identifying variance, links and trends between soil C distribution and forest soil properties such as soil horizon thickness and soil bulk density.

Global and Canadian forest soils are vulnerable to alterations caused by the effects of climate change on temperature, precipitation, and their impact on geomorphic erosion (Hu et al., 2016; Wei et al., 2017; Holz & Augustin, 2021; Sothe et al., 2022). The impacts of climate change can lead to differences in annual and seasonal temperature and the intensity and quantity of precipitation which will affect forest soil C transport and erosion altering soil C storage and distribution temporally in such sites (Rosenbloom, Doney, & Schimel, 2001; Pacific et al., 2011; Koch et al., 2013; Bowering et al., 2020).

Post-glaciated forest landscapes are highly susceptible to erosion through hydrological impacts, particularly in shallow mineral soil horizons (Bonan, 1989; Reichle et al., 1999; IPCC, 2013; Scharlemann et al., 2014; Sothe et al., 2022). Precipitation changes will influence C inputs to the underlying soil by hydrological erosion and impact the mobilization of surface soil C sources available for deeper soils (Jobbagy & Jackson, 2000; Bowering et al., 2020). Shifts in total and seasonal precipitation intensity can interact with shallow forest soils impacting soil processes through alterations to water transport, which influences soil C stores through weathering rate controls on reactive minerals (Holz and Augustin, 2021). Variations in the intensity and form of precipitation over time will also promote or constrain plant production and organic matter decomposition in forest environments. Precipitation changes will influence C inputs to the underlying soil by hydrological erosion and impact the mobilization of surface soil C sources available for deeper soils (Jobbagy & Jackson, 2000; Bowering et al., 2020). Furthermore, forest hillslope environments commonly support morphological processes controlling soil properties and C pools, such as groundwater flow and particle transport, which can result in hillslope soil C trends across the forest landscape as a function of these factors (Hoffmann et al., 2014; Hu et al., 2016; Wei et al., 2017; Holz and Augustin, 2021). This effect is more pronounced across steeper hillslopes, leading to the transport of sediment towards a depositional area causing an infilling process which increases soil content downslope (Yoo et al., 2006). Preferential flow paths and antecedent soil conditions will also affect if soils reach saturation which can further transport soil C deeper and further out from the initial mineral soils measured along the boreal forest hillslope.

Increased temperatures can also lead to increased decomposition in forest soils, enhancing the release of soil C into the atmosphere and lowering soil C stocks over time (von Haden, Yang, & DeLucia, 2020; Sothe et al., 2022). When higher temperatures occur in tandem with lower precipitation soil C decomposition rates will further increase and slow the accumulation of soil organic carbon (Sothe et al., 2022). Middle to high latitude forest ecosystems at high elevations, common across Canadian boreal forests, experience generally colder temperatures and slower soil organic C decomposition then lower latitudes and elevations (Sothe et al, 2022). As these latitudes and elevations are predicted to experience increased temperatures due to climate change, Canadian forest soil organic C decomposition and storage could be undergoing temporal alteration. As such, temporal changes to forest landscapes that alter soil volumes such as temperature, precipitation, land-use, harvesting, erosion, compaction, and hydrological interaction can further alter soil C distribution in the future (Doolittle et al., 2006; von Haden, Yang, & DeLucia, 2020). The impacts of such temperature and precipitation on soil C may also change with depth, as generally climate has more of an effect on shallow soils and less of an effect on deeper soils where clay content and soil texture will exert more control on soil C distribution (Jobbagy & Jackson, 2000). However, higher resolution and deeper soil data is needed to better understand the relationships temperature and precipitation have with soil organic C distribution and decomposition (Jobbagy & Jackson, 2000).

Geomorphic erosion, particularly through hydrological processes, can further distribute soil and soil properties across forest ecosystems in patterns reflecting site conditions such as topography and vegetation (Jobbagy & Jackson, 2000; Yoo et al., 2006). Soil erosion driven by climate, surface runoff, and groundwater processes can also exert soil mixing and cycling by physical (ex. groundwater transport) and biological factors (ex. soil acidification and leeching), transporting less stable, shallow mineral soils and C across landscapes and leading to infilling and C enrichment in depositional areas (Jobbagy & Jackson, 2000; Yoo et al., 2006; Bowering et al., 2020). Erosion processes in post-glaciated, boreal forests can lead to a complex set of mineral soil enrichment by various mechanisms as coarse aggregates can be broken down into smaller particles and contribute to a negative relationship between SOC enrichment and coarse aggregates, leading to a preferential transport of soil content and C (Wei et al., 2017; Holz & Augustin, 2021). This selective movement of SOC during erosion can lead to a shift in C and nitrogen (N) dynamics in different landscape areas, such as slope positions, and thus an increase in the spatial variability of C and N along the slope (Holz & Augustin, 2021). Additionally, forest hillslope environments commonly support topographic morphological controls on soil properties and C pools, such as promoting more intense groundwater flow and particle transport along steep slope gradients, which can result in soil C distribution that is influenced by the geometry of the hillslope across the forest landscape as a function of these factors (Hoffmann et al., 2014; Hu et al., 2016; Wei et al., 2017; Holz & Augustin, 2021). Such sediment transport mechanics can result in thicker soil horizons which the riparian zone, dependent on hillslope dip, curvature, erosional rates, and relief (Pacific et al., 2011; Patton et al., 2018). Smaller size soil particles such as clay and silt may be transported with less force resulting deposition of these particles at the bottom of forested hillslopes (Rosenbloom et al., 2001). Meta-analysis of previous forest studies has indicated that both C and nitrogen (N) can be preferentially transported during erosion events and that this preferential transport leads to an accumulation of soil organic matter and soil organic C in lower slope positions (Holz & Augustin, 2021). Furthermore, increased soil erosion across a forested hillslope can lead to the transport of fine soil content and C from shallow horizons into deeper layers (Jobbágy & Jackson, 2000; Rosenbloom et al., 2001; Yoo et al., 2006; Haden et al., 2020). Through erosion soil organic C is selectively re-deposited downslope depending on factors influencing the transport distances of the soil particles (Holz & Augustin, 2021). As soil C storage has been shown to correlate with soil particle size, the impacts of landscape trends in soil texture across a study site can be associated with soil C distribution and thus requires dense spatial data collection to properly represent C stock totals (Jobbágy & Jackson, 2000).

1.2 Background on ground penetrating radar surveying methods for measuring forest soil properties.

Despite their importance, size, and vulnerability, our current understanding of the total quantity and distribution of forest and terrestrial soil C remains relatively poor (Scharlemann et al., 2014; Dincă et al., 2015; von Haden, Yang, & DeLucia, 2020; Sothe et al., 2022). The impacts of this poor understanding have been seen in recent modelling estimates which demonstrate high variability in Canadian forest biomes and significant uncertainty in global SOC stocks with depth relative to C storage or emission (Doolittle & Collins, 1995; Butnor et al., 2003; Barton & Montagu, 2004; Doolittle et al., 2006; Gerber et al., 2007, 2010; Laamrani et al., 2013; Patton et al., 2018). These small-scale soil investigations may not readily enable the identification of links between landscape processes and trends to soil properties across forest sites, including along hillslopes and topographical gradients (Doolittle & Collins, 1995; Rosenbloom, Doney, & Schimel, 2001; Anderson et al., 2009; Gerber et al., 2010; Pacific et al., 2011; Laamrani et al., 2013; Patton et al., 2018). Additionally, most estimates of forest soil properties and C distribution are not collected at a resolution high enough to uncover geomorphological trends across landscapes like hillslopes or topographic features (Pacific et al., 2011). Small-scale, localized measurements obtained through discrete points using PSSM thus may not accurately represent landscape-scale soil variance in regional datasets that cover thousands of square kilometers (Parsekian et al., 2012; Vadeboncoeur et al., 2012; Hoffmann et al., 2014; Jandl et al., 2014).

Advancements in expanding the depth and spatial scales of forest soil investigations have been hampered by a reliance on traditional physical soil sampling methods. These methods have provided reliable measurements of physical soil properties, such as soil horizon thickness and soil bulk density, as well as estimates of soil C and N stocks, at small scales such as within soil pits (~ 1 m^2). However, the accuracy of discrete point sampling does not scale for larger surveying efforts (> 1000 m^2) that are necessary to accurately interpret soil heterogeneity and C content distribution across landscapes. To obtain high-resolution soil sampling data across landscape scales using these methods, considerable cost, destruction, labour, and time is required which is commonly not feasible for these types of investigations. Additionally, physical soil sampling methods such as soil coring and soil pit excavation are routinely limited to sampling only to depths of 30 cm, which cannot adequately represent soil C storage with depth. For example, global soil organic carbon (SOC) storage estimates for the top 3 m of soil (2344 Pg C) were > 56% more than estimates for just the first meter (1500-1600 Pg C) in previous investigations (Jobbagy & Jackson, 2000).

Ground-penetrating radar (GPR) is a noninvasive geophysical tool that can be used to investigate subsurface materials and provide images of shallow (0 to 30 m) soils, rocks, roots, and other subsurface targets (Doolittle et al., 2006). Ground-penetrating radar operates by transmitting pulses of radio-frequency electromagnetic energy into the subsurface. GPR systems generally produce a pulse of high frequency electromagnetic energy between 10 and 1000 MHz, which is applied to a transmitting antenna and directed into the subsurface soils (Davis & Annan, 1987). The electromagnetic waves generated propagate in different patterns depending on the electrical properties (primarily dielectric permittivity and electrical conductivity) of the ground. For example, the dielectric permittivity, which is a measure of a substance's ability to hold a charge is dependent on heavily dependent on soil moisture (Davis & Annan, 1987; Doolittle et al., 2006). Waves generated by the electromagnetic pulse will reflect in unique patterns when they encounter layers or objects of highly contrasting dielectric properties, such as the transition between organic and mineral soil layers or large rock bodies in a soil matrix (Barton et al., 2004; Doolittle et al., 2006). The variations in amplitude values measured by the GPR system over distance and time for these reflections can be interpreted to identify boundaries between different soil layers, allowing for measurements of soil horizon thickness, and the size and position of rocks and roots to determine soil bulk density in tandem with soil density samples (Barton et al., 2004; Butnor et al., 2003; Davis & Annan, 1987; Doolittle et al., 2006).

Electrically resistive soils with high sand content and low clay content are more favorable for GPR investigations but forest soils are generally electrically conductive and more radar opaque (Doolittle & Collins, 1995; Butnor et al., 2003). Forest soils that have high electrical conductivity will dissipate and scatter the electromagnetic wave energy transmitted by a GPR system, limiting the depths at which GPR can survey soils and the strength of reflections from soil horizon, rock, and root boundaries (Doolittle & Collins, 1995). In a forest setting, electromagnetic waves will travel and propagate through the soil subsurface until they encounter either an isolated body or layer with contrasting dielectric properties which will cause a portion of the transmitted electromagnetic wave energy to be reflected and captured by a receiving antenna (Doolittle et al., 2006). The amount of this electromagnetic energy that is reflected by an interface is dependent upon the contrast in the relative dielectric permittivity of the two materials. In a forest setting, the relative dielectric permittivity of different soils will depend on metal and elemental content, relative soil water content and holding capacity, groundwater solution, soil particle size and texture, and many other varying environmental factors. Soil horizons can demonstrate abrupt contrasts with underlying and overlying horizons due to physical soil properties including texture, soil bulk density, moisture, and organic carbon content (Doolittle & Collins, 1995). Abrupt boundaries that separate contrasting materials reflect more energy than gradual boundaries that separate layers with similar dielectric permittivity. Thus, different horizons of mineral soils in post-glaciated forest sites may have lower contrasts in dielectric permittivity than other distinct soil layers and environments, leading to less electromagnetic energy being reflected and captured by the GPR antenna. This would result in weaker, less interpretable soil horizon reflections in forest investigations compared to surveying conducted over more contrasting soil layers. For example, linear, well-defined boundaries between layers of contrasting material, such as loose mineral soil and an underlying bedrock horizon, will reflect more energy than a gradual, transitional boundary, such as boundaries between mineral soil horizons of similar content, resulting in higher amplitude responses at these contrasting positions in the resulting GPR data (Doolittle et al., 2006). Contrasts in the dielectric permittivity between bulk soil and buried objects such as rocks and roots will also create reflections with a higher amplitude the greater the difference in dielectric permittivity (Barton et al., 2004). Furthermore, the dielectric permittivity of soil can vary with temperature (phase-dependent), density, and antenna frequency (Doolittle, 2006).

Variations in the two-way travel time (TWTT) of the GPR signal can indicate buried objects, further identified by contrasting dielectric properties, and will result in characteristic reflections for identifying these subsurface targets. The TWTT of signals captured over a buried target will minimize when the antenna is directly above the object and maximize as the antenna moves away from the object, resulting in a hyperbola-shaped reflection in the GPR radar profile (Barton et al., 2004). Linear soil targets, such as the boundaries between soil horizons, aligned with the travel path of the antennas, will produce linear reflections on the radar profile (Barton et al., 2004).

GPR surveying has been applied to make a variety of soil, rock, root, and hydrology measurements across many diverse landscapes (Davis & Annan, 1989; Doolittle & Collins, 1995; Butnor et al., 2003; Barton & Montagu, 2004; Gerber et al., 2010; Zajícová & Chuman, 2019). GPR methods have been used to successfully measure ice thickness, water depth, water table position, ground water flow patterns, till and bedrock depth, soil stratigraphy, soil texture, rock and root positions, and rock and root sizes (Davis & Annan, 1989; Butnor et al., 2003; Barton & Montagu, 2004; Doolittle et al., 2006; Gerber et al., 2007, 2010; Pacific et al., 2011; Zajícová & Chuman, 2019). The application of such measurements has been and may continue to be advantageous in forests as they are cost and time effective, and able to capture continuous, non-destructive, and repeatable samples (Zajícová & Chuman, 2019). Advancements in the power, resolution, size, and durability of modern GPR systems have also promoted more work in previously avoided forest territory.

When operating a GPR system the antennas are dragged across the surface along a linear transect and the system triggers an electromagnetic pulse (either automatically or using a trigger) at regular intervals of either time or position (Barton et al., 2004). This process is not easy to carry out in forest sites containing dense vegetation, a bumpy and variable microtopography, and many surface obstacles such as litterfall, bushes, stumps and fallen branches. Generally, mobile sampling devices for GPR systems such as SmartCarts or odometer wheels are unsuccessful in forest soil investigations as mobile triggering over the rough forest floor results in missed trace data and scattering in radargram data.

1.3. Thesis organization.

This thesis consists of 4 chapters altogether. Chapters 1 and 4 are general introduction and conclusion chapters, respectively. Chapters 2 and 3 are manuscripts prepared based on the study completed in fulfilment of this master's program.

Chapter 1 is an overview of the current state of forest soil C research and its lack of large-scale spatial data. The chapter starts with an overview of current forest soil C investigations as well as the motivations, rationale, goals, and potential impacts of this study. Theoretical background on the use of GPR for forest soil C investigations is also provided for context.

Chapter 2 establishes an optimized methodology utilizing GPR for estimating soil HT and BD across heterogenous forest landscapes. This is accomplished through an extensive literature review of past and present successes in forest GPR research and provides recommendations on system settings, surveying practices and data processing to improve forest GPR data quality.

Chapter 3 details the primary experiment completed for this study. Physical soil sampling and GPR methods for estimates of soil horizon thickness and soil bulk density were completed at a boreal forest hillslope site along small (1 m) and large (80 m) scales. The site, methods, results, and landscape-based conclusions from this experiment are detailed to support the use of GPR for large-scale forest soil data capture.

Chapter 4 includes a general discussion and conclusions based on the previous chapters of this study while also putting forward ideas for new directions and future research in forest GPR soil surveying.

1.4. The potential of expanding the scale of forest soil carbon investigations with ground penetrating radar.

Large spatial scale GPR surveying for soil horizon thickness and soil bulk density estimates can assess forest hillslope soil properties at a resolution which upscales investigations into mineral soil C distribution and their landscape controls. This study presents modern methods, optimized for use in forest soil surveys, that utilize GPR to provide larger spatial accounts of soil property and stock estimates and variance. If these methods are adopted and employed, this can aid to constrain high variability in measurements of regional and global forest soil C distribution, primarily through soil C stock calculations. Furthermore, GPR methods for estimating soil properties in aid of understanding soil C distribution can achieve deeper measurements than comparative PSSM investigations, providing complete estimates for soil properties and soil C across the full depth of organic and mineral soil layers.

GPR methods, when compared to physical soil sampling methods (demonstrated in Chapter 2 and Chapter 3), highlight how optimized, large-scale spatial methods can overcome the limitations of traditional forest soil investigations. With alterations expected to occur for annual and seasonal temperature and precipitation intensity within forests as a response to climate change, these GPR methods are important to future soil studies via virtue of their sensitivity to soil structure changes and capability for repeated surveys over time. As climate change effects will occur over yearly and decadal time scales, the temporal measurement capabilities of repeated and continuous

GPR soil surveying can be very useful in monitoring changes to forest soil C distribution by erosion and transport over time.

GPR methods have been demonstrated to measure and track soil content accumulation across landscape gradients through estimates of soil horizon thickness and soil bulk density, and the technology may be uniquely equipped for tracking the effects of soil erosion and transport in forest soils. Furthermore, temporal changes in soil C due to alterations in soil volume by land use, harvesting, compaction, and hydrological interactions can be temporally measured in repeated surveys using optimized GPR methods. The technology and optimized methodology present possible climate mitigation purposes in examining landscape trends and distribution of soil C through processes of sequestration and emission through continuous monitoring of soil C and root dynamics at depth and across sites. Thus, throughout this research, the viability, and capabilities of continuous GPR data capture are evaluated in forests for organic and total mineral soil horizons to estimate properties such as soil horizon thickness and soil bulk density in aid of determining the quantity and distribution of soil C stocks.

References

Anderson, A. E., Weiler, M., Alila, Y., Hudson, R. O., 2009. Subsurface flow velocities in a hillslope with lateral preferential flow. *Water Resources Research*, 45(11). doi: 10.1029/2008WR007121.

Barton, C.V.M., Montagu, K.D., 2004. Detection of tree roots and determination of root diameters by ground penetrating radar under optimal conditions. *Tree Physiology*, 24(12), pp. 1323–1331. doi: 10.1093/treephys/24.12.1323.

Bowering, K. L., Edwards, K., Prestegaard, K., Zhu, X., Ziegler, S., 2020. Dissolved organic carbon mobilized from organic horizons of mature and harvested black spruce plots in a mesic boreal region. *Biogeosciences,* 17(3), pp. 581–595. doi: 10.5194/bg-17-581-2020.

Butnor, J. R., Doolittle, J. A., Johnsen, K. H., Samuelson, L., Stokes, T., Kress, L., 2003. Utility of ground-penetrating radar as a root biomass survey tool in forest systems. *Soil Science Society of America Journal*, 67(5), pp. 1607–1615. doi: 10.2136/sssaj2003.1607.

Davis, J. L., Annan, A.P., 1989. Ground-penetrating radar for high resolution mapping of soil and rock stratigraphy. *Geophysical Prospecting*, 37(5), pp. 531–551. doi: 10.1111/j.1365-2478.1989.tb02221.x.

Dincă, L. C., Dincă, M., Vasile, D., Spârchez, G., Holonec, L., 2015. Calculating organic carbon stock from forest soils. *Notulae Botanicae Horti Agrobotanici Cluj-Napoca*, 43(2), pp. 568–575. doi: 10.15835/nbha43210041.

Doolittle, J. A., Jenkinson, B., Hopkins, D., Ulmer, M., Tuttle, W., 2006. Hydropedological investigations with ground-penetrating radar (GPR): Estimating water-table depths and local ground-water flow pattern in areas of coarse-textured soils. *Geoderma*, pp. 317–329. doi: 10.1016/j.geoderma.2005.03.027.

Doolittle, J. A., Collins, M. E., 1995. Use of soil information to determine application of ground penetrating radar. *Journal of Applied Geophysics*, 33(1–3), pp. 101–108. doi: 10.1016/0926-9851(95)90033-0.

Gerber, R., Salat, C., Junge, A., Felix-Henningsen, P., 2007. GPR-based detection of Pleistocene periglacial slope deposits at a shallow-depth test site. *Geoderma*, 139(3–4), pp. 346–356. doi: 10.1016/j.geoderma.2007.02.014.

Gerber, R., Felix-Henningsen, P., Behrens, T., Scholten, T., 2010. Applicability of ground-penetrating radar as a tool for nondestructive soil-depth mapping on pleistocene periglacial slope deposits. *Journal of Plant Nutrition and Soil Science*, 173(2), pp. 173–184. doi: 10.1002/jpln.200800163.

von Haden, A.C., Yang, W.H., DeLucia, E.H., 2020. Soils' dirty little secret: Depth-based comparisons can be inadequate for quantifying changes in soil organic carbon and other mineral soil properties. *Global Change Biology*, 26(7), pp. 3759–3770. doi: 10.1111/gcb.15124.

Hoffmann, U., Hoffmann, T., Johnson, E., Kuhn, N., 2014. Assessment of variability and uncertainty of soil organic carbon in a mountainous boreal forest (Canadian Rocky Mountains, Alberta). *Catena*, 113, pp. 107–121. doi: 10.1016/j.catena.2013.09.009.

Holz, M., Augustin, J., 2021. Erosion effects on soil carbon and nitrogen dynamics on cultivated slopes: A meta-analysis. *Geoderma*, 397. Available at: doi: 10.1016/j.geoderma.2021.115045.

Hu, Y., Berhe, A., Fogal, M., Heckrath, G., Kuhn, N., 2016. Transport-distance specific SOC distribution: Does it skew erosion induced C fluxes. *Biogeochemistry*, 128(3), pp. 339–351. doi: 10.1007/s10533-016-0211-y.

Jandl, R. et al., 2014. Current status, uncertainty and future needs in soil organic carbon monitoring. *Science of the Total Environment*, 468–469, pp. 376–383. doi: 10.1016/j.scitotenv.2013.08.026.

Jobbagy, E. G., & Jackson, R. B., 2000. The vertical distribution of soil organic carbon and its relation to climate and vegetation. *Ecological Applications*, 10(2), p. 423. doi: 10.2307/2641104.

Klotzsche, A., Jonard, F., Looms, M., van der Kruk, J., Huisman, J., 2018. Measuring soil water content with ground penetrating radar: A decade of progress. *Vadose Zone Journal*, 17(1). doi: 10.2136/vzj2018.03.0052.

Koch, J. C., Runkel, R., Striegl, R., McKnight, D., 2013. Hydrologic controls on the transport and cycling of carbon and nitrogen in a boreal catchment underlain by continuous permafrost. *Journal of Geophysical Research: Biogeosciences*, 118(2), pp. 698–712. doi: 10.1002/jgrg.20058.

Laamrani, A., Valeria, O., Cheng, L., Bergeron, Y., Camerlynck, C., 2013. The use of ground penetrating radar for remote sensing the organic layer - mineral soil interface in paludified boreal forests. *Canadian Journal of Remote Sensing*, 39(1), pp. 74–88. doi: 10.5589/m13-009.

Pacific, V. J., McGlynn, B., Riveros-Iregui, D., Welsch, D., Epstien, H., 2011. Landscape structure, groundwater dynamics, and soil water content influence soil respiration across riparian-hillslope transitions in the Tenderfoot Creek Experimental Forest, Montana. *Hydrological Processes*, 25(5), pp. 811–827. doi: 10.1002/hyp.7870.

Parsekian, A. D., Slater, L., Ntarlagiannis, D., Nolan, J., Sebesteyen, S., Kolka, R., Hanson, P., 2012. Uncertainty in peat volume and soil carbon estimated using ground-penetrating radar and probing. *Soil Science Society of America Journal*, 76(5), pp. 1911–1918. doi: 10.2136/sssaj2012.0040.

Patton, N. R., Lohse, K., Godsey, S., 2018. Predicting soil thickness on soil mantled hillslopes. *Nature Communications*, 9(1). doi: 10.1038/s41467-018-05743-y.

Rosenbloom, N. A., Doney, S. C., Schimel, D. S., 2001. Geomorphic evolution of soil texture and organic matter in eroding landscapes. *Global Biogeochemical Cycles*, 15(2), pp. 365–381. doi: 10.1029/1999GB001251.

Scharlemann, J. P. W., Tanner, E. V. J., Hiederer, R., Kapos, V., 2014. Global soil carbon: Understanding and managing the largest terrestrial carbon pool. *Carbon Management*, pp. 81–91. doi: 10.4155/cmt.13.77.

Sothe, C., Gonsamo, A., Arabian, J., Kurz, W., Finkelstein, S., Snider, J., 2022. Large soil carbon storage in terrestrial ecosystems of Canada. *Global Biogeochemical Cycles*, 36(2). doi: 10.1029/2021GB007213.

Vadeboncoeur, M. A., Hamburg, S., Blum, J., 2012. The quantitative soil pit method for measuring belowground carbon and nitrogen stocks. *Soil Science Society of America Journal*, 76(6), pp. 2241–2255. doi: 10.2136/sssaj2012.0111.

Wei, S., Zhang, X., McLaughlin, N., Chen, X., Jia, S., Liang, A., 2017. Impact of soil water erosion processes on catchment export of soil aggregates and associated SOC. *Geoderma*, 294, pp. 63–69. doi: 10.1016/j.geoderma.2017.01.021.

Yoo, K., Amundson, R., Heimsath, A., Dietrich, W., 2006. Spatial patterns of soil organic carbon on hillslopes: Integrating geomorphic processes and the biological C cycle. *Geoderma*, 130(1–2), pp. 47–65. doi: 10.1016/j.geoderma.2005.01.008.

Zajícová, K., Chuman, T., 2019. Application of ground penetrating radar methods in soil studies: A review. *Geoderma*, pp. 116–129. doi: 10.1016/j.geoderma.2019.02.024.

Chapter 2

Optimized ground penetrating radar methods for soil property estimates informing forest soil carbon distribution

Abstract

To understand biogeomorphological and hydrological influences on soil carbon (C) across forest landscapes soil properties must be observed with appropriate resolution at full soil depths and across spatial scales. Forest soil properties are typically measured using physical soil sampling methods like core sampling or soil pit excavation, which are limited in assessing vertical and horizontal spatial variance across landscapes. Ground penetrating radar (GPR), a potential approach for obtaining soil properties at greater resolution and depth, has been demonstrated to estimate forest soil horizon thickness and soil bulk density continuously and non-destructively via the size and position of soil horizon, rock, and root reflections. Optimized GPR methods have allowed researchers to collect high-resolution data from localized heterogeneous forest soil plots capturing the full depth of mineral soil and improving estimates of key soil properties. We review current GPR-based studies of forest soil properties examining how to optimize GPR methodology for investigating heterogeneous forest soils at higher resolution across landscape-relevant spatial scales. By applying relevant findings this review to our own boreal forest investigation, we provide recommendations on how to optimize GPR methodology for measurements of soil horizon thickness and bulk density for landscape-scale assessment of forest soil property distribution. These findings should enable future collection of soil datasets informing the distribution of soil stocks and their relationship to landscape features thus contributing to our understanding of how soils respond to environmental change.

2.1 Introduction

Forest soil carbon (C) stores are vulnerable to alterations associated with increased temperature and precipitation (form and intensity) attributed to climate change (Scharlemann et al., 2014; Sothe et al., 2022). Understanding the distribution of current soil C stocks and their controls remains paramount to mitigation efforts and our ability to incorporate forest C-climate feedbacks into Earth System Models. This remains challenging, however, due to the heterogeneity of forest soil and methodological challenges.

Post-glaciated boreal forest ecosystems have particularly heterogeneous soil content and C distribution which has imposed limitations on investigating these landscapes spatially and with depth (Scharlemann et al., 2014; Dincă et al., 2015; von Haden, Yang, & DeLucia, 2020; Sothe et al., 2022). Dynamic forest site factors such as vegetation, topography, and soil water content which are controlled by biogeochemical and geomorphological processes can vary significantly over short distances (Jobbagy & Jackson, 2000; Scharlemann et al., 2014; Klotzsche et al., 2018; Sothe et al., 2022). This makes it challenging to associate these site factors with soil properties given typical resolution of physical soil sampling.

Furthermore, it is difficult to obtain deep soil samples in forest environments using physical soil sampling methods due to the abundance of large rock and root content in these soils. High quantities of large rock content limits soil core sampling or soil pit excavation at many forest locations and with depth. This limitation can bias physical soil measurements towards areas of higher soil content, impacting measurements such as soil horizon thickness and soil bulk density. As around 50% of forest soil C stores are found below depths of 30 cm, which is commonly the maximum depth for physically collected soil samples, there is a demand for deeper, increased spatial assessment of forest soil properties and soil C distribution for more accurate soil C stocks

(Jobbagy & Jackson, 2000; Scharlemann et al., 2014; Klotzsche et al., 2018; Sothe et al., 2022). However, it is challenging to obtain deep soil samples in forest environments, particularly those in post-glaciated landscapes, using physical soil sampling methods due to the abundance of rock and root content in these soils. High quantities of large rock content often prevent core sampling and limit soil pit excavation at many forest locations. This limitation can bias physical soil measurements towards shallow depths and areas of higher soil content, impacting measurements such as soil horizon thickness and soil bulk density.

Highly heterogeneous soil conditions with depth across forest landscapes result in variable estimates of soil properties, including soil horizon thickness and bulk density, which can contribute to high variability in forest soil C estimates (Dincă et al., 2015; von Haden, Yang, & DeLucia, 2020; Sothe et al., 2022). This variability typically prevents the establishment of associations among geomorphic, biogeochemical, and soil features required to establish an understanding of soil change (Sullivan et al. 2021). This prevents the representation of landscape trends that might be used to inform hydrological and biogeomorphological controls on soil properties and stocks (Hoffmann et al., 2014; Jandl et al., 2014; Dincă et al., 2015). Thus, to understand controls on soil properties and stocks within heterogeneous forest environments high-resolution sampling at landscape-relevant scales is needed but not typically feasible with physical soil sampling approaches due to limitations on labour, time, cost, and site destruction (Parsekian et al., 2012; Scharlemann et al., 2014).

2.1.1 The potential for identifying landscape trends in forest soil properties via ground penetrating radar.

Successes in nondestructive, ground penetrating radar (GPR) soil data collection across homogeneous soil landscapes indicate significant potential for identifying and observing key soil properties with an increased resolution for forest landscape observation (Davis & Annan, 1989; Pelletier, Davis, & Rossiter, 1991; Wijewardana & Galagedara, 2010; Parsekian et al., 2012; Liu et al., 2018; Illawathure et al., 2019; Illawathure et al., 2020). Small-scale GPR soil data collection efforts have been successfully used to develop estimates of soil content and C for agricultural, peatland, and forest landscapes via inspecting a portion of representative areas within a site. This has been demonstrated in relatively homogenous soils, such as in agricultural and peatland sites where the site-level representation of the landscape is appropriate (Davis & Annan, 1989; Pelletier, Davis, & Rossiter, 1991; Gerber et al., 2010; Wijewardana & Galagedara, 2010; Parsekian et al., 2012; Han et al., 2016; Klotzsche et al., 2018; Liu et al., 2018; Zajícová & Chuman, 2019; Illawathure et al., 2020).

A GPR system collects high-resolution subsurface data in a near-continuous, non-destructive manner by generating electromagnetic waves that are reflected and captured by the GPR receiving antennas at contrasting material boundaries such as soil horizons and rocks and roots within a soil matrix (Figure 2.1; Collins & Doolittle, 1987; Davis & Annan, 1989; Jol & Bristow, 2003; Sucre, Tuttle, & Fox, 2011; Parsekian et al., 2012; Proulx-McInnis et al., 2013). These systems produce relative amplitude maps (i.e., radargrams) from transmitted and captured electromagnetic waves which allow for interpretations of various soil properties (Davis & Annan, 1989; Laamrani et al., 2013; Liu et al., 2018). The reflected radar waves from large rocks and roots or layered boundaries can be used to estimate the GPR's ground wave velocity allowing for interpretations of the shape and size of the source of reflections (i.e., soil horizon boundaries, rocks, and roots) with depth (Davis & Annan, 1989; Huisman et al., 2003; Jol & Bristow, 2003; Sucre, Tuttle, & Fox, 2011). Through this process, researchers can interpret estimates of soil horizon thickness as well as rock and root content for soil bulk density measurements based on the location, size, and nature of reflections sourced from soil horizon boundaries (linear and continuous, or strong hyperbolic reflections).

While GPR systems do not measure direct quantities of elements within the soil, GPR estimates of soil horizon thickness and soil bulk density can be combined with physical soil sampling measurements of soil elemental content (e.g., % C) to determine landscape soil content distribution and calculate landscape soil elemental stocks. In some cases, it may be possible to establish associations between soil content and horizon with C content (Borchers & Perry, 1991; Périé & Ouimet, 2007; Xu, He & Yu, 2016; Poeplau, Vos & Don, 2017). For example, soil bulk density in boreal forest soils have been found to decrease as soil organic matter concentration increases such that soil bulk density may be estimated from these concentrations accurately in loamy to sandy loam forest soils (Périé & Ouimet, 2007).

In this paper we examine previous small-scale forest soil GPR investigations to determine capabilities of GPR methods to estimate key soil properties, soil horizon thickness and soil bulk density, required in estimating soil C stocks across field scales (Klotzsche et al., 2018; Proulx-McInnis et al., 2013; Zajícová & Chumana, 2019). We use this examination to specifically inform and outline steps to optimize GPR methodology for investigating heterogenous forest soils at landscape relevant spatial scales and resolution. This involved determining the obstacles of conducting GPR surveying in difficult forest sites, identifying what previous studies have done to optimize their GPR methods, including system settings, survey design, and data processing, and compiling the common optimization steps taken for estimates of forest soil horizon thickness and soil bulk density. To evaluate the optimized GPR methodology for estimates of soil horizon thickness and bulk density we collected GPR survey data from a boreal forest hillslope in the Pynn's Brook Experimental Watershed Area in western Newfoundland, Canada. The objectives of this study were to; 1) review current forest literature from various successful, small-scale GPR studies across different soil features to compile optimized settings and data processing steps for estimating of soil horizon thickness and bulk density, 2) test optimized settings and data processing steps in a recently deglaciated boreal forest site, 3) evaluate the capability of GPR to collect landscape-scale resolution soil horizon thickness and bulk density estimates, and 4) present the tested recommendations for optimizing GPR system settings and data processing steps to achieve better interpretability of soil horizon thickness and bulk density estimates in difficult forest soil radargram data.

2.2 The challenges of utilizing ground penetrating radar to estimate forest soil horizon thickness and soil bulk density.

GPR system settings and surveying techniques used to evaluate homogenous, sandy loam and loam soils are generally not capable of achieving the suitable depth and resolution for measuring forest soil properties relevant to soil C stock calculations. In relatively wet forests, soil water content and electrical conductivity can be highly variable and greatly influence the ability of the GPR signal to identify soil horizons, rocks, and roots that are below the resolution of the system (Collins & Doolittle, 1995; Doolittle et al., 2006; Klotzsche et al., 2018). Furthermore, the abundance of shallow rocks and roots in the forest setting can cause scattering and diffraction of the initial GPR signal, weakening the relative amplitude of the resulting measured reflections and

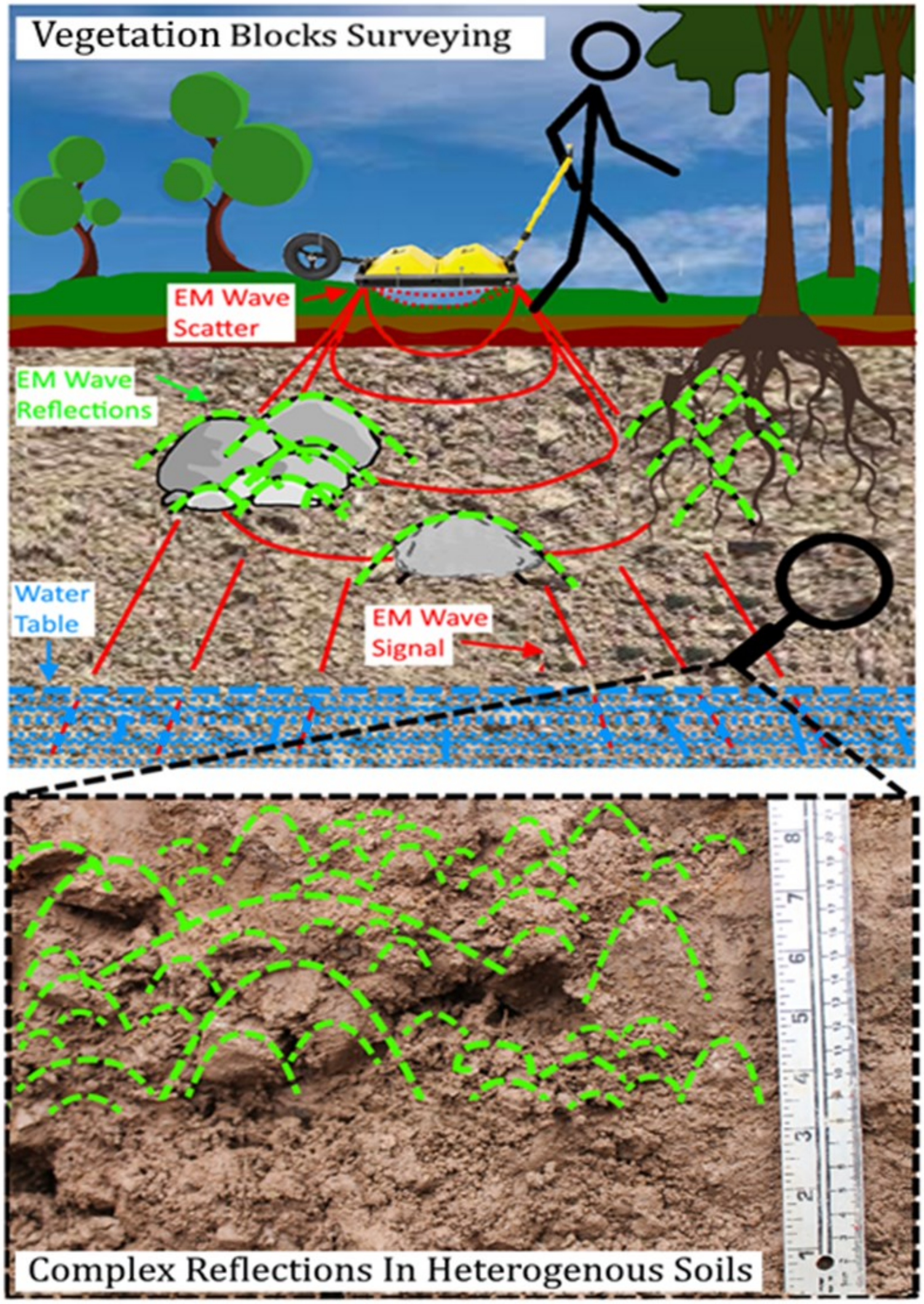

Figure 2.1. The path of a transmitted electromagnetic (EM) signal from a ground penetrating radar (GPR) system, the reflectors, and sources of attenuation. The propagation of the wave (solid red lines) is interrupted by obstacles such as rocks and roots which result in hyperbolic reflections (green dashed lines). Signal attenuation (broken red lines) may also occur when passing through different material layer boundaries, such as a water table (shown in blue). A variable microtopography may result in scattering of the EM wave (dotted red line under GPR unit).

obscuring soil horizon boundaries (Figure 2.1; Barton & Montagu, 2004; Sucre, Tuttle, & Fox, 2011; Winkelbauer et al., 2011; Liu et al., 2018). These typical forest terrain and soil conditions impede system operation and interpretation quality limiting the scale of forest soil GPR investigations without extensive labour and optimization (Gerber et al., 2010; Wijewardana & Galagedara, 2010; Han et al., 2016; Wijewardana et al., 2017; Klotzsche et al., 2018; Illawathure et al., 2019; Zajícová & Chuman, 2019).

The terrain within many forest sites can also impede GPR survey design and impact the quality of collected soil data. High tree density within forest sites with a buildup of surface litterfall, including dead wood, can prevent subsurface sampling and attenuate shallow GPR signal (Butnor et al., 2003; Barton & Montagu, 2004; Ardekani et al., 2014; André et al., 2019). A variable microtopography across forest terrain can also impede GPR soil surveying through air gaps between the ground coupling of the GPR system and the forest floor (Figure 2.1; Gerber et al., 2010). In dense forest strands with closely packed trees and vegetation, surveying can be quite restricted without significant clearing, limiting the amount of available spatial soil data. Overlying vegetation, organic layer thickness, slope, elevation, and preferential surface and groundwater flow paths further contribute to variations in soil properties within forest sites and across landscape gradients (Doolittle & Collins, 1995; Gerber et al., 2010; Laamrani et al., 2013). Many of these obstacles were observed when conducting our own surveying to test and evaluate GPR optimization methods.

When the GPR antennas cannot make complete contact with the forest floor, the GPR signal will freely propagate through air, scatter, and dissipate before entering the subsurface with a weakened amplitude (Figure 2.1; Jol & Bristow, 2003; Gerber et al., 2010). Furthermore, the forest terrain generally limits the access of many parts of the study area for surveying, either through physical blocks to access like fallen trees or an inability to collect interpretable data through such surface obstacles like understory vegetation and shrubs. When a survey line can be continuously set up through a forest site, sections of long survey lines (~100 m) may yield unusable due to surface obstacles scattering too much of the initial GPR signal and corrupting data. In addition to areas of large survey lines being inaccessible which also occurs frequently in forest surveys, corrupted or skipped sections of GPR data may have to be removed from the final, interpretable radargram (Figure 2.1). Obstacles such as tree trunks, thick vegetation, or burrows from wildlife will also impede the ability to follow a perfectly straight, linear survey line through forest sites which can introduce additional variation in resulting radargram data.

2.3 Successful applications of ground penetrating radar methods for measurements of forest soil horizon thickness and soil bulk density.

Successes in GPR soil investigations have been mainly documented for environments with homogeneous soils, including agricultural (Davis & Annan, 1989; Pelletier, Davis, & Rossiter, 1991; Wijewardana & Galagedara, 2010; Illawathure et al., 2019; Illawathure et al., 2020) and peatland ecosystems (Parsekian et al., 2012; Liu et al., 2018). In these more favorable GPR surveying locations, soil conditions can actively aid in identifying survey targets. Agricultural soils are generally sandy or loam, well-drained and have relatively homogenous soil content that produces more interpretable, repeatable radargrams (Doolittle & Collins, 1995; Wijewardana & Galagedara, 2010; Liu et al., 2018; Illawathure et al., 2019; Illawathure et al., 2020). Data processing practices have been developed and applied specifically for agricultural sites, resulting in accurate and consistent estimates of root position and size (Liu et al., 2018).

Table 2.1. A compilation of forest GPR soil studies with listed soil property targets, divided into categories of horizon thickness (a) and rock and root content (b), a description of the target measurement of the study, the spatial scale and antenna frequency used for each of these GPR investigations, the optimized settings and practices used by the researchers, and listed advancements drawn from these forest GPR surveying investigations.

Study	Target	Scale	* Freq (MHz)	Results	Optimized Settings	Optimized Practices	Advancements in forest GPR surveying
			a. Horizon Thickness Studies				
Gerber et al., 2010	Mineral soil thickness	220 m line	400	Measured horizons > 15 cm	Mean depth of 1.5 m	Layer based velocity corrections	- Achieved accurate soil-depth prediction using a practical method for shallow soil deposits over 10 m distance
Laamrani et al., 2013	Organic soil thickness	30 x 40 m grid	200	Accuracy within 2 cm	Stack = 32, 20 cm sample rate	Optimized system settings	- Reliably identified the organic layer – mineral soil interface across a boreal forest.
Winkelbauer et al., 2011	Organic soil thickness	30 x 30 m grid	800	Accuracy within 2 cm	Sampling rate of 0.102 ns	Odometer wheel attachment	- Achieved accurate measurements of organic layer thickness over large plots. - High frequency antenna and high resolution radargrams.
Han et al., 2016	Mineral soil thickness	16 m line	800	Measured horizons > 9 cm	0.05 m sample rate	High resolution sampling	- High frequency antenna. - Ground truthing using auger.
			b. Rock and Root Content Studies				
Barton et al., 2004	+ Root diameter	4 x 4 m grid	800, 1000	Roots found 50 cm deep	0.95 cm sample rate	Multiple antenna frequencies	- Found roots reliably at depth with high resolution imaging. - Evaluated the results between different antenna frequencies.
Butnor et al., 2003	Root diameter	2.5 x 4 m grid	1500	Measured roots > 5 cm thick	Mean depth of 70 cm, Stack = 256	Optimized system settings	- High significance between root biomass core and GPR estimates.
Molon et al., 2017	Root diameter	20 x 20 m grid	1000	Measured roots > 1.4 cm thick	0.5 cm sample rate	Optimized system settings	- Novel use of the Hilbert Transform for root identification. - High resolution, 3-D GPR surveying
Sucre et al., 2011	Rock content	20 x 20 m grid	200, 400	Accuracy to ground truthing	N/A	Layer based velocity corrections	- Evaluated the results between different antenna frequencies. - Accurate GPR estimates with depth compared to soil auger.

* Freq = Frequency, + = lab study

Advances in GPR methods for small-scale investigations of soil properties including soil horizon thickness, rock, and root content have been made for agricultural and forest ecosystems, presenting important information for optimizing GPR methods for forest soil investigations. A practical approach in the forest setting for obtaining accurate measurements of thick soil horizons (> 15 cm) at shallow depths and over distances greater than 10 m was demonstrated in small-scale, heterogenous, forest study sites (Gerber et al., 2010). In this example, variable soil depth was resolved from GPR survey data with an accuracy of 10 cm using a 400 MHz antenna frequency and mean penetration depth of 1.5 m (Table 2.1; Gerber et al., 2010). Using similar parameters at a low sampling rate of every 0.5 m, we found soil horizon depth estimates from GPR were less variable than the accompanying soil pit measurements conducted (Gerber et al., 2010). Furthermore, in studies in a boreal forest using a 200 MHz center frequency GPR antenna with shallower depth penetration, the interface between organic and mineral soil horizons was interpreted at a similar resolution of 10 cm (Table 2.1; Laamrani et al., 2013). The use of higher frequency GPR antennas (800 – 1000 MHz) in forest soil surveying have also yielded high resolution, accurate results. In a forest hillslope in China, researchers collected measurements of soil horizon thickness for horizons < 10 cm thick that were comparable with physical sampling estimates using a high sampling rate (0.05 m) over 16 m survey lines (Han et al., 2016).

Additionally, much effort has gone into studying the capabilities of GPR to measure the size and position of isolated bodies in soil matrices, including rock and root content. In lab tests completed by filling pits with damp sand and burying roots at specific depths, GPR methods could resolve the position and size of roots ≥ 5 cm reliability up to 50 cm deep (Table 2.1; Barton & Montagu, 2004). In field tests under similar conditions in Georgia, USA, root biomass for roots of similar diameter was measured up to 30 cm deep (Table 2.1; Butnor et al., 2003). Furthermore, in rocky forest soils across sites in the southern Appalachian Mountains, GPR methods were able to resolve soil depth up to twice as deep as soil auger measurements with similar variability (Sucre, Tuttle, & Fox, 2011). A study conducted in a temperate pine forest demonstrated success in identifying coarse root biomass using high frequency GPR antennas (1000 MHz) and additional data processing using a Hilbert Transformation (Molon et al., 2017). The detailed processing steps taken and application of the Hilbert Transformation to produce interpretable radargrams for GPR estimates of root biomass demonstrate valuable methods for obtaining usable forest radargram data (Molon et al., 2017).

2.4 Optimized, landscape-scale ground penetrating radar methods for forest soil horizon thickness and soil bulk density estimates.

Following the techniques and settings reviewed from previous successful GPR forest survey approaches, we identified soil horizon boundaries and soil horizon thickness of the organic layer and mineral soil horizons across 1 m long and 1 m deep survey lines using the optimized GPR methods along a boreal forest hillslope (Figure 2.2). Soil horizon boundaries were identified in radargrams collected by interpreting the position of strong, linear, continuous reflections which occur between two soil horizons (organic, mineral, or till) of contrasting electrical conductivity such as dielectric permittivity and electrical conductivity. This contrast is mainly due to the material and moisture of the different soil horizons. Initial radargram data collected in such forest environments with minimal or 'raw' data processing may be partially or fully interpretable based upon reflections observed (Figure 2.2a).

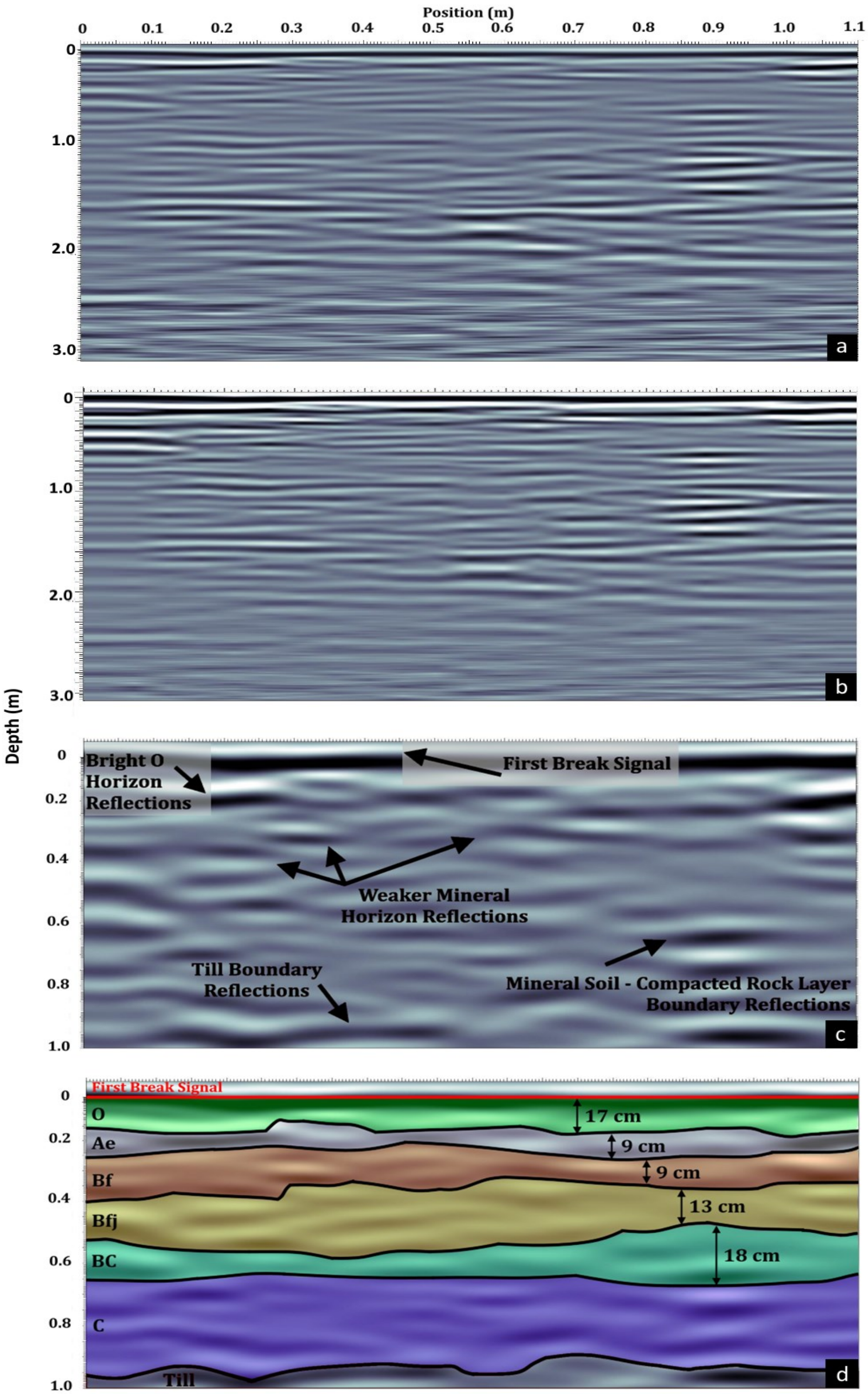
Position (m)
0
0.1
0.2
0.3
0.4
0.5
0.6
0.7
0.8
0.9
1.0
1.1
Depth (m)
1.0
2.0
3.0
a
b
0.2
0.4
0.6
0.8
Bright O Horizon Reflections
First Break Signal
Weaker Mineral Horizon Reflections
Till Boundary Reflections
Mineral Soil - Compacted Rock Layer Boundary Reflections
c
First Break Signal
O
Ae
Bf
Bfj
BC
C
Till
17 cm
9 cm
9 cm
13 cm
18 cm
d

Figure 2.2. Radargram data collected from a forest hillslope in the Pynn's Brook Experimental Watershed Area, western Newfoundland, Canada utilizing optimized GPR methods as recommended in this paper. This radargram data, collected along a 1 m section parallel and 0.5 m upslope from an excavated soil pit where physical soil sampling and interpretation was conducted for reference, is displayed as raw, unprocessed data (a). This same data, which has undergone all soil horizon thickness data processing steps as recommended in this paper, is given just below (b), and then given with accompanying interpretations of the position of specific soil horizon boundary reflections (c). Finally, the colour-mapped interpretations for soil horizon positions and thickness are provided (d). Soil horizons are labelled as an organic layer (O), an eluviated mineral soil layer (Ae), the three underlying mineral soil horizons (Bf, Bfj, and BC in descending order), the compacted rock layer (C) and an underlying till layer.

Considerable data processing must be taken after data is collected to be able to fully interpret the data for estimates of soil horizon thickness (Figure 2.2b). Once recommended data processing steps were taken, the linear, continuous reflections associated with soil horizon boundaries were stronger, more visible, and therefore easier to interpret fully across the radargram section (Figure 2.2c). Once the soil horizon boundaries could be fully interpreted following GPR data processing, the position and thickness of soil horizons across the full radargram section were interpreted, mapped, and allowed for continuous and spatial averages of individual soil horizon thickness (Figure 2.2d).

GPR methods used to determine the position and size of isolated rock and root bodies can aid in estimating soil bulk density. Reflections in GPR radargrams associated with rock and root content appear as strong, isolated, hyperbolic reflections where the shape of the hyperbola relates to the size of the rock or root. The transmitting antenna of a GPR system will produce an elliptical, cone shaped pulse which will extend with a long axis into the subsurface with depth (Barton et al., 2004). When completing GPR surveying by moving the device along the soil surface, the travel time of the signal which is reflected off rocks and roots in the underlying soil will decrease to a minimum when the GPR system is directly over the reflecting rock or root (Barton et al., 2004).

This travel time will increase as the GPR antenna is moved away from the object, resulting in the characteristic hyperbolic shape of rock and root reflections (Barton et al., 2004).

Following optimized data processing steps as synthesized from previous studies, we were able to identify rock and root content in highly rocky and root filled soils in boreal forest hillslope site (Figure 2.3). These results highlight the need for optimized data processing to account for rocks and roots, particularly at depth, as their associated reflections are not clearly interpretable in the raw, unprocessed radargram (Figure 2.3a). The raw radargrams collected from this boreal forest site demonstrate the anomalies in amplitude content against a consistent grayscale background as the soil content reflects electromagnetic wave energy (Figure 2.3a). Key GPR data processing steps including distance normalization, background noise removal, and migration were taken and enabled more detailed identification of rock and root locations (Figure 2.3b). Higher amplitude reflections indicating rock or root content were easily interpretable in these conditions as shown by the brighter white or darker black coloring (Figure 2.3c). Locating high amplitude reflection content left after processing can be used to produce a map of near-surface relative rock and root content in forest soils when informed by physical soil sampling. This is commonly achieved by applying a Hilbert Transformation to the processed GPR data (Figure 2.3d). The Hilbert transform imparts a phase shift on a signal data set of ± 90° for all frequencies of the function (Luo et al., 2003). This is achieved for the dataset, u(t), by performing a convolution with the Cauchy kernel function $h(t) = 1 / \pi t$ (Eq. 2.1). Explicitly, the Hilbert transformation can be written as a principal value integral:

$$H(u)(t) = -\pi^{-1}\lim_{\varepsilon\to 0}\int_{\varepsilon}^{\infty} (u(t+\tau)-u(t-\tau))\, \partial\tau \qquad \text{(Eq. 2.1)}$$

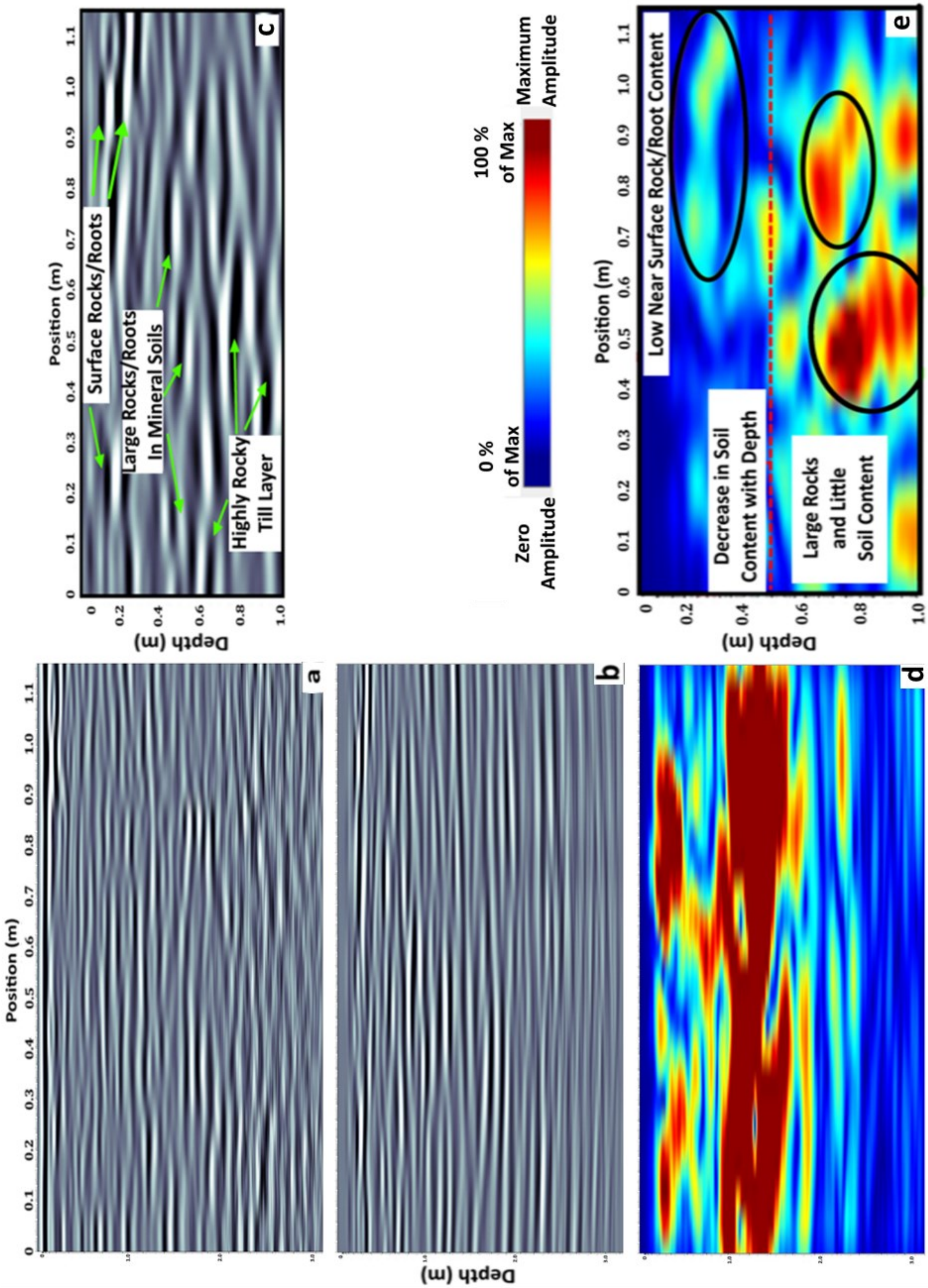

Position (m)
Depth (m)
a
b
c
d
e
Surface Rocks/Roots
Large Rocks/Roots In Mineral Soils
Highly Rocky Till Layer
0 % of Max
100 % of Max
Zero Amplitude
Maximum Amplitude
Low Near Surface Rock/Root Content
Decrease in Soil Content with Depth
Large Rocks and Little Soil Content

Figure 2.3. Radargram data collected by Zachary Gates and Lakshman Galagedara from a forest hillslope in the Pynn's Brook Experimental Watershed Area, western Newfoundland, Canada utilizing optimized GPR methods as recommended in this paper. This radargram data, collected along a 1 m section parallel and 0.5 m upslope from an excavated soil pit labelled D-1 at which physical soil sampling and interpretation was conducted for reference, is displayed as raw, unprocessed data (a), data which has undergone all soil bulk density data processing steps as recommended in this paper (b). The processed GPR data is further examined with accompanying interpretations of the position of specific rock and root reflections (c). To interpret the spatial distribution of rock and root content across the collected radargram data, a non-polarized Hilbert Transform was conducted on the processed GPR data (d). Interpretations for rock and root content can be made following the Hilbert transformations and interpreted using an associated amplitude scale, where higher amplitude indicates a higher concentration of rock and roots (e).

In practice, the Hilbert transformation filter will scale and colour-map amplitude energy from a non-polarized zero background level to the maximum amplitude (Luo et al., 2003; Molon, Boyce, & Arain, 2017). This process, when applied over lines of radargram data, will convert reflection data into a scaled, nonpolarized colour map that shows areas of high and low amplitude responses (Figure 2.3c; Butnor et al., 2003; Molon, Boyce, & Arain, 2017). Following the Hilbert transformation, interpretations for rock and root content can be made using an associated amplitude scale, where higher amplitudes indicate a higher concentration of rock and roots.

2.4.1 Optimized ground penetrating radar system settings for measuring forest soil horizon thickness and soil bulk density.

For accurate interpretations of soil targets, a calibration of GPR interpreted depth relative to the ground wave's two-way travel time is routinely performed before line surveying using ground wave velocity (Jol & Bristow, 2003). Frequently, common midpoint and wide-angle reflection and refraction surveying are employed to make measurements of ground wave velocity with depth in forest GPR investigations (Pelletier, Davis, & Rossiter, 1991; Huisman et al., 2003;

Jol & Bristow, 2003; Zajícová & Chuman, 2019). Additionally, during standard common offset surveying for soil targets, hyperbolic reflections can be captured from rock and root content, or in their absence from buried reflectors like metal pipes or rebar, to estimate the ground wave velocity at varying depths (Sucre, Tuttle, & Fox, 2011; Wijewardana et al., 2017; Illawathure et al., 2019).

Modern GPR systems have high frequency antennas that have improved the resolution achieved in various soil investigations when targeting shallow soil properties (Table 2.1; Gerber et al., 2010; Sucre, Tuttle, & Fox, 2011; Winkelbauer et al., 2011; Proulx-McInnis et al., 2013; Han et al., 2016; Molon, Boyce, & Arain, 2017). GPR soil investigations generally employ antenna frequencies between 100 to 1000 MHz, but frequencies of 500 MHz or greater are recommended to provide the best interpretability for shallow soil layering and rock and root content while achieving the required penetration depth to image the full mineral soil layer (Table 2.1; Gerber et al., 2010; Sucre, Tuttle, & Fox, 2011; Winkelbauer et al., 2011; Proulx-McInnis et al., 2013; Zajícová & Chuman, 2019). Investigations of organic layer thickness in an alpine forest using high frequency (800 MHz) GPR methods, for example, indicate low variation in thickness measurements ($\pm$ 2 cm) compared to physical measurements (Winkelbauer et al., 2011). However, in this case, individual horizons within the organic layer could not be resolved (Winkelbauer et al., 2011). High frequency antennas are also generally smaller and more mobile than older, lower frequency models, and have allowed researchers to achieve depth penetration of roughly 2.0 m in forest sites which is ideal for imaging the total mineral soil depth in postglacial landscapes, including individual horizon features $\geq$ 10 cm (Table 2.1; Barton & Montagu, 2004; Sucre, Tuttle, & Fox, 2011; Winkelbauer et al., 2011; Laamrani et al., 2013; Han et al., 2016; Molon, Boyce, & Arain, 2017). Through our GPR surveying tests in a boreal forest site, we found that 500 MHz antennas improved the interpretability of shallow soil features, such as roots in the organic soil (<

10 cm), rocks and soil horizon boundaries in the shallow mineral soil horizons (< 30 cm), by producing stronger reflections for these targets than those obtained using a lower frequency (250 MHz) antenna.

Review of other studies, and our own application based upon those studies, indicates that optimizing the depth penetration with a focus on shallow soil targets (< 1 m) can improve the image resolution of those targets. This can be achieved by using GPR antenna center frequency between 500 and 1000 MHz with a maximum depth set at 2 m. Using such frequencies can increase the image resolution of the soil targets in complex forest environments enabling clear identification of individual mineral soil horizons (Table 2.1; Gerber et al., 2010). At the boreal forest site we surveyed, a mean depth penetration of 2 m was achieved (50 ns time window) when using a 500 MHz center frequency GPR system which encompassed the full depth of the organic, mineral, and compacted soil and rock layers as well as part of the underlying till, providing the entire soil profile at this site.

GPR settings including trace stacking and step size were also evaluated to determine how they can improve the interpretability of soil targets in difficult forest soils (Laamrani et al., 2013). Using a 400 MHz antenna frequency to investigate soil layer thickness over Pleistocene periglacial soil deposits in a rocky forest, researchers were able to tailor system settings to achieve a vertical resolution of 0.5 cm in wet soils with an average ground wave velocity of 0.9 m ns^{-1}. In similar studies, a high stacking rate (> 32) and a low trace spacing (~0.05 m) and sampling interval (50 ns) resulted in smooth traces (i.e. the time between two sampling points) and were used to further improve the interpretability of soil horizon boundaries to achieve better measurements of soil horizon thickness (Table 2.1; Laamrani et al., 2013; Warner et al., 1990).

The number of GPR pulses summed to create each averaged sample trace comprising the radargram, called trace stacking, may be increased to provide a more representative average summed from a high quantity of replicate radar data measurements (Jol & Bristow, 2003). Increasing the GPR trace stacking allows for the influence of random noise and variations in GPR signal transmission and recapture to be reduced while amplifying reflections that consistently appear in all traces, such as those related to soil horizon boundary, rock, and root content positions (Jol & Bristow, 2003). This has been used to improve the imaging of high amplitude reflections associated with linear horizon boundaries and point reflections from rocks and roots, as lower amplitude background noise is filtered out through repeated stacking (Table 2.1; Warner, Nobes, & Theimer, 1990; Butnor et al., 2003). In our testing, a variety of different stack rates, step size, and system settings were used in tandem to determine which parameters provided the best quality radargrams for soil horizon interpretations. In line with the literature, a minimum stack rate of 32 was found to provide reliable trace averages for estimates of both forest soil horizon thickness and bulk density when tested using various GPR systems of different antenna frequencies (i.e., 250, 500, and 1000 MHz) (Table 2.1; Figure 2.2).

The GPR sampling interval will control how frequently the system triggers an electromagnetic signal and measurement of the resulting trace data at sampling locations based on distance or time intervals across the landscape (Jol & Bristow, 2003). The appropriate trace spacing (distance between sampling points) varies with site conditions, but generally, a lower sampling interval and trace spacing is preferred as it results in a more continuous dataset (Laamrani et al., 2013). To capture reflections from smaller rocks or roots (diameter < 10 cm), a trace spacing of no more than half the size of the desired minimum target diameter is used to provide enough resolution to interpret targets of this size according to the Nyquist theorem (Table 2.1; Molon, Boyce, & Arain, 2017).

The resolution obtained in a GPR survey depends on the wavelength of the GPR signal as the resolution is defined as a fourth of the inverse of wavelength. As wavelength is equal to the ground wave velocity divided by the frequency of the wave, a higher frequency or lower ground wave velocity will lower the wavelength and result in a higher resolution. Ground wave velocity depends on soil water content. The higher water content in soils results in higher dielectric permittivity, lowering ground wave velocity and thus wavelength, increasing resolution. Thus, the lowest trace spacing possible should be used in forest GPR surveying to achieve the highest resolution for interpreting soil targets. For example, a trace spacing of 5 cm provides the resolution to resolve soil targets around 10 cm in diameter or greater through radargram interpretation (Table 2.1; Winkelbauer et al., 2011; Han et al., 2016). In general, a trace spacing of 5 cm is recommended with a 500 MHz center frequency in heterogeneous forest settings, based on analogous studies, the Nyquist theorem, and for obtaining representative data while maintaining efficiency in time and labour (Table 2.1; Han et al., 2016; Molon, Boyce, & Arain, 2017). The GPR surveying conducted at our boreal forest site was consistent with this. The soil horizon thickness and compacted zones of rock or root content were generally ≥ 10 cm in diameter and thus a trace spacing of 5 cm was found to be appropriate (Figures 2.2 & 2.3). We recommend this sampling interval for analogous, post-glaciated forest soil targets, but the sampling interval should be adjusted following the Nyquist theorem based on the average size of the desired soil target.

2.4.2 Optimized data processing steps for ground penetrating radar measurements of forest soil horizon thickness.

To measure forest soil horizon thickness in aid of determining soil C distribution using GPR methods, researchers interpret soil horizon boundaries from radargrams only after the data undergoes processing to improve the signal-to-noise ratio such that these horizon boundary reflections are clearly visible (Jol & Bristow, 2003). Processing will be unique to each site as factors of soil content, electrical conductivity, and external electrical signals (i.e., overhead wires, powered research equipment) will introduce noise into the radar section (Jol & Bristow, 2003). GPR dataset processing steps derived from previous studies aimed at obtaining forest soil horizon thickness (Table 2.1) are summarized here and, with their application in difficult boreal forest terrain, demonstrate improved data interpretability for accurate soil horizon thickness estimates (Figure 2.4).

1) Application of filters to remove noise. A dewow style filter is commonly applied, which eliminates low-frequency noise created by the close spacing of the GPR transmitter and receiver antenna (Figure 2.4; Jol & Bristow, 2003; Winkelbauer et al., 2011; Laamrani et al., 2013). Using such filters, the linear reflections from forest soil horizon boundaries become more apparent as the signal-to-noise ratio is improved (Figure 2.4). Additional noise filtering tools may be applied at this stage to further improve data clarity, such as background average subtraction filters (Table 2.1; Barton & Montagu, 2004; Molon, Boyce, & Arain, 2017).

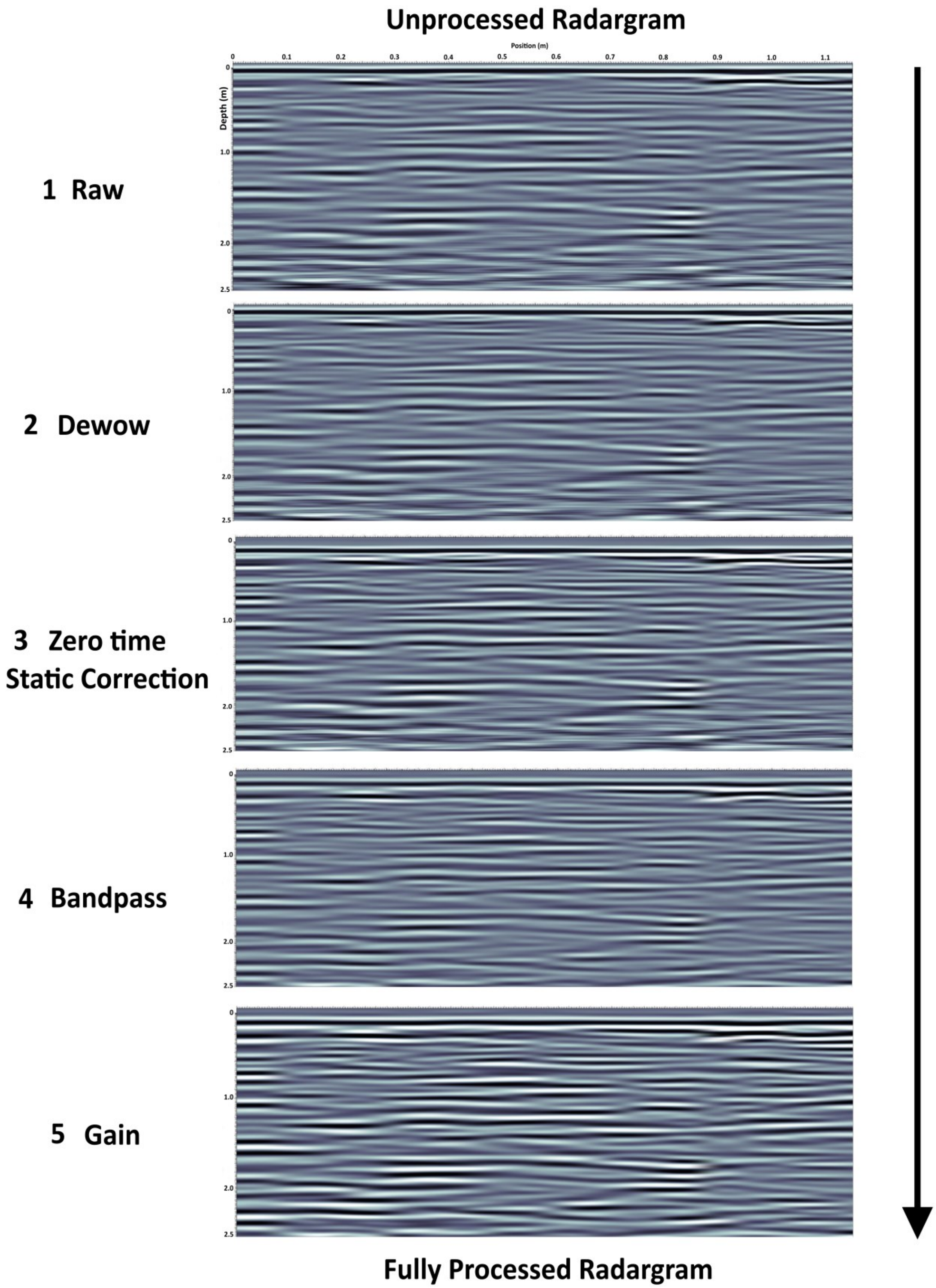

Unprocessed Radargram
Position (m)
Depth (m)
1 Raw
2 Dewow
3 Zero time
Static Correction
4 Bandpass
5 Gain
Fully Processed Radargram

Figure 2.4. Radargram data collected along a 1 m survey line within a boreal forest site in the Pynn's Brook Experimental Watershed Area, western Newfoundland, Canada. The data is displayed under raw field processing settings (1) and after undergoing data processing following the recommended steps to highlight soil horizon thickness results (5). Resulting radargram data following processing steps in between include using a dewow filter (2; Laamrani et al., 2013; Winkelbauer et al., 2011), adjusting first break signals (3; Gerber et al., 2010; Laamrani et al., 2013), applying a bandpass filter (4; Gerber et al., 2010; Han et al., 2016), and running gain functions (5; Laamrani et al., 2013; Pelletier et al., 1991) to improve interpretability.

2) A zero-time static correction applied by editing or repicking at the first break signals, where the GPR interprets the first interaction of the GPR wave with the subsurface (Figure 2.4; Gerber et al., 2010; Winkelbauer et al., 2011). This can also correct errors in the interpretation of subsurface depth caused by poor ground coupling when surveying over the variable forest microtopography (Jol & Bristow, 2003; Laamrani et al., 2013; Han et al., 2016). By testing different parameters of these settings through our forest GPR surveying, we achieved the best radargram interpretability when the dewow filter was set to a standard value (1.33 pulse widths) and the first breaks parameters were repicked at a threshold of 5 mV (Figure 2.4; Gerber et al., 2010; Laamrani et al., 2013).

3) The application of bandpass filters to remove low and high-frequency reflections and smooth out data along the GPR section (Figure 2.4d; Gerber et al., 2010; Winkelbauer et al., 2011). Additional data smoothing before applying gain can improve normalization and clarity in reflection amplitude distribution which helps to find continuous linear reflections and remove hyperbolic reflections associated with rock and root content (Gerber et al., 2010; Winkelbauer et al., 2011). The effect of this tool is most prominently seen in removing near-surface smearing effects caused by high reflection contrasts between organic and mineral soil horizon boundaries (Figure 2.4; Gerber et al., 2010; Han et al., 2016). The bandpass filter worked best to improve

radargram interpretability at our boreal forest site when a more gradual taper was applied, thus frequency parameters of F_1 = 40 %, F_2 = 80 %, F_3 = 120 %, F_4 = 160 % are recommended (Figure 2.4; Gerber et al., 2010; Han et al., 2016).

4) The application of gain control to enhance weak continuous reflections in the radargram is the final processing step (Jol & Bristow, 2003). Many types of gain can be applied, including spherical and exponential compensation gain and automatic gain control. The right gain control to apply will be determined by the target depth as well as site conditions and the GPR system (Pelletier, Davis, & Rossiter, 1991; Winkelbauer et al., 2011; Laamrani et al., 2013; Molon, Boyce, & Arain, 2017). Heterogenous forest soils with complex reflections may require significant gain to amplify target reflections, especially at depth, which has undergone scattering and amplitude loss through many rocks and roots (Figure 2.4e; Laamrani et al., 2013). For radargrams collected in our boreal forest site, we tested a range of gain control to obtain the right range for horizon thickness measurements, and found that a spherical and exponential compensation gain with a high gain attenuation of ten, a moderate start gain of three, and a maximum gain of 500 provided the best detection of strong linear reflections that identified horizon boundary positions (Figure 2.4; Pelletier, Davis, & Rossiter, 1991; Laamrani et al., 2013).

2.4.3 Optimized data processing steps for ground penetrating radar measurements of forest soil bulk density.

Optimized processing steps for interpreting hyperbolic reflections associated with shallow rock and root content in forest soils to make measurements of their abundance and inform soil bulk density estimates also involve applying filters to remove noise and the zero-time correction stage as described for horizon thickness. The same settings and application of a dewow filter and repicking first breaks used in soil horizon thickness are recommended for GPR data processing aimed at rock and root content and soil bulk density (Barton & Montagu, 2004; Raz-Yaseef, Koteen, & Baldocchi, 2013). However, subsequent steps differ as described below.

1) Additional background noise removal is applied to better isolate high amplitude, hyperbolic reflections associated with high root and rock content. This can be achieved by using background subtraction filters which average trace amplitude data and then subtract the average from each trace to isolate high amplitude content (Figure 2.5; Barton & Montagu, 2004; Winkelbauer et al., 2011; Molon, Boyce, & Arain, 2017). We found that automatic background average subtraction filters which calculate the average amplitude worked best at removing additional noise and improve radargram interpretations for estimating soil horizon thickness and soil bulk density at our boreal forest site (Figure 2.5; Barton & Montagu, 2004).

2) Gain functions as previously outlined for the GPR data processing procedure for soil horizon thickness must be similarly modified for detecting strong rock and root reflections at depth (Figure 2.5; Pelletier, Davis, & Rossiter, 1991; Winkelbauer et al., 2011; Laamrani et al., 2013; Molon, Boyce, & Arain, 2017). When conducting GPR surveying for rock and root content in aid of estimating soil bulk density in our boreal forest site, for example, gain had to be specifically applied to each radargram for optimal interpretability (Figure 2.5; Butnor et al., 2003).

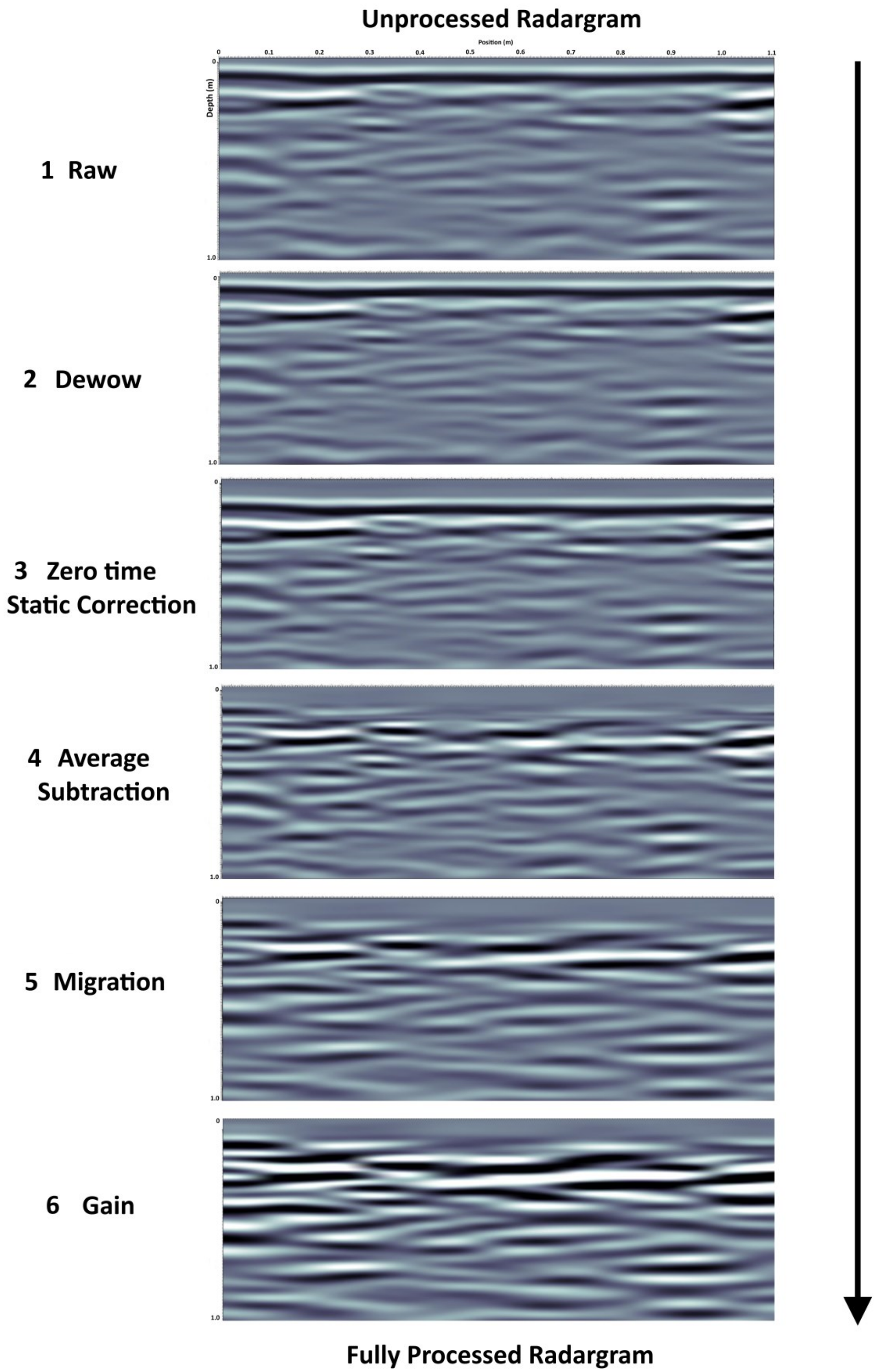
Unprocessed Radargram
Position (m)
Depth (m)
1 Raw
2 Dewow
3 Zero time
Static Correction
4 Average
Subtraction
5 Migration
6 Gain
Fully Processed Radargram

Figure 2.5. Radargram data collected along a survey line in the Pynn's Brook Experimental Watershed Area in western Newfoundland, Canada. The data is displayed under raw field processing settings (1) and after undergoing data processing following the recommended steps to highlight soil bulk density results (6). Processing steps included using a dewow filter (2; Laamrani et al., 2013; Winkelbauer et al., 2011), adjusting first break signals (3; Gerber et al., 2010; Laamrani et al., 2013), background average amplitude subtraction (4; Barton et al., 2004), frequency-wavelength domain (F-K) migration (5; Molon et al., 2017), and running gain functions (6; Laamrani et al., 2013; Pelletier et al., 1991) to improve interpretability (Table 2.1).

3) The application of a migration procedure is recommended to correct the positioning of point reflections to their source location (Figure 2.5; Raz-Yaseef, Koteen, & Baldocchi, 2013; Molon, Boyce, & Arain, 2017). Migration is a key step for rock and root content interpretations as reflections in shallow soils may migrate by centimeters under this correction which could significantly influence interpretations of horizon rock content and bulk density (Figure 2.5; Molon, Boyce, & Arain, 2017). The frequency-wavenumber domain migration and Kirchhoff migration are the most popular tools for this application (Raz-Yaseef, Koteen, & Baldocchi, 2013; Molon, Boyce, & Arain, 2017). The parameter for velocity used by the frequency-wavenumber domain migration applied to GPR data collected at our boreal forest site was matched to the average measured ground wave velocity at the time of the survey, which was 0.10 m/s, as is the recommended procedure for this filter (Raz-Yaseef, Koteen & Baldocchi, 2013; Molon, Boyce, & Arain, 2017). In the data processing software used for this testing, EkkoProject 5 (Sensors & Software Inc., Mississauga, ON, Canada), a migration process is applied before the Hilbert transformation takes place when using the assisted pick processing tool.

4) Transformation of data from a polarized reflection set to a normalized, amplitude map for easy identification of the abnormal rock and root content is a final processing step useful in high rock and root content soils (Figure 2.5; Butnor et al., 2003; Luo et al., 2003; Molon, Boyce,

& Arain, 2017). This is commonly achieved by using filters or tools that employ a Hilbert transformation of the data, like assisted pick processing. The Hilbert transformation procedure was applied as the final processing step for all radargrams collected during GPR surveying at our boreal forest site for interpreting the spatial position of rock and root content to inform both GPR and physical estimates of soil bulk density (Butnor et al., 2003; Luo et al., 2003; Molon, Boyce, & Arain, 2017). This allows for the identification of rock and root content at positions of high amplitude responses over the entire collected GPR survey line which is important to scaling forest soil investigations for soil C stocks (Figure 2.5; Butnor et al., 2003; Luo et al., 2003; Molon et al., 2017). Identification of rock and root content in forest subsurface allows for quantification of the total non-soil, coarse fragment (> 2 mm diameter) portion of the subsurface and thus an inverse measurement of the quantity of soil fraction (< 2 mm diameter) over the surveyed soil volume. By using soil density measurements determined by physical soil excavation and sampling across a forest site, these inverse measurements of total soil content can be used to estimate soil bulk density.

2.5 Combining spatial datasets with ground penetrating radar holds potential for large-scale assessment of forest soil properties and controls.

Much potential to understand landscape influence and controls on soil properties and their distribution lies in the tandem use of available spatial data products and methods with continuous GPR survey capabilities for large-scale, high-resolution soil property data (Pelletier, Davis, & Rossiter, 1991; Hubbard et al., 2013). In this paper, and through our own testing conducted in a boreal forest site, we demonstrate optimized methods for successful GPR investigations of forest soil properties such as soil horizon thickness and rock and root content informing soil bulk density at smaller, plot scales (Table 2.1; Proulx-McInnis et al., 2013; Klotzsche et al., 2018; Zajícová &

Chuman, 2019). The application of these methods across hillslope or landscape scales has the potential to provide continuous data to assess forest landscape-scale variation in soil properties and the opportunity for integration of these with other surface and above-ground spatial datasets, such as those obtained via airborne geophysical and LiDAR surveys (Gerber et al., 2010; Laamrani et al., 2013; Molon, Boyce, & Arain, 2017). Integration of these datasets can contribute to our understanding of controls on forest soil properties and thus soil responses to climate and environmental change (Collins & Doolittle, 1987; Davis & Annan, 1989; Gerber et al., 2010; Molon, Boyce, & Arain, 2017).

Combining GPS and topographical data with continuous GPR surveying enables georeferencing of soil datasets for establishing potential controls on soil properties across hillslope positions relevant to soil formation processes (Pelletier, Davis, & Rossiter, 1991). Technologies for obtaining additional site measurements to use in tandem with GPR surveying include direct GPS attachments to the GPR system for measurements of position and elevation, satellite-based estimates of surface content and processes such as tree biomass, distribution, and net primary production , and airborne surveying for additional geophysical measurements (Worsfold, Parashar, & Perrott, 1986; Pelletier, Davis, & Rossiter, 1991; Raz-Yaseef, Koteen, & Baldocchi, 2013; Henry et al., 2015). Through combining such datasets, such as those obtained using optimized GPR methods described here, with site information derived from these additional methods, soil property data may be linked with forest site factors relevant to controls on soil stocks and properties such as landscape level variation in net primary production or evapotranspiration. Combining such datasets may also lead to opportunities for scaling up soil stocks informed by a larger quantity and spatial coverage of soil property data. Such datasets, paired with well-chosen physical sampling, can inform our understanding of the relationships between soil bulk density distribution, topography, soil stratigraphy, and ultimately soil C distribution along forest hillslope sites.

Satellite mobile laser technologies can also expand forest surveys by increasing spatial data collection and coverage as well as providing surface and subsurface measurements such as vegetation and tree canopy height (Henry et al., 2015). LiDAR, a high-resolution spatial mapping method using laser measurements, provides geomorphic metrics such as topographical and organic growth data across sites (Næsset & Gobakken, 2008; Hubbard et al., 2013). Coupling such datasets with continuous GPR soil surveying enables the establishment of above and belowground associations (Hubbard et al., 2013). For example, GPR estimates of root biomass were combined with tree distribution data derived from LiDAR imaging linking tree root biomass measurements to forest structure (Raz-Yaseef, Koteen, & Baldocchi, 2013). Cluster analysis of both LiDAR and GPR data has been used to better capture soil distribution across hydrologic, geochemical, and geomorphic gradients (Hubbard et al., 2013).

The optimized GPR methodology presented here provides the means to collect estimates of forest soil horizon thickness and soil bulk density such that they can be combined with physical soil sampling measurements of soil elemental content (e.g., C or N) to determine landscape scale soil content distribution and calculate landscape soil elemental stocks. This type and scale of tandem GPR and physical soil sampling investigation will be important for developing and monitoring mitigation efforts and informing forest C-climate feedbacks. For example, repeated surveying possible through non-destructive, continuous GPR surveying allows for temporal analysis of soil content changes across forest landscapes over time which will be useful for understanding the impacts of climate changes on forest ecosystems and their soil stocks. For this kind of temporal investigation, physical soil sampling informed by GPR surveying can limit site

Table 2.2. Recommended data processing steps for obtaining forest measurements of soil horizon thickness and soil bulk density using ground penetrating radar (GPR). Data processing steps should be applied in the order listed in the table and with the specific parameters listed for each soil property measurements. These data processing steps will work optimally when data is collected using GPR system settings tailored for forest soil property surveying which include: ≥ 500 MHz antenna center frequency; a high stacking rate ≥ 32; a low trace spacing ≤ 5 cm for a 10 resolution; a low sampling interval time window of ≤ 50 ns; and a mean depth penetration of 2 m.

Order	Process	Goal	Horizon Thickness Method Parameter	Bulk Density Method Parameter
1.	Dewow	Eliminate low frequency noise	≤ 1.33 pulse widths	≤ 1.33 pulse widths
2.	Zero-time Static Correction	Correct subsurface depth scale	Threshold of ≥ 5 mV	Threshold of ≥ 5 mV
3.	Background Average Subtraction	Isolate high amplitude reflections	N/A	Calculated background amplitude average
4.	Bandpass Filter	Remove low and high frequency noise to smooth trace data	F_1 = 40 % F_2 = 80 % F_3 = 120 % F_4 = 160 %	N/A
5.	Gain	Amplify high amplitude reflections	Attenuation = 10 Start gain = 3 Max gain = 500	Attenuation = 10 Start gain = 3 Max gain = 500
6.	Migration	Correct positions of high amplitude reflections	N/A	V_{gw} = 0.10 ns or in-situ average from CMP/WARR surveying
7.	Hilbert Transformation	Transform data from polarized (-max to +max) to normalized (0 to max) scale	N/A	Transform calculated using Eq. 1

destruction and inform targeted sampling to capture landscape trends critical for best estimates and representation.

Optimized GPR methods for forest surveying as presented in this paper, which are summarized in Table 2.2, and additional spatial data methods can expand both the spatial resolution of soil content measurements and depth of measurements through high-resolution, continuous data collection (Table 2.2; Worsfold, Parashar, & Perrott, 1986; Pelletier, Davis, & Rossiter, 1991; Raz-Yaseef, Koteen, & Baldocchi, 2013; Henry et al., 2015). The continuous and high-resolution data captured through these methods show the potential, through landscape scale application, to reveal relationships between soil properties and forest site conditions, such as vegetation, topography, or hydrology (Table 2.2).

2.6 Conclusion.

Through a review of relevant, current literature and our own tests completed along a boreal forest hillslope we demonstrate that continuous GPR data collection can be used to inform physical soil properties that may be captured at spatial scales and depths relevant to forest landscape studies. Furthermore, common system settings, surveying practices, and data processing steps from successful forest GPR studies were compiled into an optimized GPR methodology for collecting forest estimates of soil horizon thickness and soil bulk density. The optimized GPR methodology presented was successfully used to improve the interpretability of radargram data collected from a boreal forest hillslope site, demonstrating continuous, high-resolution acquisition of soil horizon and content data across segments of a heterogenous forested hillslope and over a meter depth. These optimized GPR methods for estimating forest soil horizon thickness and soil bulk density indicate potential landscape representation of soil C stocks, variance, hydro-biogeochemical, and morphological controls through the ability to efficiently collect large-spatial datasets in difficult, forest soil environments.

References

Anderson, A. E., Weiler, M., Alila, Y., Hudson, R. O., 2009. Subsurface flow velocities in a hillslope with lateral preferential flow. *Water Resources Research*, 45(11). doi: 10.1029/2008WR007121.

André, F., Jonard, F., Jonard, M., Vereecken, H., Lambot, S., 2019. Accounting for surface roughness scattering in the characterization of forest litter with ground-penetrating radar. *Remote Sensing*, 11(7). doi: 10.3390/rs11070828.

Ardekani, M., Neyt, X., Nottebaere, M., Jacques, D., Lambot, S., 2014. GPR data inversion for vegetation layer. *Proceedings of the 15th International Conference on Ground Penetrating Radar*, Institute of Electrical and Electronics Engineers Inc., pp. 170–175. doi: 10.1109/ICGPR.2014.6970408.

Barton, C.V.M., Montagu, K.D., 2004. Detection of tree roots and determination of root diameters by ground penetrating radar under optimal conditions. *Tree Physiology*, 24(12), pp. 1323–1331. doi: 10.1093/treephys/24.12.1323.

Beaulne, J., Garneau, M., Magnan, G., Boucher, É., 2021. Peat deposits store more carbon than trees in forested peatlands of the boreal biome. *Scientific Reports*, 11(1). doi: 10.1038/s41598-021-82004-x.

Borchers, J. G., Perry, D. A., 1992. The influence of soil texture and aggregation on carbon and nitrogen dynamics in southwest Oregon forests and clearcuts. *Canadian Journal of Forest Research*, 22. doi: 10.1139/X92-039.

Bowering, K. L., Edwards, K., Prestegaard, K., Zhu, X., Ziegler, S., 2020. Dissolved organic carbon mobilized from organic horizons of mature and harvested black spruce plots in a mesic boreal region. *Biogeosciences,* 17(3), pp. 581–595. doi: 10.5194/bg-17-581-2020.

Borchers, J. G., Perry, D. A., 1991. The influence of soil texture and aggregation on carbon and nitrogen dynamics in southwest Oregon forests and clearcuts. *Canadian Journal of Forest Research*, 22.

Butnor, J. R., Doolittle, J. A., Johnsen, K. H., Samuelson, L., Stokes, T., Kress, L., 2003. Utility of ground-penetrating radar as a root biomass survey tool in forest systems. *Soil Science Society of America Journal*, 67(5), pp. 1607–1615. doi: 10.2136/sssaj2003.1607.

Collins, M. E., Doolittle, J. A., 1987. Using ground-penetrating radar to study soil microvariability. *Soil Science Society of America Journal*, 51(51), pp. 491–493.

Davis, J. L., Annan, A.P., 1989. Ground-penetrating radar for high resolution mapping of soil and rock stratigraphy. *Geophysical Prospecting*, 37(5), pp. 531–551. doi: 10.1111/j.1365-2478.1989.tb02221.x.

Dincă, L. C., Dincă, M., Vasile, D., Spârchez, G., Holonec, L., 2015. Calculating organic carbon stock from forest soils. *Notulae Botanicae Horti Agrobotanici Cluj-Napoca*, 43(2), pp. 568–575. doi: 10.15835/nbha43210041.

Doolittle, J. A., Jenkinson, B., Hopkins, D., Ulmer, M., Tuttle, W., 2006. Hydropedological investigations with ground-penetrating radar (GPR): Estimating water-table depths and local ground-water flow pattern in areas of coarse-textured soils. *Geoderma*, pp. 317–329. doi: 10.1016/j.geoderma.2005.03.027.

Doolittle, J. A., Collins, M. E., 1995. Use of soil information to determine application of ground penetrating radar. *Journal of Applied Geophysics*, 33(1–3), pp. 101–108. doi: 10.1016/0926-9851(95)90033-0.

Gerber, R., Salat, C., Junge, A., Felix-Henningsen, P., 2007. GPR-based detection of Pleistocene periglacial slope deposits at a shallow-depth test site. *Geoderma*, 139(3–4), pp. 346–356. doi: 10.1016/j.geoderma.2007.02.014.

Gerber, R., Felix-Henningsen, P., Behrens, T., Scholten, T., 2010. Applicability of ground-penetrating radar as a tool for nondestructive soil-depth mapping on 56leistocene periglacial slope deposits. *Journal of Plant Nutrition and Soil Science*, 173(2), pp. 173–184. doi: 10.1002/jpln.200800163.

von Haden, A.C., Yang, W.H., DeLucia, E.H., 2020. Soils' dirty little secret: Depth-based comparisons can be inadequate for quantifying changes in soil organic carbon and other mineral soil properties. *Global Change Biology*, 26(7), pp. 3759–3770. doi: 10.1111/gcb.15124.

Han, X., Liu, J., Zhang, Z., 2016. Identifying soil structure along headwater hillslopes using ground penetrating radar based technique. *Journal of Mountain Science*, 13(3), pp. 405–415. doi: 10.1007/s11629-014-3279-7.

Hedges, J. I., Stern, J. H., 1984. Carbon and nitrogen determinations of carbonate-containing solids. *Limnology and Oceanography*, 29(3), pp. 657–663. Available at: doi: 10.4319/lo.1984.29.3.0657.

Henry, M. et al., 2015. An overview of existing and promising technologies for national forest monitoring. *Annals of Forest Science*, 72(6), pp. 779–788. doi: 10.1007/s13595-015-0463-z.

Hoffmann, U., Hoffmann, T., Johnson, E., Kuhn, N., 2014. Assessment of variability and uncertainty of soil organic carbon in a mountainous boreal forest (Canadian Rocky Mountains, Alberta). *Catena*, 113, pp. 107–121. doi: 10.1016/j.catena.2013.09.009.

Holz, M., Augustin, J., 2021. Erosion effects on soil carbon and nitrogen dynamics on cultivated slopes: A meta-analysis. *Geoderma*, 397. Available at: doi: 10.1016/j.geoderma.2021.115045.

Hu, Y., Berhe, A., Fogal, M., Heckrath, G., Kuhn, N., 2016. Transport-distance specific SOC distribution: Does it skew erosion induced C fluxes. *Biogeochemistry*, 128(3), pp. 339–351. doi: 10.1007/s10533-016-0211-y.

Hubbard, S.S. et al., 2013. Quantifying and relating land-surface and subsurface variability in permafrost environments using LiDAR and surface geophysical datasets. *Hydrogeology Journal*, 21(1), pp. 149–169. doi: 10.1007/s10040-012-0939-y.

Huisman, J. A., Hubbard, S., Redman, J., Annan, A., 2003. Measuring soil water content with ground penetrating radar: A review. *Soil Science Society of America*, 2, pp. 476–491.

Illawathure, C., Parkin, G., Lambot, S., Galagedara, L., 2019. Evaluating soil moisture estimation from ground-penetrating radar hyperbola fitting with respect to a systematic time domain reflectometry data collection in a boreal podzolic agricultural field. *Hydrological Processes*, October 2019, 1-18.

Illawathure, C., Cheema, M., Kavanagh, V., Galagedara, L., 2020. Distinguishing capillary fringe reflection in a GPR profile for precise water table depth estimation in a boreal podzolic soil field. *Water* (Switzerland), 12(6). doi: 10.3390/W12061670.

Jandl, R. et al., 2014. Current status, uncertainty and future needs in soil organic carbon monitoring. *Science of the Total Environment*, 468–469, pp. 376–383. doi: 10.1016/j.scitotenv.2013.08.026.

Jobbagy, E. G., & Jackson, R. B., 2000. The vertical distribution of soil organic carbon and its relation to climate and vegetation. *Ecological Applications*, 10(2), p. 423. doi: 10.2307/2641104.

Jol, H. M., & Bristow, C. S., 2003. GPR in sediments: advice on data collection, basic processing and interpretation, a good practice guide. *Geological Society, London, Special Publications*, 211(1), pp. 9–27. doi: 10.1144/GSL.SP.2001.211.01.02.

Klotzsche, A., Jonard, F., Looms, M., van der Kruk, J., Huisman, J., 2018. Measuring soil water content with ground penetrating radar: A decade of progress. *Vadose Zone Journal*, 17(1). doi: 10.2136/vzj2018.03.0052.

Koch, J. C., Runkel, R., Striegl, R., McKnight, D., 2013. Hydrologic controls on the transport and cycling of carbon and nitrogen in a boreal catchment underlain by continuous permafrost. *Journal of Geophysical Research: Biogeosciences*, 118(2), pp. 698–712. doi: 10.1002/jgrg.20058.

Laamrani, A., Valeria, O., Cheng, L., Bergeron, Y., Camerlynck, C., 2013. The use of ground penetrating radar for remote sensing the organic layer – mineral soil interface in paludified boreal forests. *Canadian Journal of Remote Sensing*, 39(1), pp. 74–88. doi: 10.5589/m13-009.

Liu, X., Dong, X., Xue, Q., Leskover, D., Jifon, J., Butnor, J., Marek, T., 2018. Ground penetrating radar (GPR) detects fine roots of agricultural crops in the field. *Plant and Soil*, 423(1–2), pp. 517–531. doi: 10.1007/s11104-017-3531-3.

Luo, Y., Al-Dossary, S., Marhoon, M., Alfaraj, M., 2003. Generalized Hilbert transform and its applications in geophysics. *Leading Edge* (Tulsa, OK), 22(3), pp. 198–202. doi: 10.1190/1.1564522.

Molon, M., Boyce, J. I., Arain, M. A., 2017. Quantitative, nondestructive estimates of coarse root biomass in a temperate pine forest using 3-D ground-penetrating radar (GPR). *Journal of Geophysical Research: Biogeosciences*, 122(1), pp. 80–102. doi: 10.1002/2016JG003518.

Moroni, M.T., Shaw, C. H., Otahal, P., 2010. Forest carbon stocks in newfoundland boreal forests of harvest and natural disturbance origin I: Field study. *Canadian Journal of Forest Research*, 40(11), pp. 2135–2145. doi: 10.1139/X10-154.

Næsset, E., Gobakken, T., 2008. Estimation of above- and below-ground biomass across regions of the boreal forest zone using airborne laser. *Remote Sensing of Environment*, 112(6), pp. 3079–3090. doi: 10.1016/j.rse.2008.03.004.

Pacific, V. J., McGlynn, B., Riveros-Iregui, D., Welsch, D., Epstien, H., 2011. Landscape structure, groundwater dynamics, and soil water content influence soil respiration across riparian-hillslope transitions in the Tenderfoot Creek Experimental Forest, Montana. *Hydrological Processes*, 25(5), pp. 811–827. doi: 10.1002/hyp.7870.

Parsekian, A. D., Slater, L., Ntarlagiannis, D., Nolan, J., Sebesteyen, S., Kolka, R., Hanson, P., 2012. Uncertainty in peat volume and soil carbon estimated using ground-penetrating radar and probing. *Soil Science Society of America Journal*, 76(5), pp. 1911–1918. doi: 10.2136/sssaj2012.0040.

Patton, N. R., Lohse, K., Godsey, S., 2018. Predicting soil thickness on soil mantled hillslopes. *Nature Communications*, 9(1). doi: 10.1038/s41467-018-05743-y.

Pelletier, R. E., Davis, J. L., Rossiter, J. R., 1991. Peat analyses in the Hudson Bay lowlands using ground penetrating radar. *[Proceedings] IGARSS'91 Remote Sensing: Global Monitoring for Earth Management*, IEEE, pp. 2141–2144. doi: 10.1109/IGARSS.1991.575463.

Péiré, C., Ouimet, R., 2008. Organic carbon, organic matter and bulk density relationships in boreal forest soils. *Canadian Journal of Soil Science*, 88(3): 315-325. doi: 10.4141/CJSS6008.

Poeplau, C., Vos, C., Don, A., 2017. Soil organic carbon stocks are systematically overestimated by misuse of the parameters bulk density and rock fragment content. *Soil,* 3, 61-66. doi: 10.5194/soil-3-61-2017.

Proulx-McInnis, S., St-Hilaire, A., Rosseau, A., Jutras, S., 2013. A review of ground-penetrating radar studies related to peatland stratigraphy with a case study on the determination of peat thickness in a northern boreal fen in Quebec, Canada. *Progress in Physical Geography*, SAGE Publications Ltd, pp. 767–786. doi: 10.1177/0309133313501106.

Raz-Yaseef, N., Koteen, L., Baldocchi, D. D., 2013. Coarse root distribution of a semi-arid oak savanna estimated with ground penetrating radar. *Journal of Geophysical Research: Biogeosciences*, 118(1), pp. 135–147. doi: 10.1029/2012JG002160.

Rosenbloom, N. A., Doney, S. C., Schimel, D. S., 2001. Geomorphic evolution of soil texture and organic matter in eroding landscapes. *Global Biogeochemical Cycles*, 15(2), pp. 365–381. doi: 10.1029/1999GB001251.

Scharlemann, J. P. W., Tanner, E. V. J., Hiederer, R., Kapos, V., 2014. Global soil carbon: Understanding and managing the largest terrestrial carbon pool. *Carbon Management*, pp. 81–91. doi: 10.4155/cmt.13.77.

Slessarev, E. W., Chadwick, O, Sokol, N., Nuccio, E., Pett-Ridge, J., 2022. Rock weathering controls the potential for soil carbon storage at a continental scale. *Biogeochemistry*, 157(1). doi: 10.1007/s10533-021-00859-8.

Sothe, C., Gonsamo, A., Arabian, J., Kurz, W., Finkelstein, S., Snider, J., 2022. Large soil carbon storage in terrestrial ecosystems of Canada. *Global Biogeochemical Cycles*, 36(2). doi: 10.1029/2021GB007213.

Sucre, E. B., Tuttle, J. W., Fox, T. R., 2011. The use of ground-penetrating radar to accurately estimate soil depth in rocky forest soils. *Forest Science*, 57(1), pp. 59–66. doi: 10.1093/forestscience/57.1.59.

Sullivan, P. L., Billings, S. A., Hirmas, D., Li, L., Zhang, X., Ziegler, S., Murenbeeld, K., Ajami, H., Guthrie, A., Singha, K., Giménez, D., Duro, A., Moreno, V., Flores, A., Cueva, A., Koop, Aronson, E. L., Barnard, H. R., Banwart, S. A., Keen, R. M., Nemes, A., Nikolaidis, N. P., Nippert, J. B., Richter, D., Robinson, D. A., Sadayappan, K., de Souza, L. F. T., Unruh, H. W., 2022. Embracing the dynamic nature of soil structure: a paradigm illuminating the role of life in critical zones of the Anthropocene. *Earth-Science Reviews*, 10387. doi: 10.1016/j.earscirev.2021.103873

Vadeboncoeur, M. A., Hamburg, S., Blum, J., 2012. The quantitative soil pit method for measuring belowground carbon and nitrogen stocks. *Soil Science Society of America Journal*, 76(6), pp. 2241–2255. doi: 10.2136/sssaj2012.0111.

Warner, B. G., Nobes, D .C., Theimer, B. D., 1990. An application of ground penetrating radar to peat stratigraphy of Ellice Swamp, southwestern Ontario, *Can. J. Earth Sci*.

Wei, S., Zhang, X., McLaughlin, N., Chen, X., Jia, S., Liang, A., 2017. Impact of soil water erosion processes on catchment export of soil aggregates and associated SOC. *Geoderma*, 294, pp. 63–69. doi: 10.1016/j.geoderma.2017.01.021.

Wijewardana, Y. G. N. S., Galagedara, L. W., 2010. Estimation of spatio-temporal variability of soil water content in agricultural fields with ground penetrating radar. *Journal of Hydrology*, 391(1–2), pp. 24–33. doi: 10.1016/j.jhydrol.2010.06.036.

Wijewardana, Y. G. N. S., Shilpadi, A., Mowjood, M., Kawamoto, K., Galagedara, L., 2017. Ground-penetrating radar (GPR) responses for sub-surface salt contamination and solid waste: modeling and controlled lysimeter studies. *Environmental Monitoring and Assessment,* 189(2). doi: 10.1007/s10661-017-5770-4.

Winkelbauer, J., Völkel, J., Leopold, M., Bernt, N., 2011. Methods of surveying the thickness of humous horizons using ground penetrating radar (GPR): An example from the Garmisch-Partenkirchen area of the Northern Alps. *European Journal of Forest Research*, 130(5), pp. 799–812. doi: 10.1007/s10342-010-0472-2.

Worsfold, R. D., Parashar, S. K., Perrott, T., 1986. Depth profiling of peat deposits with impulse radar, *Can. Geotech. J.*

Xu, L., He, N., Yu, G., 2016. Methods of evaluating soil bulk density: impact on estimating large scale soil organic carbon storage. *Cantena,* 144, pp. 94-101

Yoo, K., Amundson, R., Heimsath, A., Dietrich, W., 2006. Spatial patterns of soil organic carbon on hillslopes: Integrating geomorphic processes and the biological C cycle. *Geoderma*, 130(1–2), pp. 47–65. doi: 10.1016/j.geoderma.2005.01.008.

Zajícová, K., Chuman, T., 2019. Application of ground penetrating radar methods in soil studies: A review. *Geoderma*, pp. 116–129. doi: 10.1016/j.geoderma.2019.02.024.

Co-author statement

Lakshman Galagedara, Susan Ziegler, and Zachary Gates conceptualized the review topic. Zachary Gates investigated the concept and developed a methodology with direct input from Susan Ziegler. Zachary Gates conducted the literature review and writing for the original review draft with direct input from Susan Ziegler, and with verification, editing and revision completed by all three authors.

Appendix

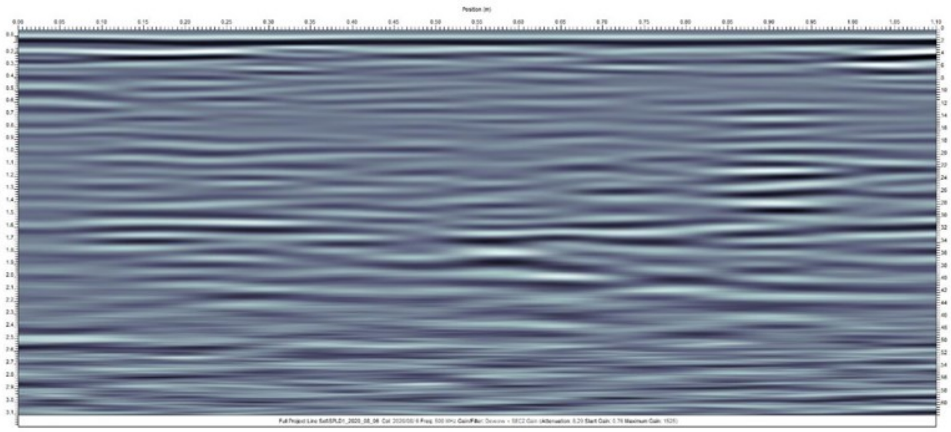

a

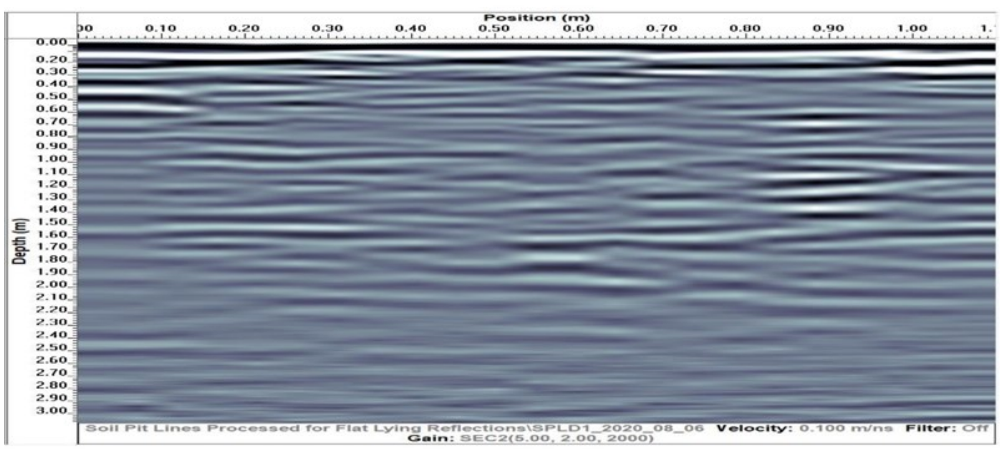

b

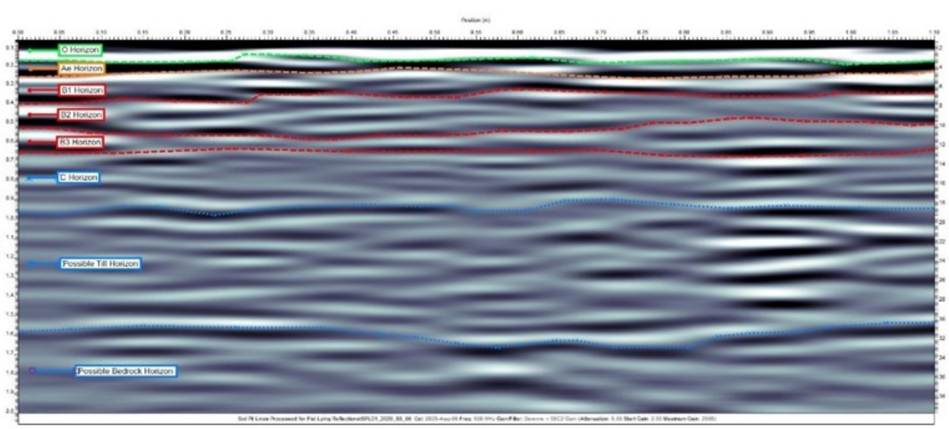

c

Figure 2.A1. Radargrams collected along a 1 m survey line within a boreal forest site 0.5 m upslope and parallel to soil pit D-1 in the Pynn's Brook Experimental Watershed Area, Newfoundland, Canada, using a 500 MHz Sensors & Software PulseEkko GPR system. The radargram data collected is presented in its unprocessed form (a) and after it has undergone processing for soil horizon thickness measurements as outlined Section 2.4.2 (b). Interpretations made for soil horizon boundary positions (c) based on the processed radargram data were used for the evaluation of GPR estimates for forest soil thickness in this study.

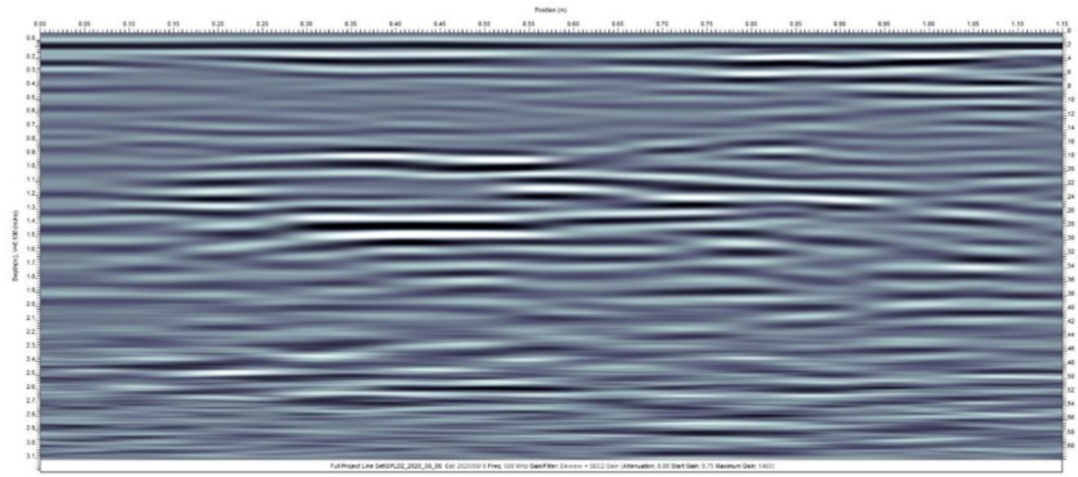

a

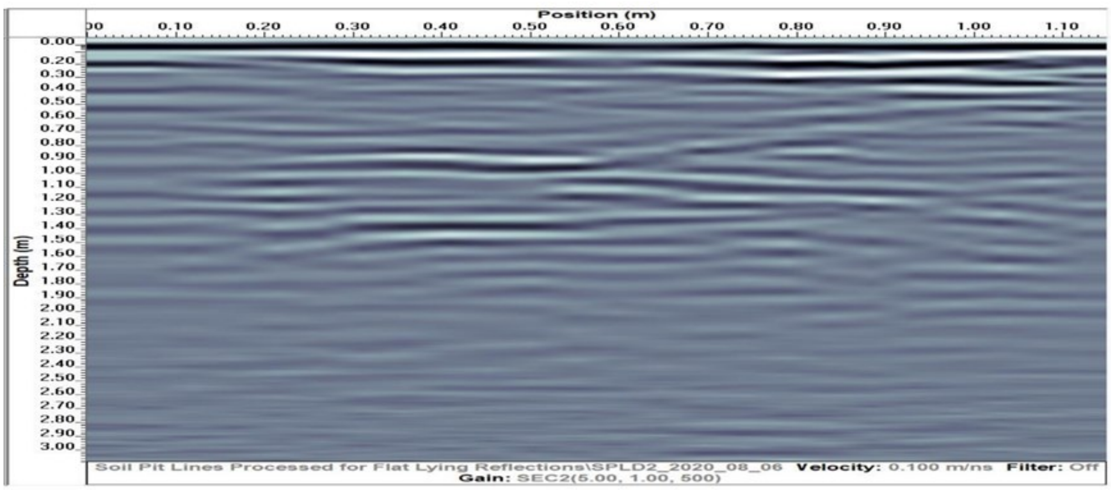

Position (m)
Depth (m)
Soil Pit Lines Processed for Flat Lying Reflections\SPLD2_2020_08_06 Velocity: 0.100 m/ns Filter: Off
Gain: SEC2(5.00, 1.00, 500)

b

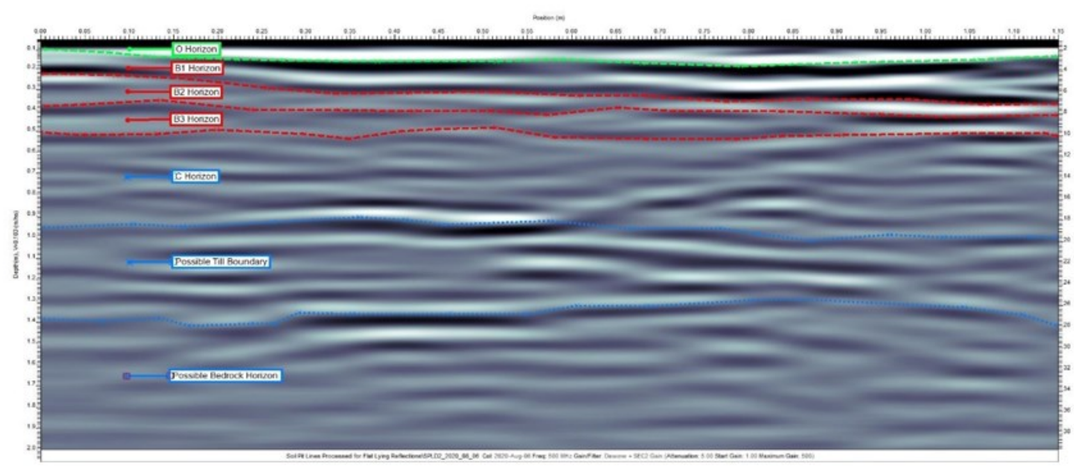

O Horizon
B1 Horizon
B2 Horizon
B3 Horizon
C Horizon
Possible Till Boundary
Possible Bedrock Horizon

c

Figure 2.A2. Radargrams collected along a 1 m survey line within a boreal forest site 0.5 m upslope and parallel to soil pit D-2 in the Pynn's Brook Experimental Watershed Area, Newfoundland, Canada, using a 500 MHz Sensors & Software PulseEkko GPR system. The radargram data collected is presented in its unprocessed form (a) and after it has undergone processing for soil horizon thickness measurements as outlined Section 2.4.2 (b). Interpretations made for soil horizon boundary positions (c) based on the processed radargram data were used for the evaluation of GPR estimates for forest soil thickness in this study.

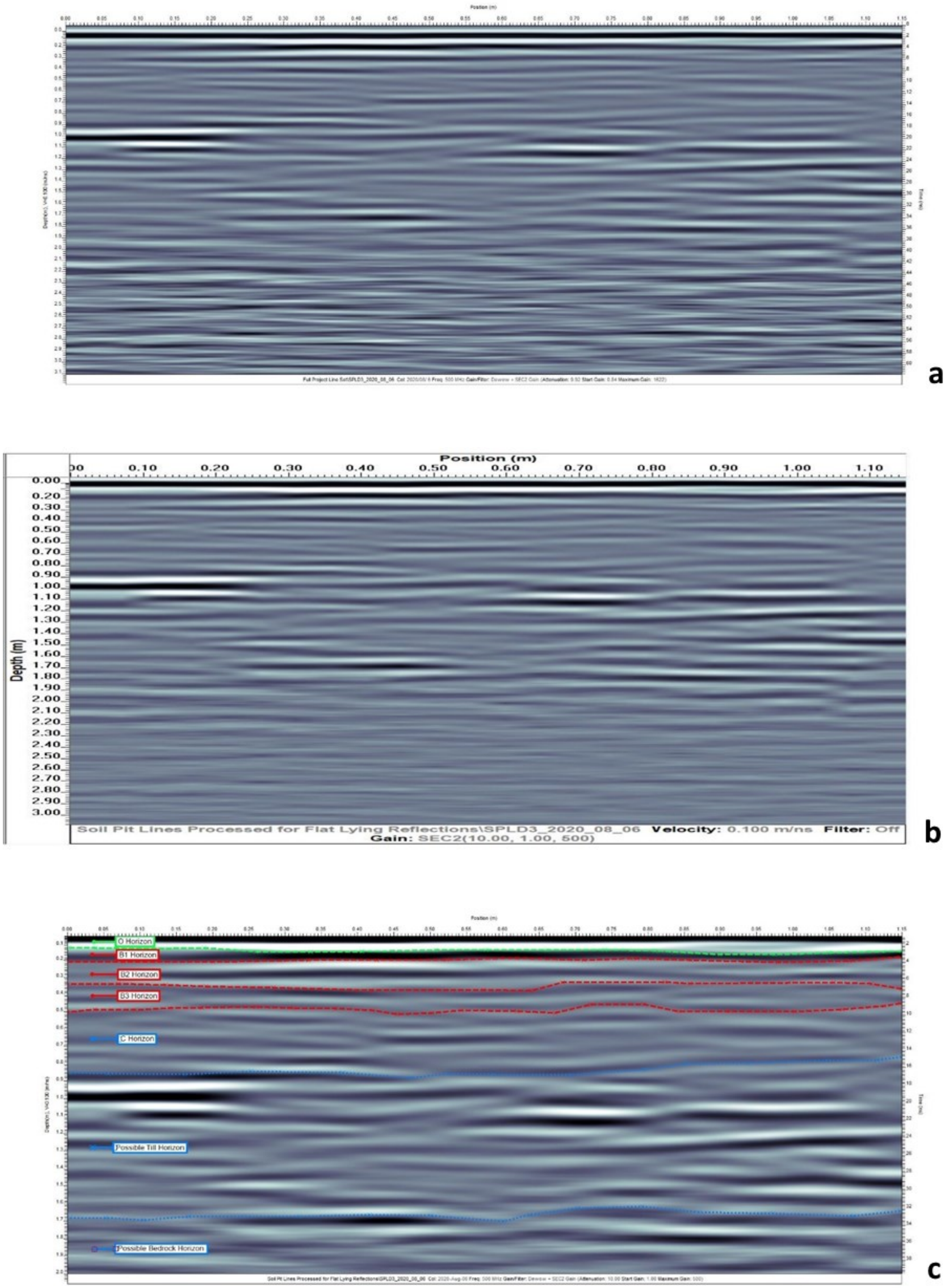
a
Position (m)
Depth (m)
Soil Pit Lines Processed for Flat Lying Reflections\SPLD3_2020_08_06 Velocity: 0.100 m/ns Filter: Off
Gain: SEC2(10.00, 1.00, 500)
b
O Horizon
B1 Horizon
B2 Horizon
B3 Horizon
C Horizon
Possible Till Horizon
Possible Bedrock Horizon
c

Figure 2.A3. Radargrams collected along a 1 m survey line within a boreal forest site 0.5 m upslope and parallel to soil pit D-3 in the Pynn's Brook Experimental Watershed Area, Newfoundland, Canada, using a 500 MHz Sensors & Software PulseEkko GPR system. The radargram data collected is presented in its unprocessed form (a) and after it has undergone processing for soil horizon thickness measurements as outlined Section 2.4.2 (b). Interpretations made for soil horizon boundary positions (c) based on the processed radargram data were used for the evaluation of GPR estimates for forest soil thickness in this study.

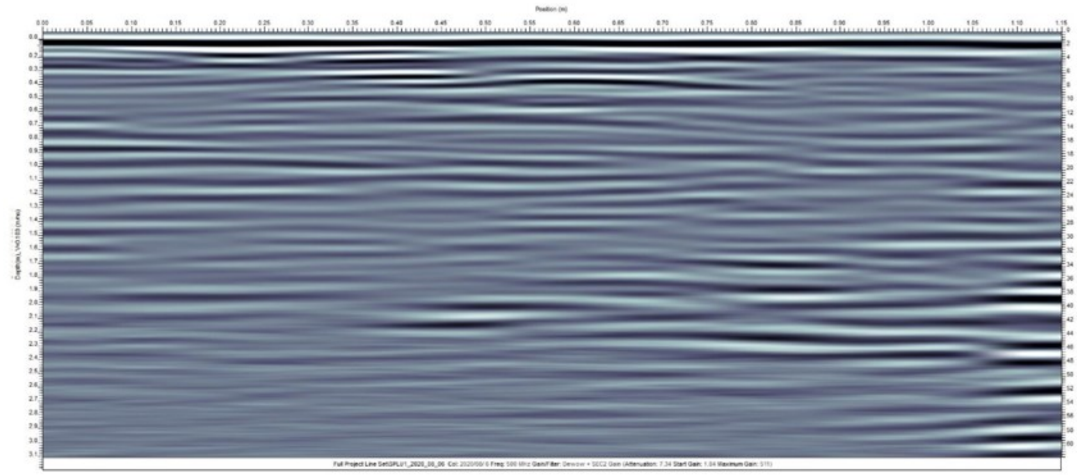

a

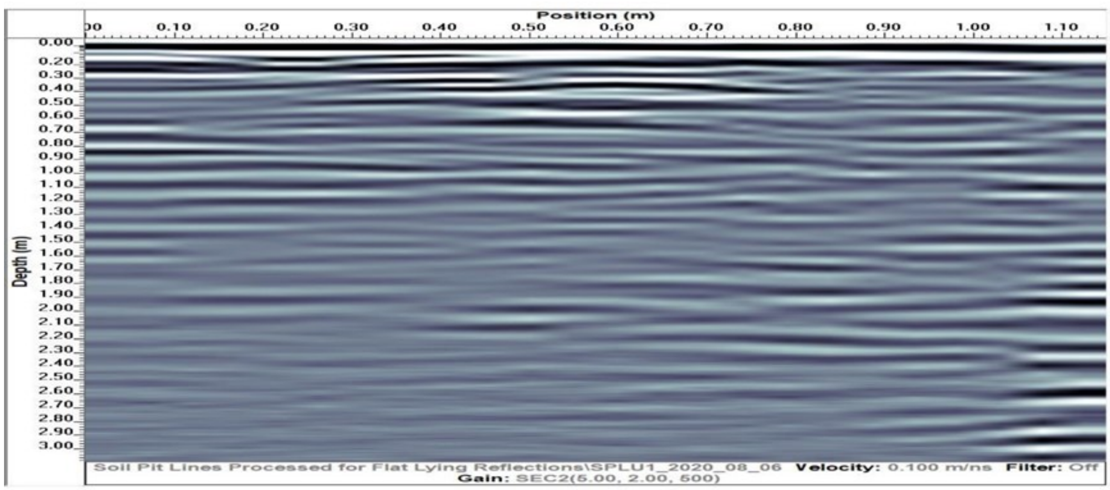
Position (m)
Depth (m)
Soil Pit Lines Processed for Flat Lying Reflections\SPLU1_2020_08_06 Velocity: 0.100 m/ns Filter: Off
Gain: SEC2(5.00, 2.00, 500)

b

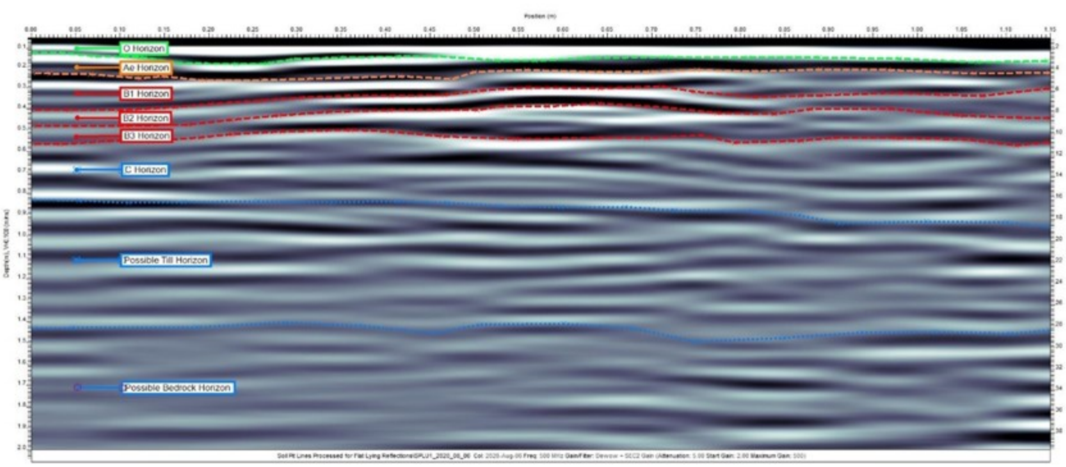
O Horizon
Ae Horizon
B1 Horizon
B2 Horizon
B3 Horizon
C Horizon
Possible Till Horizon
Possible Bedrock Horizon

c

Figure 2.A4. Radargrams collected along a 1 m survey line within a boreal forest site 0.5 m upslope and parallel to soil pit U-1 in the Pynn's Brook Experimental Watershed Area, Newfoundland, Canada, using a 500 MHz Sensors & Software PulseEkko GPR system. The radargram data collected is presented in its unprocessed form (a) and after it has undergone processing for soil horizon thickness measurements as outlined Section 2.4.2 (b). Interpretations made for soil horizon boundary positions (c) based on the processed radargram data were used for the evaluation of GPR estimates for forest soil thickness in this study.

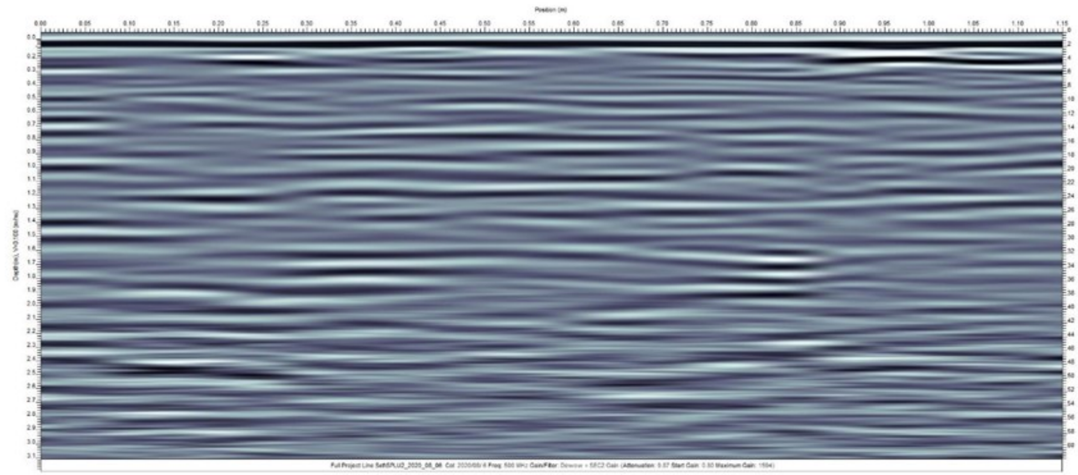

a

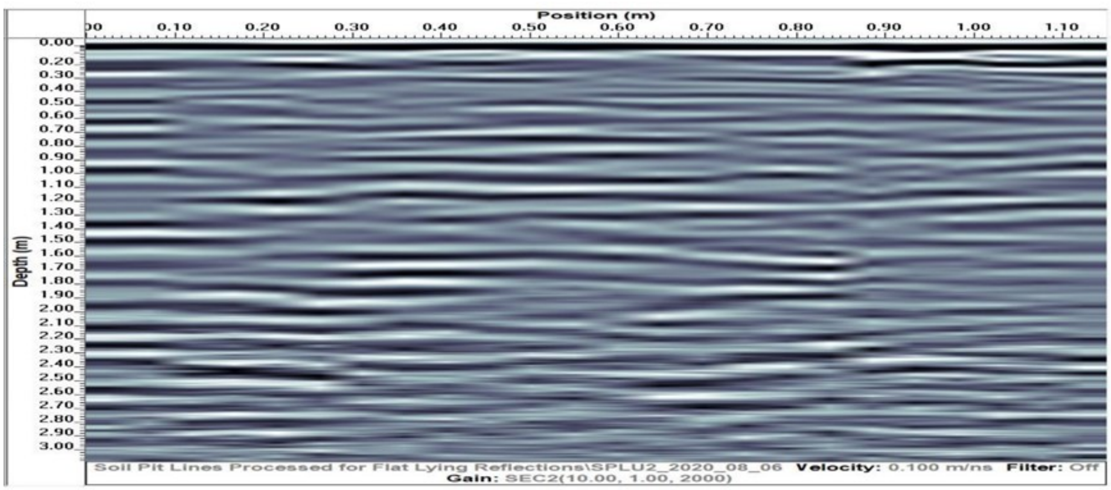

Position (m)
Depth (m)
Soil Pit Lines Processed for Flat Lying Reflections\SPLU2_2020_08_06 Velocity: 0.100 m/ns Filter: Off
Gain: SEC2(10.00, 1.00, 2000)

b

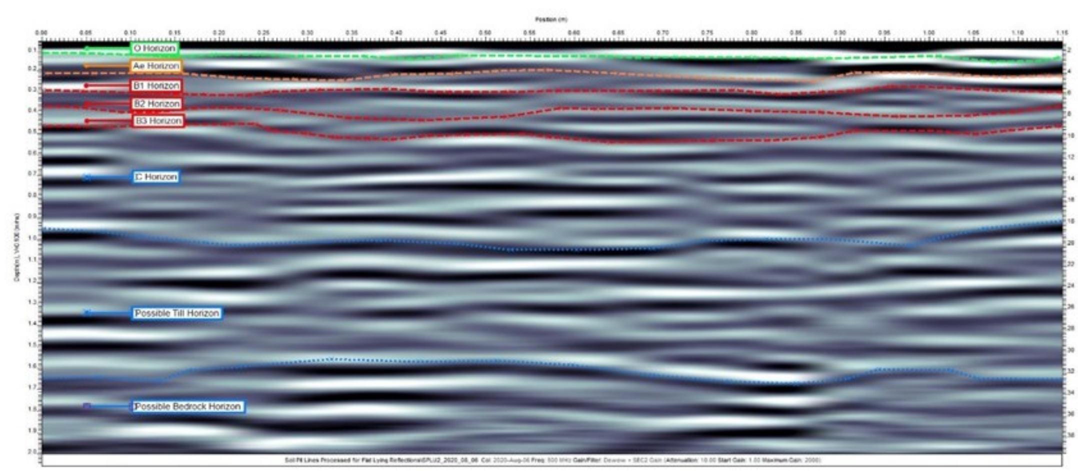

O Horizon
Ae Horizon
B1 Horizon
B2 Horizon
B3 Horizon
C Horizon
Possible Till Horizon
Possible Bedrock Horizon

c

Figure 2.A5. Radargrams collected along a 1 m survey line within a boreal forest site 0.5 m upslope and parallel to soil pit U-2 in the Pynn's Brook Experimental Watershed Area, Newfoundland, Canada, using a 500 MHz Sensors & Software PulseEkko GPR system. The radargram data collected is presented in its unprocessed form (a) and after it has undergone processing for soil horizon thickness measurements as outlined Section 2.4.2 (b). Interpretations made for soil horizon boundary positions (c) based on the processed radargram data were used for the evaluation of GPR estimates for forest soil thickness in this study.

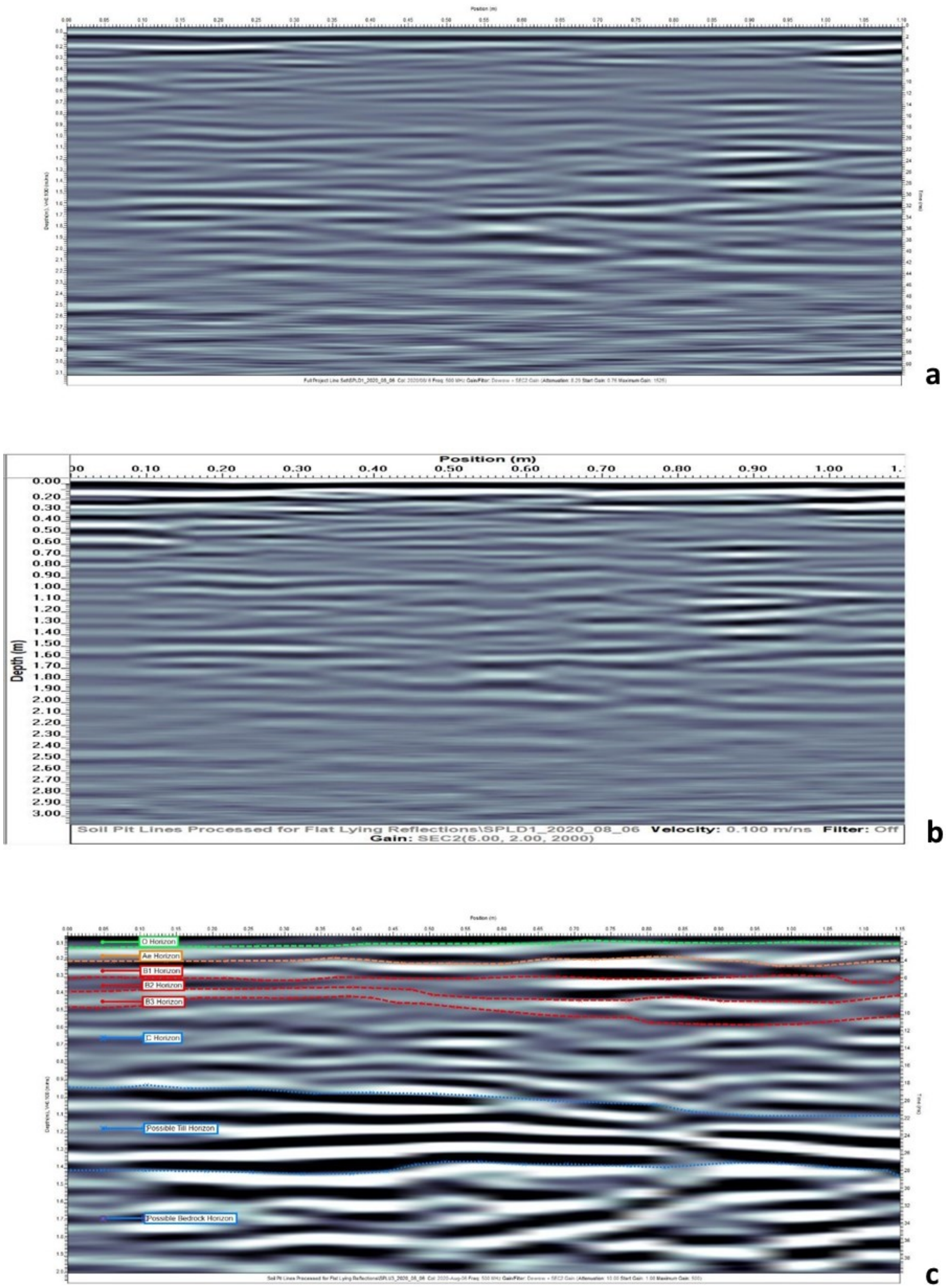

a
Position (m)
Depth (m)
0.00
0.20
0.30
0.40
0.50
0.60
0.70
0.80
0.90
1.00
1.10
1.20
1.30
1.40
1.50
1.60
1.70
1.80
1.90
2.00
2.10
2.20
2.30
2.40
2.50
2.60
2.70
2.80
2.90
3.00
0.10 0.20 0.30 0.40 0.50 0.60 0.70 0.80 0.90 1.00
Soil Pit Lines Processed for Flat Lying Reflections\SPLD1_2020_08_06 Velocity: 0.100 m/ns Filter: Off
Gain: SEC2(5.00, 2.00, 2000)
b
O Horizon
Ae Horizon
B1 Horizon
B2 Horizon
B3 Horizon
C Horizon
Possible Till Horizon
Possible Bedrock Horizon
c

Figure 2.A6. Radargrams collected along a 1 m survey line within a boreal forest site 0.5 m upslope and parallel to soil pit U-3 in the Pynn's Brook Experimental Watershed Area, Newfoundland, Canada, using a 500 MHz Sensors & Software PulseEkko GPR system. The radargram data collected is presented in its unprocessed form (a) and after it has undergone processing for soil horizon thickness measurements as outlined Section 2.4.2 (b). Interpretations made for soil horizon boundary positions (c) based on the processed radargram data were used for the evaluation of GPR estimates for forest soil thickness in this study.

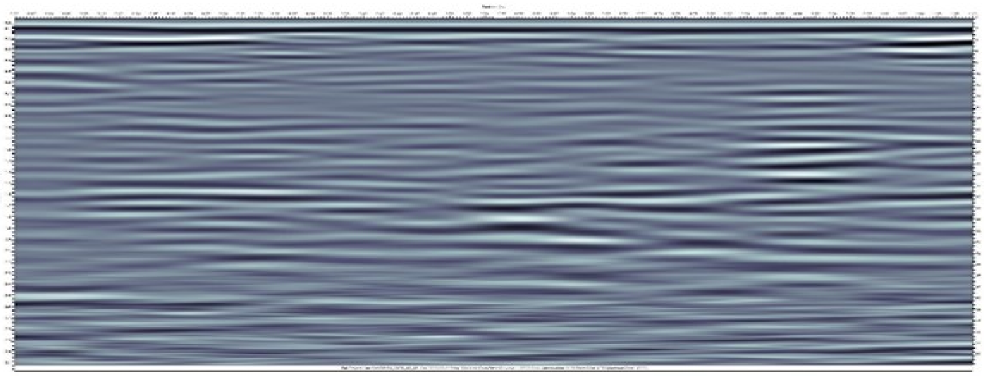
a

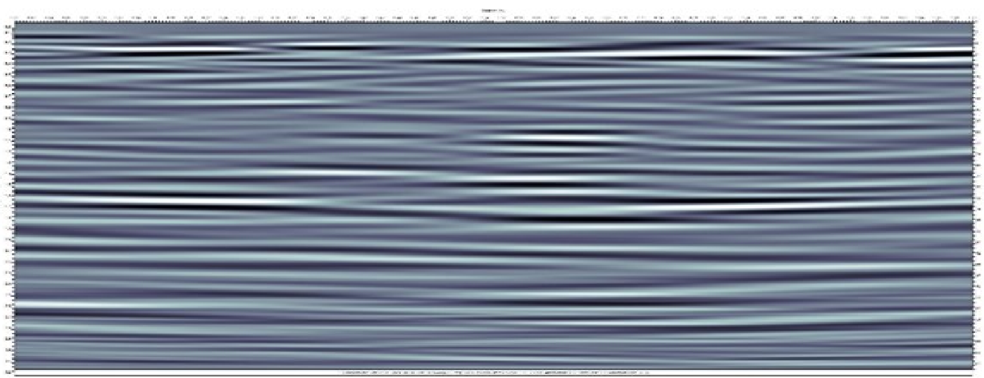
b

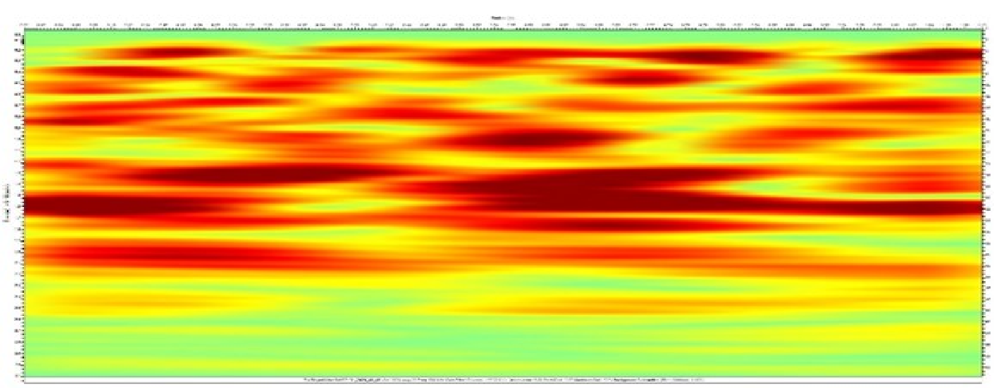
c

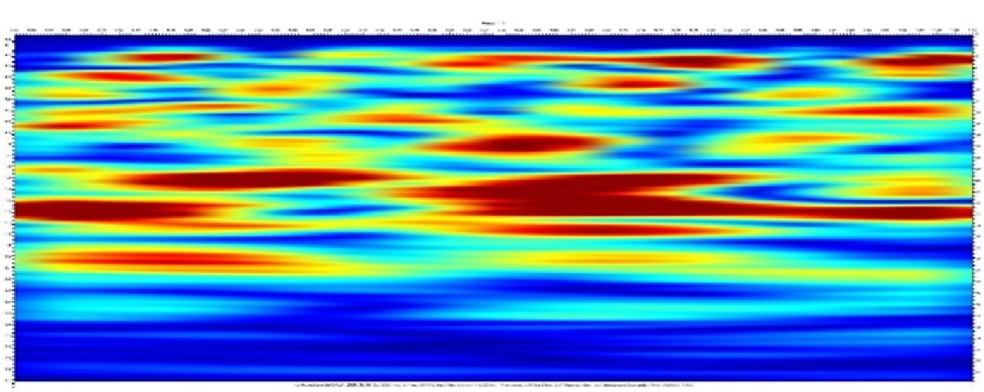
d

Figure 2.A7. Radargrams collected along a 1 m survey line within a boreal forest site 0.5 m upslope and parallel to soil pit D-1 in the Pynn's Brook Experimental Watershed Area, Newfoundland, Canada, using a 500 MHz Sensors & Software PulseEkko GPR system. The radargram data collected is presented in its unprocessed form (a) and after it has undergone processing for soil bulk density measurements as outlined Section 2.4.3 (b). The processed radargram data underwent Hilbert Transformation using EkkoProject 5's Assisted Pick Processing tool. The transformed radargram data is displayed under polarized (c) and nonpolarized (d) scaling and used to assess soil, rock, and root distribution for estimates of forest soil bulk density.

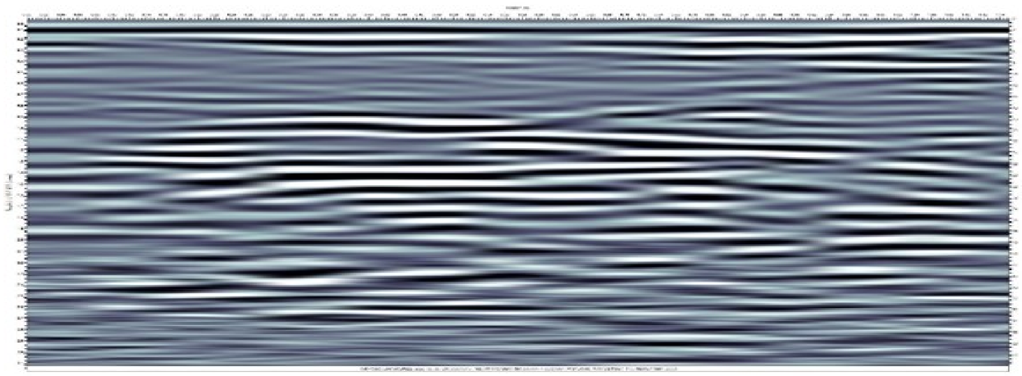

a

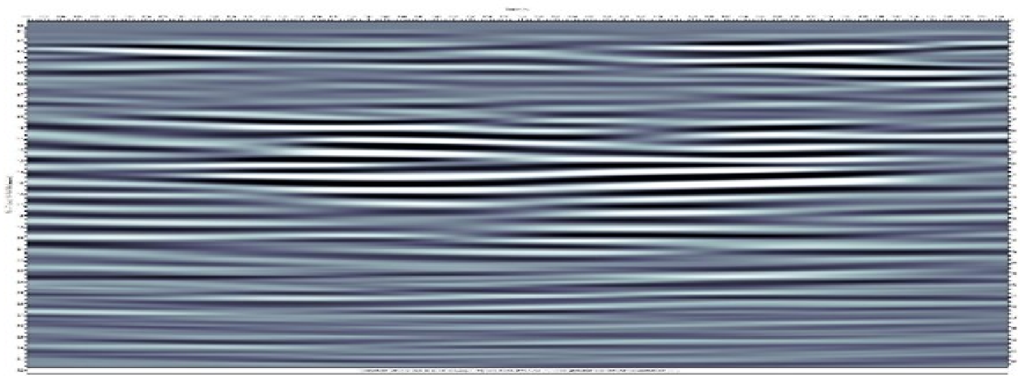

b

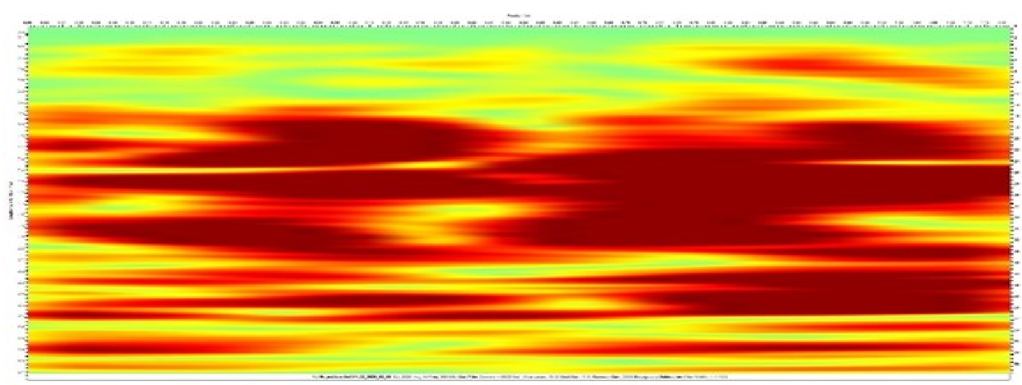

c

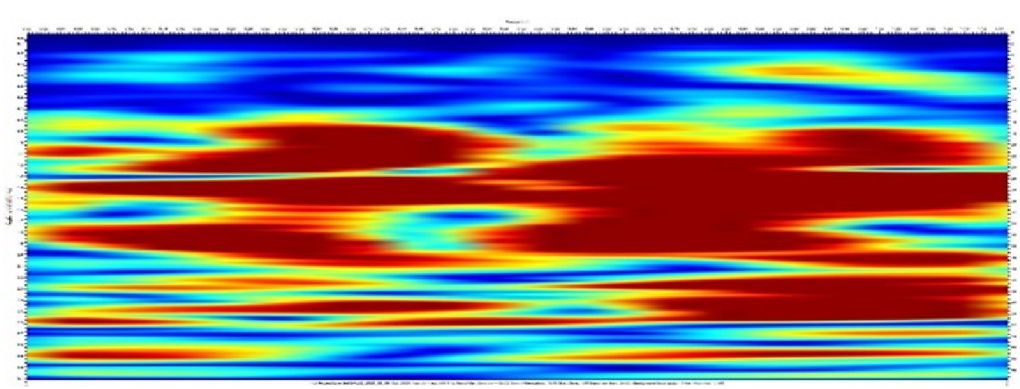

d

Figure 2.A8. Radargrams collected along a 1 m survey line within a boreal forest site 0.5 m upslope and parallel to soil pit D-2 in the Pynn's Brook Experimental Watershed Area, Newfoundland, Canada, using a 500 MHz Sensors & Software PulseEkko GPR system. The radargram data collected is presented in its unprocessed form (a) and after it has undergone processing for soil bulk density measurements as outlined Section 2.4.3 (b). The processed radargram data underwent Hilbert Transformation using EkkoProject 5's Assisted Pick Processing tool. The transformed radargram data is displayed under polarized (c) and nonpolarized (d) scaling and used to assess soil, rock, and root distribution for estimates of forest soil bulk density.

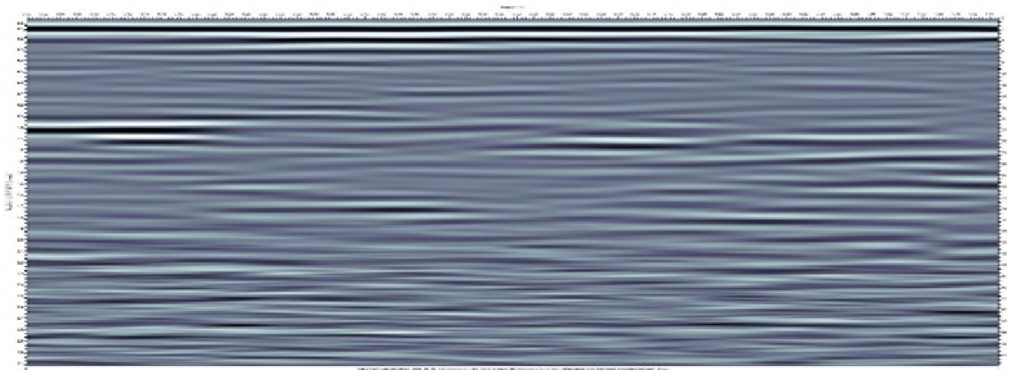

a

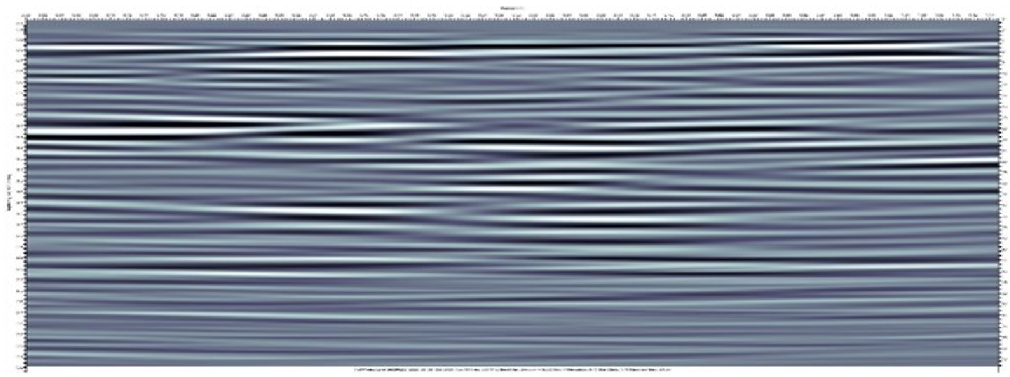

b

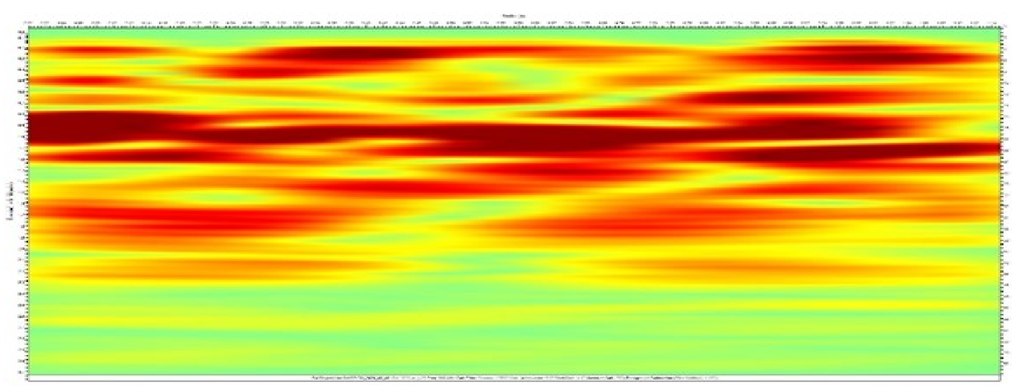

c

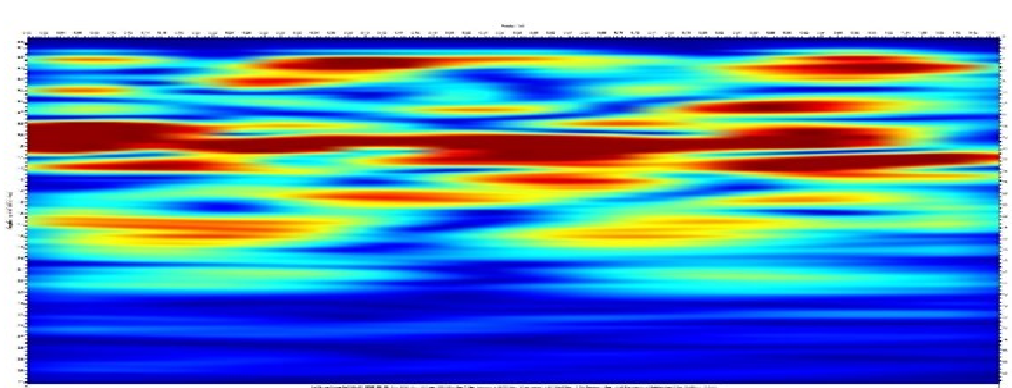

d

Figure 2.A9. Radargrams collected along a 1 m survey line within a boreal forest site 0.5 m upslope and parallel to soil pit D-3 in the Pynn's Brook Experimental Watershed Area, Newfoundland, Canada, using a 500 MHz Sensors & Software PulseEkko GPR system. The radargram data collected is presented in its unprocessed form (a) and after it has undergone processing for soil bulk density measurements as outlined Section 2.4.3 (b). The processed radargram data underwent Hilbert Transformation using EkkoProject 5's Assisted Pick Processing tool. The transformed radargram data is displayed under polarized (c) and nonpolarized (d) scaling and used to assess soil, rock, and root distribution for estimates of forest soil bulk density.

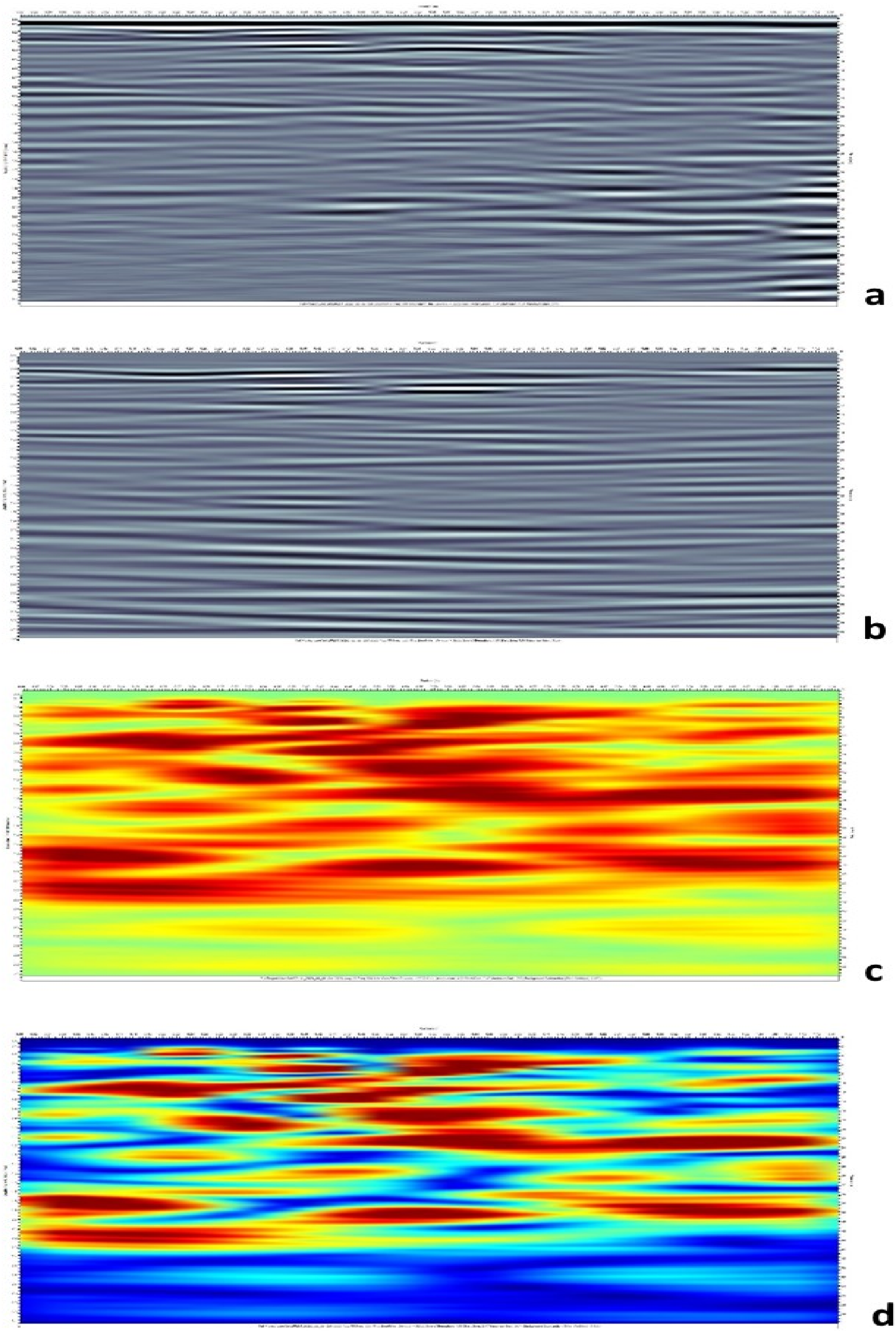
a
b
c
d

Figure 2.A10. Radargrams collected along a 1 m survey line within a boreal forest site 0.5 m upslope and parallel to soil pit U-1 in the Pynn's Brook Experimental Watershed Area, Newfoundland, Canada, using a 500 MHz Sensors & Software PulseEkko GPR system. The radargram data collected is presented in its unprocessed form (top) and after it has undergone processing for soil bulk density measurements as outlined Section 2.4.3 (middle). The processed radargram data underwent Hilbert Transformation using EkkoProject 5's Assisted Pick Processing tool. The transformed radargram data is displayed under polarized (c) and nonpolarized (d) scaling and used to assess soil, rock, and root distribution for estimates of forest soil bulk density.

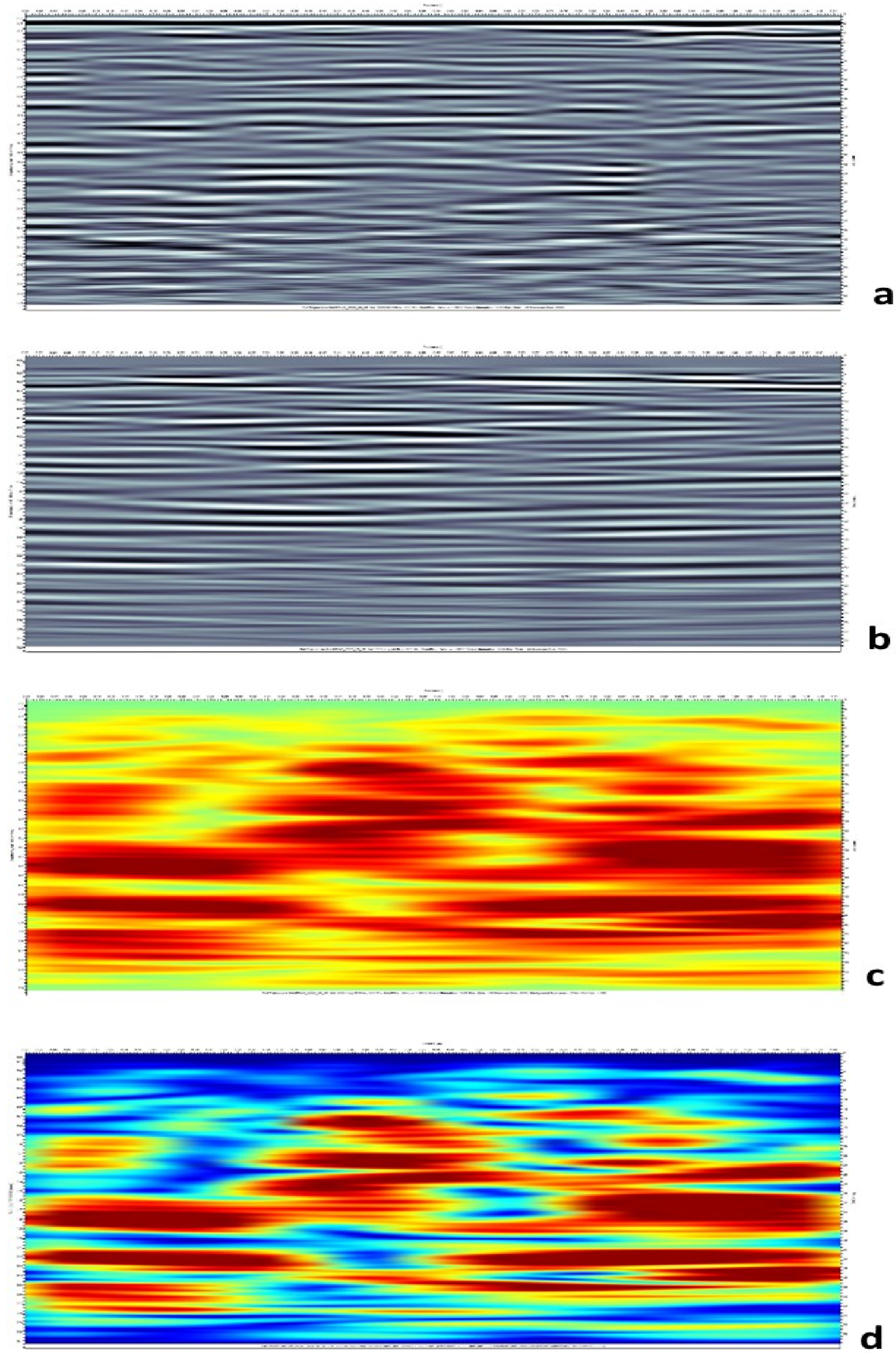
a
b
c
d

Figure 2.A11. Radargrams collected along a 1 m survey line within a boreal forest site 0.5 m upslope and parallel to soil pit U-2 in the Pynn's Brook Experimental Watershed Area, Newfoundland, Canada, using a 500 MHz Sensors & Software PulseEkko GPR system. The radargram data collected is presented in its unprocessed form (top) and after it has undergone processing for soil bulk density measurements as outlined Section 4.3 (middle). The processed radargram data underwent Hilbert Transformation using EkkoProject 5's Assisted Pick Processing tool. The transformed radargram data is displayed under polarized (c) and nonpolarized (d) scaling and used to assess soil, rock, and root distribution for estimates of forest soil bulk density.

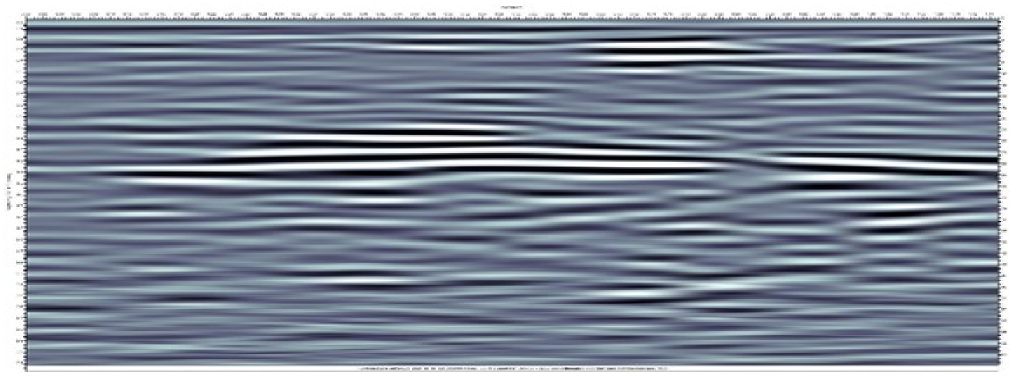
a

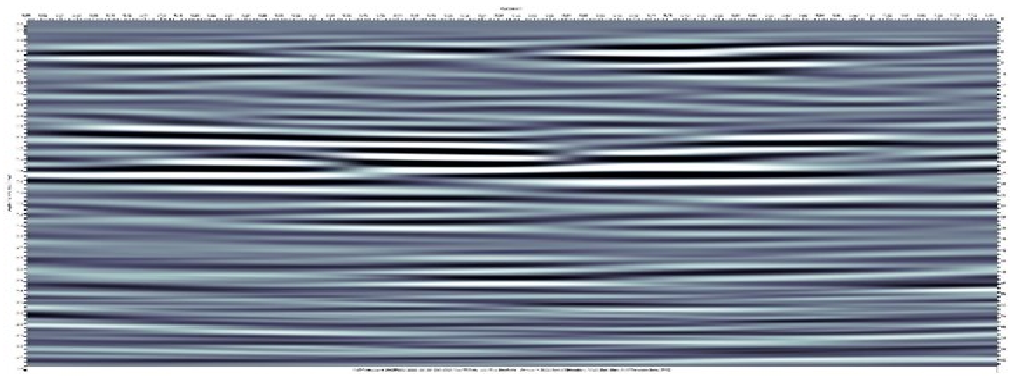
b

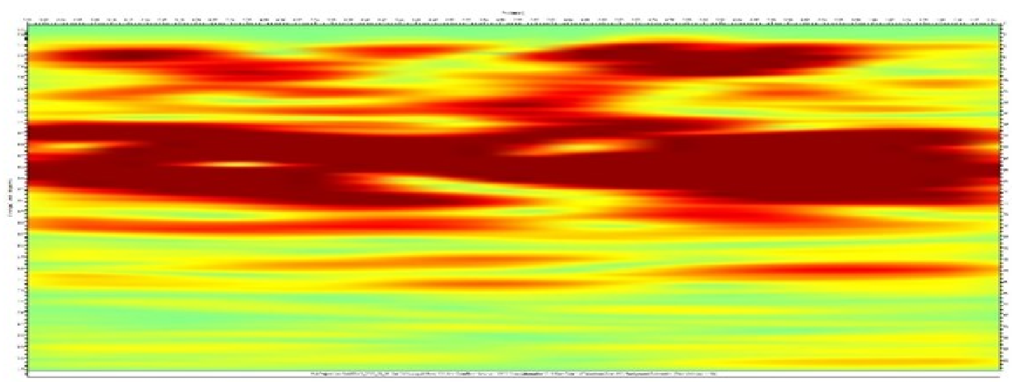
c

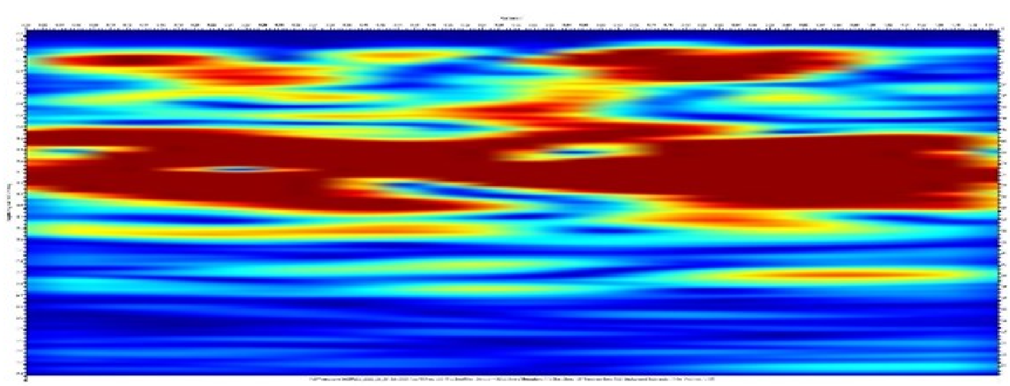
d

Figure 2.A12. Radargrams collected along a 1 m survey line within a boreal forest site 0.5 m upslope and parallel to soil pit U-3 in the Pynn's Brook Experimental Watershed Area, Newfoundland, Canada, using a 500 MHz Sensors & Software PulseEkko GPR system. The radargram data collected is presented in its unprocessed form (top) and after it has undergone processing for soil bulk density measurements as outlined Section 2.4.3 (middle). The processed radargram data underwent Hilbert Transformation using EkkoProject 5's Assisted Pick Processing tool. The transformed radargram data is displayed under polarized (c) and nonpolarized (d) scaling and used to assess soil, rock, and root distribution for estimates of forest soil bulk density.

Chapter 3

Ground penetrating radar estimates of soil horizon thickness and soil bulk density inform boreal forest hillslope carbon distribution

Abstract

Forest ground penetrating radar (GPR) investigations of soil properties relevant to soil carbon (C) distribution remain to be tested across landscapes at a resolution that upscales vertical and horizontal spatial assessment of mineral soils. By conducting physical soil sampling and GPR surveying methods for estimates of mineral soil horizon thickness and soil bulk density across a boreal forest hillslope in Pynn's Brook, Newfoundland, Canada, we demonstrate the use of GPR to inform our understanding on forest hillslope soil horizon thickness, soil bulk density, and C stock distribution. Continuous GPR estimates across the full forest hillslope (80 m) of soil horizon thickness exhibited increases in thickness in downslope, shallow mineral soil horizons (Bf, Bfj) which were not apparent from physical sampling efforts. Furthermore, GPR estimates of soil bulk density were consistently lower, especially downslope, than analogous soil sampling results. Total mineral soil C stock estimates (Bf + Bfj + BC) by GPR averaged for 50 x 50 m grids were 2.51 ± 2.0 Kg C m^{-2} in the upslope and 1.35 ± 0.8 Kg C m^{-2} downslope, not significantly different from physical soil sampling estimates of 2.25 ± 0.7 Kg C m^{-2} and 1.75 ± 2.0 Kg C m^{-2}, respectively. Through this investigation we show that landscape scale, non-destructive, continuous GPR methods for measuring soil horizon thickness and soil bulk density can further expand investigations of soil C stock distribution in boreal forest hillslope sites and identify links in landscape processes to the heterogeneity observed in forest soil and C content.

3.1 Introduction

Many forests, especially boreal strands in high-latitude and post-glaciated areas, exhibit high heterogeneity in soil, rock, and root content. This can lead to high variability in the distribution of soil properties, fluxes, and stocks. Accurate measurements that represent landscape variability of forest soil properties impacting soil C storage and transport are needed to understand the alterations taking place to these forest soils due to climate change. Shifts in total and seasonal precipitation quantity and intensity changes can interact with shallow forest mineral soils at both small and large scales, impacting soil processes through changes to hydrological soil erosion, transport, and weathering rate controls on reactive minerals (Holz & Augustin, 2021; Slessarev et al., 2022). This is needed as soil and ecosystem properties which influence soil C distribution in shallow mineral soil horizons are influenced by erosion, hydrology, and climate (Jobbagy & Jackson, 2000; Yoo et al., 2006; Koch et al., 2013; Hoffmann et al., 2014; Scharlemann et al., 2014; von Haden, Yang, & DeLucia, 2020; Sothe et al., 2022).

In these types of boreal forests, landscape scale representative measurements with depth are especially needed as surface and deeper soil C stocks can often vary by as much as 70% to 80% respectively across such landscapes (Hoffmann et al., 2014; Sothe et al., 2022). There is a lack of deep soil property measurements in forest soil C investigations due to the difficulties in obtaining samples from these rocky, heterogenous sites. This is concerning as in high-latitude forests large stores of soil C have been found at depths that are deeper than standard soil sampling methods has indicated (Jobbagy & Jackson, 2000; Scharlemann et al., 2014; Klotzsche et al., 2018; Beaulne et al., 2021; Sothe et al., 2022). For example, more than 150 Pg C may be stored up to 3 m deep in forest systems (Jobbagy & Jackson, 2000). As such, increased assessment of soils at deeper depths is necessary to better account for total soil C storage in forest sites and to determine what biogeochemical and morphological processes control them.

To inform C to climate feedbacks in forest ecosystems it is critical to understand controls on forest soil C distribution across landscape gradients such as large hillslopes using robust, representative, high-resolution sampling of soil properties (Sucre, Tuttle, & Fox, 2011; Winkelbauer et al., 2011; Laamrani et al., 2013). The selective movement of soil organic C during erosion can lead to a shift in C and nitrogen (N) dynamics in different landscape areas, such as slope positions, and thus increase the spatial variability of C and N along the slope (Holz & Augustin, 2021). Furthermore, forest hillslope environments commonly support topographical and morphological controls on soil properties and C pools, such as promoting more intense groundwater flow and particle transport along steep slope gradients (Hoffmann et al., 2014; Hu et al., 2016; Wei et al., 2017; Holz & Augustin, 2021). This can lead to a high variability in soil content and C distribution across full hillslope systems as the high elevation, erosional section of the hillslope, the low elevation, depositional section, and the intermediate, high transport parts of the slope will all undergo different degrees of soil alteration and deposition.

3.1.1 Ground penetrating radar methods can better inform forest soil property estimates with spatial scale and depth compared to physical soil sampling.

Physical soil sampling methods are limited in capturing the variance of soil properties created by biogeochemical and morphological factors. These limits have resulted in empirical measurements and models of forest soil C distribution which exhibit high variability in their accounting (Hoffmann et al., 2014; Jandl et al., 2014; Dincă et al., 2015). Furthermore, the non-continuous nature of physical soil sampling methods often limits our ability to observe and understand trends in soil properties with landscape attributes in forest and boreal landscapes given the highly heterogenous unconsolidated till where the young soils are developed (Parsekian et al., 2012; Vadeboncoeur et al., 2012; Jandl et al., 2014). Thus, physical methods do not typically provide the sampling resolution that is needed to examine the influence of landscape trends on boreal forest soil properties, particularly at different depths, as it requires extensive labour, time, and site destruction to achieve large-scale coverage (Jol & Bristow, 2003; Sucre, Tuttle, & Fox, 2011; Parsekian et al., 2012; Jandl et al., 2014).

Ground penetrating radar (GPR), a near-surface geophysical surveying technology, has been used in forest soil surveying to collect estimates of soil horizon thickness and bulk density through measurements of soil horizon boundaries, rock, and root content (Collins & Doolittle, 1987; Davis & Annan, 1989; Jol & Bristow, 2003; Sucre, Tuttle, & Fox, 2011; Parsekian et al., 2012; Proulx-McInnis et al., 2013). The GPR technology has shown promise toward providing representative data of sitewide soil content across plot scales, particularly in agroecosystems. However, rough surfaces and sub-surfaces found in boreal forest environments due to rocks, roots, and decaying trees pose problems that have limited GPR surveying and interpretation. Optimization of GPR methodology and data processing has improved GPR data collection in heterogeneous, challenging forest environments and has been demonstrated at small plot scales (Butnor et al., 2003; Gerber et al., 2010; Laamrani et al., 2013). Applying these optimized GPR practices at scales that can provide landscape-relevant representation of boreal forest soil properties may better inform our understanding of the distribution, controls, and trends of soil content and C in these environments.

Current forest soil investigations conducted using GPR systems have been able to resolve and estimate soil property targets including soil horizon thickness, rock content, root content, and root biomass at resolutions comparable to physical soil sampling efforts while providing continuous data and limited site alteration or destruction, providing the ability to make replicate GPR measurements of the same areas of investigation (Butnor et al., 2003; Barton et al., 2004; Gerber et al., 2010; Sucre et al., 2011; Winkelbauer et al., 2011; Laamrani et al., 2013; Han et al., 2016; Molon et al., 2017). Organic and mineral soil horizons in forest ecosystems that are thicker than 10 cm have been repeatedly measured for soil horizon thickness and verified against physical soil sampling measurements such as soil coring, soil pit excavation, as soil auger sampling (Gerber et al., 2010; Winkelbauer et al., 2011; Laamrani et al., 2013; Han et al., 2016). These estimates of soil horizon thickness were generally within ± 2 cm of accompanying physical soil sampling measurements in these studies, demonstrating remarkable accuracy to previous methods. Furthermore, individual rocks and roots have been identified in GPR forest soil investigations up to 50 cm deep and with diameters > 5 cm (Butnor et al., 2003; Barton et al., 2004; Sucre et al., 2011; Molon et al., 2017). Again, the estimates of the size of these rock and root targets were comparable to accompanying physical measurements of rock and root content confirming the viability of GPR methods for these estimates. Thus, it is documented that in difficult forest environments, optimized GPR methods can achieve similar resolution and accuracy to physical soil sampling methods.

However, most of the forest soil GPR investigations that were reviewed to inform this study were completed over small spatial areas (< 1000 m^2). The limited spatial scale of these investigations restricts the ability in these studies to determine landscape trends in soil property measurements which would improve our understanding of the landscape distribution of key soil properties and soil C. This can be attributed to a lack of general, optimized methods for landscape GPR forest surveying which requires researchers to complete smaller spatial scale studies to determine the viability and optimization needed for full landscape surveying and the rough conditions of many of these forest sites which may prevent GPR surveying at landscape scales without site alteration or extensive optimization steps (Butnor et al., 2003; Gerber et al., 2010; Sucre et al., 2011; Winkelbauer et al., 2011; Laamrani et al., 2013; Han et al., 2016). As such, this study aims to bridge the gap from small to landscape scale forest GPR surveying by evaluating the previous small scale efforts, developing and testing optimized GPR methods at small and large spatial scales, and applying the verified optimized methods across a full boreal forest hillslope site (106 m x 54 m) to evaluate the resolution achieved in the results and influence of landscape distribution of soil properties and C content on individual and bulk estimates across the forest site.

In this experiment, we tested GPR results against physical soil sampling measurements made using soil excavation and direct interpretations of horizon thickness, bulk density, roots, and rock content at a hillslope scale (~80 m) in a boreal forest site in Pynn's Brook, Newfoundland, Canada. In this case, the GPR surveying was completed at a similar scale to the soil pit excavations, with a 1 m survey line collected 0.5 m upslope at each 1 m^2 soil pit of 6 total. This same GPR survey approach was then applied across the boreal forest hillslope site to assess the applicability of GPR in obtaining continuous estimates of soil properties which could then be used to assess associations with landscape attributes. This was done by collecting 6 GPR survey lines across the forest hillslope spanning from up- to down- slope. These survey lines were roughly 100 m long and yielded on average 80 m of useable GPR data. This study aims to evaluate continuous, landscape scale GPR data collections conducted across a boreal forest hillslope to; (1) assess soil heterogeneity and trends with depth and slope position, (2) observe patterns in soil horizon thickness and bulk density with slope position, and (3) identify potential associations between estimates of soil properties and hillslope morphology relevant to understanding boreal forest soil

C stocks. Therefore, this study examines soil property estimates, the key to determining soil stocks, made using GPR methods optimized for a recently deglaciated heterogenous boreal forest hillslope.

3.2 Materials and Methods

3.2.1 Site description.

Soil pit excavation and GPR surveying were carried out in the Pynn's Brook Experimental Watershed Area, or PBEWA (see Moroni, Shaw, & Otahal, 2010; Bowering et al., 2020 for more site details), located in western Newfoundland, Canada. The study site was a boreal forest hillslope, separated into 2 separate plots, 1 upslope and 1 downslope (Figure 2.1). The two plots used in this study comprise a mature black spruce-dominated forest hillslope roughly 106 m long by 54 m wide with an upslope portion exhibiting the characteristics of an eroding shoulder slope. The slope transitions from a dip of 6° when reaching the back slope midway downslope to 4°. The remaining hillslope is represented by a depositional foot slope portion with a steeper slope of 12°.

The site chosen for this study was especially difficult for completing GPR surveying due to the surface forest conditions impeding the positioning of survey lines and collection of complete survey line datasets. Dead wood, fallen trees, burrow holes and other obstacles blocked many locations for GPR surveying, limiting the amount and available space for continuous survey lines. The terrain of the forest floor further contributed corrupted and 'missed trace' data in GPR surveying, resulting in repeated surveying or unusable sections of data. Additionally, the heterogeneity displayed in these soils result in GPR data which can be very complex to process and interpret for useful measurements of soil properties such as soil horizon thickness and soil bulk density. The continuous collection of soil properties across the entire forest hillslope of ~80 m long was used to assess trends in these properties and soil C distribution in the context of morphological processes such as particle transport, groundwater, and erosion across the hillslope. This provided a means to assess how well the indirect GPR approach may be used to assess trends in key soil properties relevant to assessing soil C stocks and their controls.

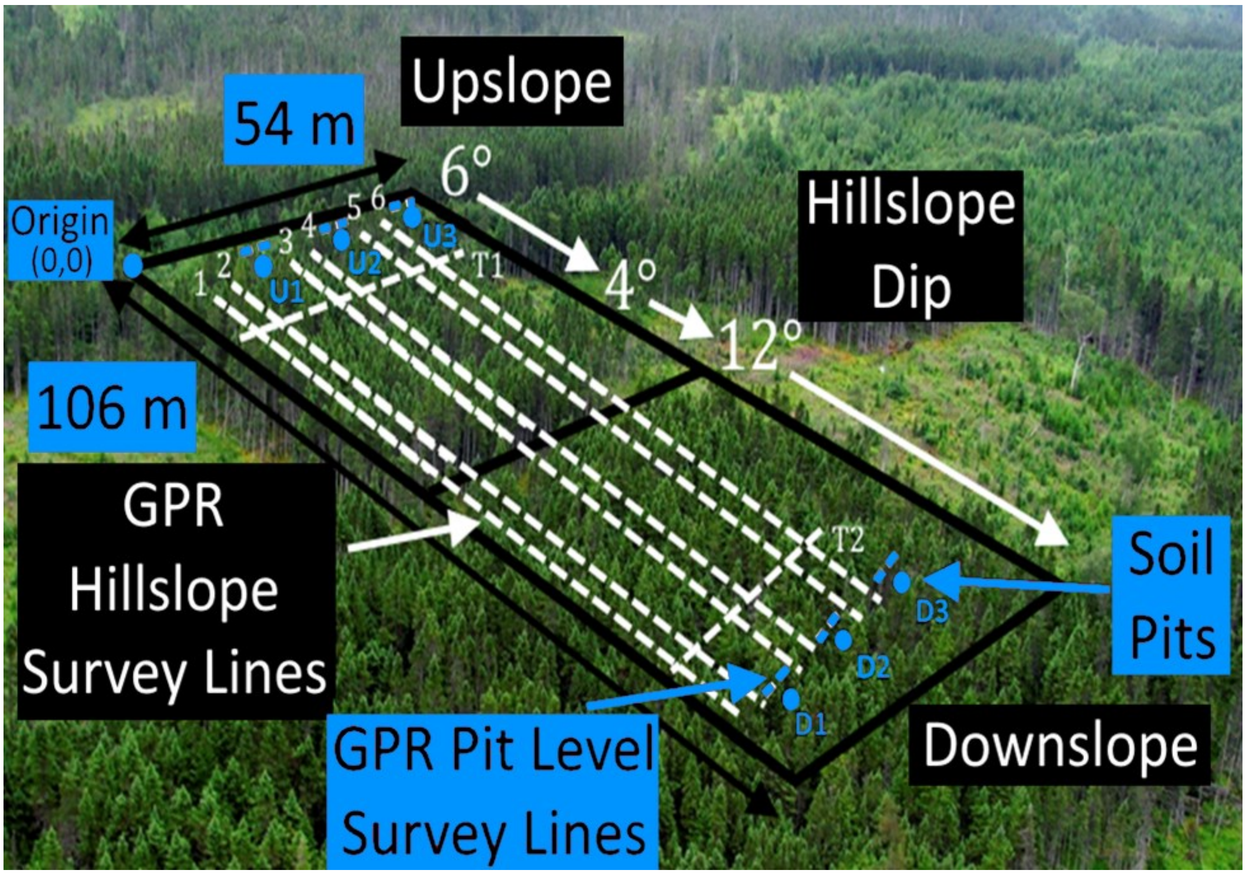

Figure 3.1. Physical soil sampling methods and ground penetrating radar surveying grid schemes overlain on an air photo of the Pynn's Brook Experimental Watershed Area (PBEWA). Soil Pits are indicated by blue dots, labelled for slope position (U = upslope, D = downslope) and numbered for the lateral position. Soil pits were positioned equally distanced across the plot at a 13.5 m lateral spacing along the same upslope and downslope gradient positions. GPR hillslope survey lines (numbered 1-6) were roughly 80 m long with two tie lines (dashed lines labelled T1 and T2) across the width of the plot at roughly 40 m in length. GPR survey lines along the hillslope were nearly spaced 4.5 m apart from each other and the soil pits and tie lines were positioned 20 m towards the middle of the plot from the soil pit positions. All credit for the air photo goes to the photographer Keri Bowering.

Soil methods used to classify the slope portions of the site included soil colour identification using a Munsell soil colour chart, measurements of soil fractionation (sand, silt, clay) through collecting, sieving, and weighing soil pit excavated samples, soil water holding capacity estimates using weight by the difference of the field wet and oven-dried weights of soil samples, electrical conductivity using conductivity probe measurements of soil sample and deionized water solutions, and elemental and isotopic analysis conducted in Memorial University of Newfoundland's CREAIT Stable Isotope Lab (Munsell Color (Firm), 2010). Soil pit sampling and GPR surveying were conducted in the upslope and downslope regions of the study site to examine soil property differences between distinct slope locations (Figure 3.1). The upslope and downslope regions were classified as separate areas with unique soil properties based on initial physical soil sampling measurements conducted at the site (Table 3.1). The downslope soils examined in through physical soil sampling had a higher quantity of soil particles (> 2 mm) and lower silt content (> 2 mm, < 53 μm) than upslope soils within the same horizons (Table 3.1). Root content was also much lower in the downslope portion of the hillslope, although roots were sparsely seen in soils deeper than the Bf horizon across the entire site (Table 3.1). During the period of sampling, soil water content was also lower in downslope soils, especially in the shallowest Bf mineral soil horizon (Table 3.1). The upslope soils also showed higher concentrations in all horizons of aluminum (Al_{py}) and iron (Fe_{py}) in g Kg^{-1} of soil and C and N in percentage of the total sample weight (Table 3.1). Electrical conductivity was more similar between the upslope and downslope soils but indicated that the Bf horizon is slightly more conductive than the underlying Bfj and BC horizons.

Table 3.1. Mineral soil properties at the Pynn's Brook Experimental Forest Watershed Area (PBEWA) study site for soil horizon classification by the Canadian System of Soil Classification (CSSC). Particle sizes are defined as sand (0.05 mm – 2 mm), silt (0.002 mm – 0.05 mm) and clay (< 0.002 mm) content and there was an average of 2% material loss between the initial and separated quantities for particle analysis. Total root concentration and rooting depth (applicable only to the Bf horizon, no roots in Bfj or BC) site values were provided by Dr. Ziegler, Dr. Prestegard, and Haley Talbot-Wendlt. Measurements of pyrophosphate extractable aluminum (Al_{py}) and iron (Fe_{py}) were taken from Patrick et al., 2022. The C:N ratios are given by weight. Electrical Conductivity was measured from slurry samples using a 5:1 deionized water to the soil mixture. The standard deviation for soil properties are in brackets.

	Upslope Horizons			Downslope Horizons		
Soil Property	**Bf**	**Bfj**	**BC**	**Bf**	**Bfj**	**BC**
Colour	7.5 YR 3/4	7.5 YR 3/3	7.5 YR 3/3	7.5 YR 4/4	7.5 YR 3/3	7.5 YR 2.5/3
Sand > 2 mm (%)	67.2 (15.6)	75.1 (7.3)	72.9 (12.7)	78.2 (5.8)	78.1 (6.2)	77.1 (4.2)
Silt < 2 mm, > 53 µm (%)	28.8 (14.5)	20.1 (7.8)	23.8 (12.3)	18.4 (4.6)	19.6 (5.6)	20.7 (4.7)
Clay < 53 µm (%)	1.3 (0.9)	1.1 (0.3)	1.0 (0.3)	1.0 (0.2)	1.2 (0.6)	1.3 (0.5)
Roots (%)	13.7 (7.2)	0.18 (0.2)	0.04 (0.1)	2.4 (1.5)	0	0
Soil Water Content (%)	77.1 (10.9)	ND	53.5 (4.1)	46.6 (3.1)	ND	39.4 (6.1)
Al_{PY} (g kg^{-1} soil)	4.9 (1.4)	ND	4.2 (0.9)	2.3 (0.8)	ND	1.7 (0.5)
Fe_{PY} (g Kg^{-1} soil)	5.5 (1.4)	ND	3.1 (0.3)	2.2 (0.4)	ND	1.7 (0.3)
C (%)	2.96 (0.76)	2.06 (0.86)	1.24 (0.43)	0.95 (0.11)	0.87 (0.46)	0.65 (0.14)
N (%)	0.16 (0.03)	0.13 (0.06)	0.09 (0.04)	0.08 (0.01)	0.08 (0.03)	0.06 (0.01)
C:N	19.2 (2.5)	16.7 (1.6)	14.0 (1.3)	11.7 (2.7)	10.8 (1.3)	10.2 (0.9)
Electrical Conductivity (µs/cm)	29.4 (6.1)	21.9 (8.3)	13.9 (2.4)	26.5 (8.2)	22.0 (8.2)	15.3 (1.9)

The upslope sampling position follows characteristics of an eroding, shoulder slope where soils would undergo erosion processes, facilitated by soil transport and groundwater flow, removing less stable soil particles from upslope portions, and transporting them downslope (Table 3.1; Yoo et al., 2006). Some of the transported particles will be deposited in the depositional footslope portion further downslope from the shoulder through infilling and infiltration processes (Table 3.1; Yoo et al., 2006). However, as this hillslope is convex with the downslope being steeper than the upslope, much more of this transported material will be passed through the downslope soils and out of the hillslope system (Table 3.1; Yoo et al., 2006; Wei et al., 2017). Although such a runoff of soil with aggregates can lead to soil enrichment in depositional areas (Wei et al., 2017). As such, soils sampled and surveyed in the upslope area (Soil pits U-1, U-2, U-3, and survey line positions 0 – 40 m) are considered part of an erosional zone at the shoulder position (Table 3.1). Furthermore, evidence of these depositional processes by a higher soil bulk density measurement and sand content through physical soil sampling and GPR estimates indicates that the downslope sampling area (Soil pits D-1, D-2, D-3, and survey line positions 40 – 80 m) is a footslope position in this depositional hillslope zone (Table 3.1).

The soils in the study sites are humo-ferro podzols with an organic (O) layer, a discontinuous bleached Ae soil layer, 3 mineral soil layers (Bf, Bfj, and BC in descending order) and a compacted rock (C) layer (Table 3.1; Soil Classification Working Group. 1998). Mineral soil layers are moderate in C, aluminum (Al) and iron (Fe) content, generally display 7.5-year to 10-year colouring with a chroma > 3 and are filled with rocks varying from pebbles to large boulders (Munsell Color (Firm), 2010). The compacted soil and rock layer (C) contains a high degree of large rock content. This horizon extends into a layer of till (> 1 m depth) made up of siliciclastic sedimentary parent material from the underlying bedrock (> 2 m depth).

3.2.2 Physical soil sampling and ground penetrating radar surveying schemes.

Soil pit and GPR measurements of soil horizon thickness and bulk density were collected to compare continuous GPR survey datasets to measurements collected by physical soil sampling methods at each of the soil pit locations. In total, 6 soil pits (3 on the upslope portion and 3 on the downslope) were excavated to interpret soil horizon thickness and sample for bulk density and C content by weight estimates (Figure 3.1). Soil pits were excavated such that the full mineral soil stratigraphy was revealed (Bf, Bfj, BC) for horizon thickness measurements and soil bulk density sampling. A square perimeter of 1 m x 1 m at each location was excavated until a transition from the mineral soil to the compacted rock C layer was observed (> 60 cm deep). These soil pits were hand excavated using trowels, shovels, rock hammers and a pry bar and samples were collected by hand from each visible mineral soil horizon using the same tools.

GPR samples were collected every 0.05 m (step size) across each survey line resulting in a high-resolution dataset for each short survey line collected next to each soil pit. Wide-angle reflection-refraction (WARR) surveying, where the spacing between the GPR's detachable transmitting and receiving antennas was increased by 0.05 m with each sample shot, was also conducted at these pit scale survey lines to estimate ground wave velocity for GPR depth calibrations. These measurements represent a soil pit scale at which operations can cover a heterogenous boreal forest soil base in 1 m segments along strategic discrete point positions. The hillslope scale GPR surveying was conducted to cover the 54 m x 106 m boreal forest site. Six survey lines, roughly 80 m long, were collected parallel to the hillslope at roughly 80 m in length (Figure 3.1). GPR data were collected at a similar resolution to the pit scale measurements, again with a step size of 0.05 m. Additionally, 2 tie lines were collected perpendicular to the hillslope, intersecting the 6 hillslope survey lines, to verify GPR measurements by depth and position. All GPR measurements were conducted by physically placing the system at sample locations and triggering the sample collection manually, rather than commonly used automatic sampling systems such as odometer wheels, as the variable forest microtopography of the site results in a high degree of noise and corrupted data when using these attachments. In total, 6 short 1 m lines adjacent to the soil pits, 6 long 80 m survey lines spanning the full forest hillslope, and 2 tie lines about 40 m were collected by the authors to evaluate the small- and large-scale abilities of optimized forest GPR surveying.

In the Pynn's Brook boreal forest site chosen for this investigation it was difficult to obtain deep soil samples in forest environments using physical soil sampling methods due to the abundance of large rock and root content in these soils. Soil pits were hand excavated to remove these rocks and roots for soil sampling procedures, which compared to GPR surveying investigations to similar depths took considerably much more time and effort. A high quantity of rocks and roots at depth also impacted GPR surveying efforts, limiting the interpretability of the radargrams collected to 1 m after optimized data processing due to high scattering of reflections. Furthermore, high tree density within the boreal forest site and surface litterfall, including dead wood, prevented both subsurface sampling and GPR surveying across many sections of the site due to limited accessibility. The variable microtopography of the forest floor also caused the GPR signal to miss traces or scatter frequently, resulting in repeated measurements or sections of GPR lines having to be skipped and interpolated.

3.2.3 Physical soil sampling methods.

All soil, rocks, and roots in each sampled soil pit (~1 m^2) were removed to provide a 1 m wide soil profile for interpretation and sample collection. Soil profiles were interpreted by depth for several different soil properties including soil particle and rock size, rock and root content, and soil colour and texture to determine soil horizon stratigraphy and boundary positions. Interpreted soil horizon positions were marked along the profiles and the resulting cross-section was measured for average soil horizon thickness for all mineral soils along the 1 m profile.

Soil samples were collected for bulk density measurements and elemental analysis for each mineral soil horizon at the 6 excavated soil pits in August 2019. Soil bulk density measurements were collected to determine the quantity of organic C bearing soil within the surveyed subsurface volumes relative to non-soil content such as rocks and roots. Soil bulk density is the oven-dry mass of soil per unit volume and is a necessary measurement for determining SOC concentration in terms of spatial units such as area or volume (Throop et al., 2012). Soil bulk density estimates are essential for accurate estimates or regional soil organic C stocks, as soil C stock calculations involving multiplication of measured soil C content by oven-dry mass soil bulk density and the depth of the soil horizon for which the C stock is for (Poeplau et al., 2017).

Methods for calculating soil bulk density from physical samples include the fine earth method where soils are sieved to excluding coarse fraction (>2 mm) particles and density is calculated using only the mass and volume of the soil particles < 2 mm particles, the core method where soils are not sieved and coarse fragments are included in the mass and volume calculations, and the hybrid method which combines these processes to correct for the volume occupied by non-organic C bearing coarse fragments (Throop et al., 2012). The alternative hybrid includes the fine earth mass (< 2 mm soil particles) and excludes the coarse fraction (> 2 mm) for appropriate soil property measurements relevant to the fine earth fraction only such as soil organic C. However, the volume of the entire fine earth and coarse fraction is used to calculate the bulk density estimate rather than that of just the fine earth fraction to account for displacement of fine earth soil particles by coarse fragments, can greatly impact the available soil organic C within an area of soil, rock, and root material (Throop et al., 2012).

Soil and non-soil content was defined based on particle size such that soil particles were < 2 mm in diameter and particles > 2 mm were not considered part of this organic C bearing soil matrix (Poeplau et al., 2017). Soil bulk density samples were collected using sheet metal plates such that the volume of the sample (4000 cm^2) was constrained and measured. This allowed for the measurement of soil content to be constrained spatially to a volume of sampled or surveyed subsurface, with the units for soil bulk density being in grams of soil per sample volume in cm^3. Samples were taken in duplicate at each horizon for a total of 56 samples. The bulk soil sampled was dry sieved at 2 mm to separate the soil (< 2 mm) from larger rock, root, and organic materials (> 2 mm) for individual density measurements. The weights of each size fraction were measured, and soil bulk density was then calculated by dividing the weight of the soil fraction (< 2 mm) by the bulk sample volume. This provided the bulk density of soil within the sampled soil horizon given as grams of dry weight soil (g dry weight) per volume (cm^3) of bulk material:

$$\text{Bulk Density [g cm}^{-3}\text{]} = \text{Soil Fraction [g dry weight]} / \text{Sample Volume [cm}^{3}\text{]} \qquad \text{(Eq 3.1)}$$

Soil bulk density has also demonstrated relationship with soil organic C and soil organic matter, with soil bulk density frequently used to estimate soil C pools and convert measurements of soil nutrient concentrations estimates in units of space and volume (Périé & Ouimet, 2007). Estimates of soil horizon thickness and soil bulk density can be combined with physical soil sampling measurements of soil elemental content (e.g., % C) to determine landscape soil content distribution and calculate landscape soil elemental stocks (Borchers & Perry, 1991; Périé & Ouimet, 2007; Xu, He & Yu, 2016; Poeplau, Vos & Don, 2017). For example, soil bulk density in boreal forest soils have been found to decrease as soil organic matter concentration increases such that soil bulk density may be estimated from these concentrations accurately in loamy to sandy loam forest soils (Périé & Ouimet, 2007). However, while soil bulk density might seem simple to estimate, measuring soil bulk density in forests can be labor intensive and time-consuming, especially in root-filled organic horizons and rock-filled mineral soil horizons which impede many physical soil sampling methods (Périé & Ouimet, 2007).

Soil samples were collected for soil C content measurements from each horizon across the full excavated profile using clean trowels and large freezer bags. Samples were collected in triplicate along each of the 3 mineral soil horizons (81 samples) at either side and in the middle of the profile. Dry combustion methods to measure organic C involve measuring the resulting CO_2 concentrating after combustion and oxidation processes (Périé & Ouimet, 2007). The amount of C in each soil horizon was measured using an elemental analyzer (Vario EL Cube, Elementar) in Memorial University of Newfoundland's CREAIT Stable Isotope Lab. Soil samples were ground using a ball mill and acidified using a vaporization technique (12 M HCl in a sealed desiccator; Hedges & Stern, 1984). The powdered, acidified, and dried soil samples were well mixed at all subsampling stages to ensure homogeneity. Acetanilide was used as a calibration standard, and a check measured at least 3 times over the course of each run. A low organic soil reference material (B2153: 1.61 ± 0.09 % C; 0.133 ± 0.023 % N) and a high organic sediment (B2151: 7.45 ± 0.14 % C; 0.52 ± 0.02 % N; Elemental Microanalysis), were ran as quality control samples in all batches analyzed. Estimates of soil C stock were made using the soil horizon thickness and soil bulk density derived from both the physical sampling and GPR interpretation, and measurements of soil C following Eq. 3.2:

Soil C Stock [g C m^{-2}] =

(Soil Horizon Thickness [m]) (Soil Bulk Density [g soil m^{-3}]) (Soil C by Weight [g C g $soil^{-1}$])

(Eq. 3.2)

3.2.4 Ground penetrating radar surveying methods and settings.

To collect quality GPR data for soil horizon thickness and soil bulk density measurements within rocky boreal forest soils, optimized practices, system settings and data collection methods as adapted from methods shared in previous forest GPR literature and reviews (Chapter 2). Data was collected using two different GPR systems, a PulseEkko PRO 500 MHz system and a Noggin 500 MHz system, for efficiency and to compare recommended optimization settings between systems (Sensors & Software Inc., Mississauga, ON, Canada). An antenna step size of 0.05 m was chosen as a default setting to provide the highest resolution sampling while maintaining efficiency, providing an interpretation resolution of 10 cm (within the range of horizon thickness and average rock diameter). For each GPR trace, 32 stacking was selected, which removed significant random noise while maintaining efficient in-field data collection time. Depth penetration settings (time window) in the GPR system were calibrated to image roughly 2 m deep for a focus on shallow soil targets. The use of a 500 MHz center frequency antenna helped for imaging shallower soil property targets and collecting reflections from within 2-3 m deep depending on soil water content and electrical conductivity. GPR settings were calibrated for accurate depth interpretation using an average ground wave velocity of 0.10 m/s as measured by WARR surveying and expected for the moist boreal forest soils as indicated by the GPR systems.

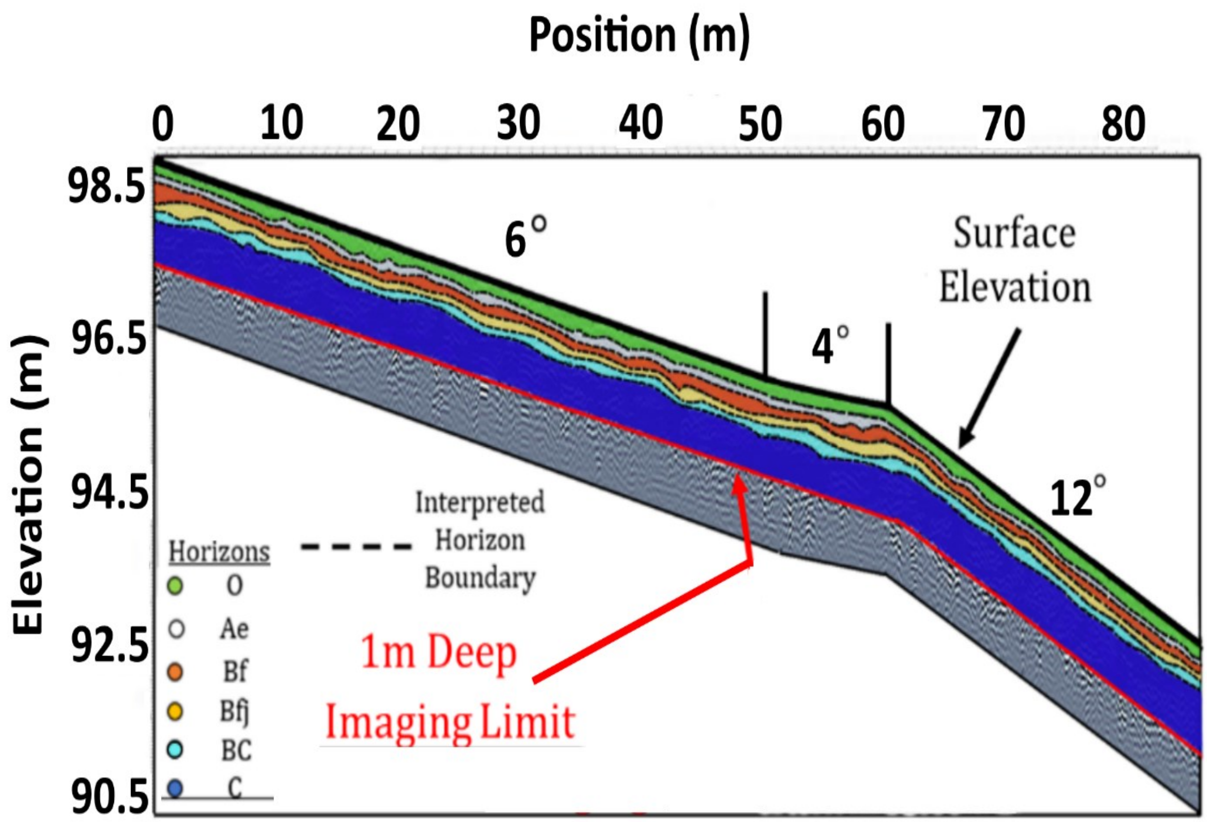

Figure 3.2. Large scale, topography corrected, processed radargram interpretations for measuring soil horizon thickness from GPR surveys across survey line 5 (Figure 3.1) in the Pynn's Brook boreal forest hillslope site. Soil horizon positions and the boundaries at depth between them could be interpreted continuously across the full hillslope and changes in slope up to 1 m deep following the method described in Section 3.2.5 and 3.2.6. 6 soil horizons, including an organic layer (O), bleached and podzolic mineral soil layers (Ae, Bf, Bfj, BC), and a compacted rock layer (C). Sections of the radargram associated with each soil horizon are color-mapped (see legend) to illustrate the variation in soil horizon thickness across the hillslope.

GPR surveying at soil pit locations and across the forest hillslope were processed and interpreted for continuous and averaged estimates of soil horizon thickness. Initial interpretations of soil horizon boundary positions based on the presence of linear, continuous, high amplitude reflections were noted, and the 'raw' radargram data (Figure 3.A1) underwent specific data processing to highlight these soil horizon boundary reflections and remove noise which can obscure these interpretations (Figure 3.A1). Following this specific data processing, which is explained in more detail in Section 3.2.6, interpretations of soil horizon boundary positions between organic, mineral soil, and compacted rock layers can be interpreted for position and depth, providing a cross-section map of soil horizon structure (Figure 3.A1). From this radargram map of soil horizon positions, the thickness of individual soil horizons can be measured based on the radargram depth scale (cm) across the entire surveyed section (Figure 3.A1). This GPR method for soil horizon thickness estimates thus provides continuous measurements across the surveyed area which can be used to calculate robust averages of landscape soil horizon thickness with a high sampling rate. This approach to soil horizon interpretations was applied over the entire hillslope, providing a detailed cross-section of soil horizon positions and morphological trends with slopes, such as the gradual reduction and loss of an Ae soil layer in the downslope (Figure 3.2).

Soil bulk density estimates can be derived from GPR radargram data aimed at illuminating and identifying reflections sourced from rocks, roots, and other particles greater than 2 mm in size. Estimates of soil bulk density for forest sites can be made by taking physical soil samples across the site for measurements of soil particle density (grams of dry soil per volume of dry soil, all particles < 2 mm in size) which can be used to convert estimates of soil volume in each surveyed area to estimates of soil bulk density. Estimates of soil volume can be defined for areas and depth over a surveyed area using GPR through identifying the relative percentage of soil content for the observed volume of subsurface material. The percentage of soil content is based on the presence, amount and strength of hyperbolic reflections sourced from rock and root content in each area where areas of 100 % soil content (no rocks or roots) would show no record of hyperbolic reflections while areas of 0 % soil content (all rocks and roots) would show many overlapping, scattered, strong hyperbolic reflections. Therefore, areas with a mixture of soil, rocks, and roots can be quantified for the relative spatial amount of organic C bearing soil based on radargram interpretations following the equation

Bulk Density [g cm^{-3}] = (Soil Particle Density [g cm^{-3}]) (Soil content (%)]). (Eq. 3.3)

Initial GPR interpretations for relative soil volume can be made from raw, unprocessed radargrams (Figure 3.A2) however specific data processing to highlight the position and quantity of rock and root sourced hyperbolic reflections is necessary for accurate interpretations (Figure 3.A2). While the interpreted hyperbolic reflections reveal the position and size of rock or roots based on their strength and size, the amplitude response created by reflections at positions of rocks and roots can be represented spatially across the surveyed subsurface using tools that employ a Hilbert Transformation filter. The Hilbert Transformation essentially collapses the hyperbolic reflections sourced from rocks and roots into point reflections that are more representative of the realistic geometry of the reflector than hyperbolic reflections. Furthermore, the Hilbert Transformation will color-map amplitude responses for these point reflections based on either a polarized scale (maximum negative to maximum positive amplitude) or non-polarized scale (0 to maximum amplitude) that can be used to compare the strength of reflections and thus quantity of rock and root content versus soil content (Figure 3.A2). Based on a non-polarized, linear color map scale where near 0 amplitude responses are mapped dark blue and the maximum amplitude responses measured are mapped dark red, the percentage of soil content (100 % = blue, 0 % = red) and/or rock and root content (0 % = blue, 100 % = red) can be interpreted for distinct sections of the GPR surveyed area, such as across an individual soil horizon or sample sections (i.e., 1 m averages) (Figure 3.A2; Butnor et al., 2003; Raz-Yaseef, Koteen & Baldocchi, 2013; Molon, Boyce & Arain, 2017).

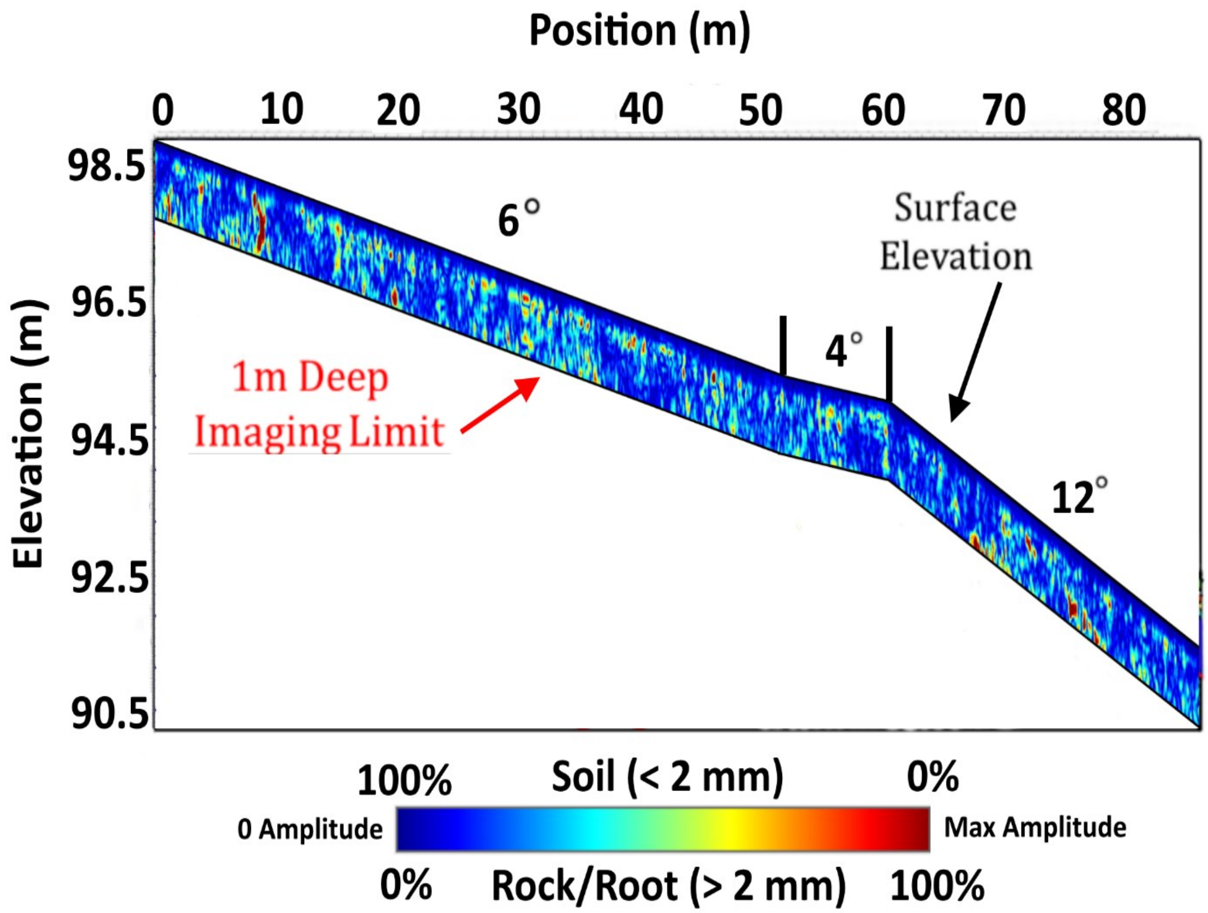

Figure 3.3. Large scale, topography corrected radargram interpretations for measuring relative soil and rock/root content percentages to estimate soil bulk density from GPR surveys across survey line 5 (Figure 3.1) in the Pynn's Brook boreal forest hillslope site. The GPR data has undergone processing as outlined in Section 3.2.5 and 3.2.7, including being filtered through a Hilbert Transformation. The position of high or low quantities of soil and rock are identified through the position and size of low (blue) or high (red) amplitude responses seen in the radargram color map. The relative percentage of soil or rock/root content are interpreted using the corresponding color-map scale relating the displayed color of the reflections to the amplitude strength of the response.

Using horizon thickness measurements collected through GPR surveying of the Pynn's Brook site, rock and root content for individual soil horizons was determined at soil pit scales and across the full hillslope (Figure 3.3). Rock content was measured at 10 cm intervals along each of the soil horizons, with the inverse measurement giving the soil content value. Soil content quantities were averaged along 10 cm segments of the collected radargram data for each mineral soil horizon. To convert the estimate of soil content to soil bulk density, the relative soil content estimate as a fraction was multiplied by the soil particle density (g cm^{-3}) determined from the physical soil measures of soil and rock content taken at each of the 6 soil pits for each horizon (Eq. 3.3).

3.2.5 Ground penetrating radar data processing for soil horizon thickness.

Specific data processing was undertaken to achieve the highest resolution and the clearest interpretations of reflections in radargrams. This was achieved by amplifying reflections associated with targeted soil properties (i.e., linear reflections at soil horizon boundaries and hyperbolic reflections at locations of the large rock and root content) while removing noise generated in heterogeneous soils. Data processing was undertaken for measurements of soil horizon thickness to boost horizon boundary reflections for easier interpretability using the EkkoProject 5 software suite (Sensors & Software Inc., Mississauga, ON, Canada). Background noise associated with soil heterogeneity and the sensitivity of GPR antennas was removed using a standard dewow filter (Window width = 1.33 pulse widths) and a bandpass filter (F_1 = 40 %, F_2 = 80 %, F_3 = 120 %, F_4 = 160 %). Additionally, the first break signals at each trace location were automatically repicked through a zero-time static correction operating under a tighter threshold (5 % average peak, 20 mV signal) to adjust the GPR's interpretation of the soil profile. A gain function was applied with settings such that shallow boundary reflections would be properly amplified for interpretation (Figure 3.A1). A spherical and exponentially compensation gain filter was chosen with specific settings of attenuation, start and maximum gain applied to present the best interpretability in each radargram and amplify deeper reflections with average values of 1-10 dB/m for attenuation, a start gain of 1-2, and a maximum gain of 200-500 were used (Figure 3.A1).

3.2.6 Ground penetrating radar data processing for soil bulk density.

Specific processing steps were used to interpret rock and root content reflections when estimating soil bulk density using GPR reflection data. Like the horizon boundary identification, a dewow filter and zero-time static correction were applied. Additional background noise removal was conducted for this data informing root and rock content using a background average subtraction filter which subtracts the average trace amplitude across the section to isolate high amplitude content (Barton & Montagu, 2004; Winkelbauer et al., 2011; Molon, Boyce, & Arain, 2017). Following noise removal, a migration tool was used to correct the GPR's positioning of hyperbolic reflections associated with rock and root content. Without migration processing, the initial interpretation of hyperbolic reflections in a raw radargram may not represent the true position of the source body due to discrepancies in the measurement of the GPR signals' two-way travel time, which can lead to an inaccurate accounting of rock and root content with depth (Raz-Yaseef, Koteen & Baldocchi, 2013; Molon, Boyce, & Arain, 2017). Hyperbolic reflections like these may be corrected by centimetres in-depth and position under migration filtering (Molon, Boyce, & Arain, 2017). To correct for this occurrence and accurately interpret rock and root positions and sizes, migration was applied along the frequency-wavenumber domain (F-K) with the parameter of velocity set to an average of 0.10 ms^{-1} (Figure 3.A2; Raz-Yaseef, Koteen, & Baldocchi, 2013; Molon, Boyce, & Arain, 2017). Finally, gain functions were applied to the entire radargram section using parameters like those used for the soil horizon thickness gain filter (Figure 3.A2).

To properly interpret rock and root content volume and geometry, reflection data were transformed into a more spatially representative form. This was accomplished using a Hilbert transform through the Assisted Pick Processing (APP) tool in EkkoProject 5 (Figure 3.3). This process transformed the data from a polarized, parabolic reflection set to a normalized, relative amplitude map that details areas of high and low amplitude interpreted here as high and low rock and root content (Butnor et al., 2003; Luo et al., 2003; Molon, Boyce, & Arain, 2017). Therefore, soil content was estimated as the inverse of the rock content interpreted through the processing steps described here. Hilbert transform tools like APP operate on GPR reflection data through a transform envelope filter which scales the radar amplitude energy from a polarized minimum background amplitude to a non-polarized scale from low background level amplitude to the maximum amplitude (Luo et al., 2003; Molon, Boyce, & Arain, 2017). Under this filtering approach, large rocks, and roots, as well as areas of high rock and root content will create strong amplitude responses that are easy to identify and quantify in terms of spatial volume (Figure 3.A2). Soil content will create relatively low or medium amplitude responses which are not very distinguishable from the background radar amplitude (Figure 3.A2).

3.2.7 Data handling and analyses.

Soil pit excavation for physical soil sampling methods and GPR methods was conducted and resulted in the sampling of 3 mineral soil horizons (Bf, Bfj, BC) at each of the 6 soil pit locations for measurement and estimation of soil horizon thickness and soil bulk density, obtaining one average value for each horizon within each soil pit. The average values of soil horizon thickness, soil bulk density, and soil C stocks were used to compare these estimates by method, slope position and horizon at the soil pit scale. Soil C stocks were calculated using C content obtained from replicate soil horizon samples, combined with soil bulk density and horizon thickness estimates derived from both physical soil excavation and GPR methods. Thus, in the case of soil C stocks, methodological comparisons were based solely upon differences in soil bulk density and horizon thickness since C content values were the same between the two methods.

GPR measurements conducted across the full hillslope length provided continuous data for estimates of soil content used to estimate soil C stocks at 0.05 m sample intervals with a 0.1 m resolution (Figure 3.2 & 3.3). This high-density data was used to generate slope position averages of these properties and evaluate observed changes with slope. Averaging was conducted along 10 m segments of the hillslope, providing estimates across each of these hillslope position segments to allow for assessment of the spatial variation of soil property across select segments and the full hillslope scale.

The effect of slope position, soil horizon and method on estimates of soil horizon thickness, bulk density, and soil C stocks was evaluated using multiple single factors ANOVA. Tests were performed in three ways; 1) among mineral soil horizons within slope position and method (physical soil sampling methods vs GPR), 2) between slope positions within mineral soil horizons and method, and 3) between methods within soil horizons and slope position. Following the results of the ANOVA, a Tukey pairwise T-test was conducted to determine if there are differences between the examined pairs of horizons (i.e., Upslope Bf vs. Upslope BC), slope position (i.e., Upslope Bfj vs. Downslope Bfj), and method (i.e., Physical measurement of Upslope Bf vs. GPR measurements of Upslope Bf). To determine if differences between horizon, slope, and method estimates are due to inherent variance from repeated testing, pairwise comparisons were evaluated as a post-hoc test of difference. To assess the comparison of the physical soil sampling methods more visually and GPR estimates of soil horizon thickness, soil bulk density, and soil C stock values obtained by each method were plotted against each other using data from across all pits and horizons. These were evaluated via linear regression. All statistical tests were performed with an alpha (a) of 0.05 in Microsoft Excel using the “Real Statistics Resource Package” developed by Charles Zaiontz.

To evaluate and compare soil pit level soil property measurements by physical soil sampling and GPR methods of soil horizon thickness, soil bulk density, and soil C stocks, each methods dataset were statistically analysed following the described methods. This was done to determine the means with standard deviation for soil properties grouped by position, space, and soil horizon (Table 3.A1), and any significant between soil property estimates by horizon between the two methods (Table 3.A2, 3.A3, & 3.A4). For this analysis only soil organic C bearing mineral soil horizons were examined. The entirety of the mineral soil layer (Bf + Bfj + BC) examined at each slope position (upslope, downslope) by each method were examined for means, standard deviation, and significant difference (P) (Table 3.A2). Pairwise comparisons with Tukey HSD testing were used to determine significant difference in soil property estimates between mineral soil horizons within method (Q, P, T) (Table 3.A2). Furthermore, the relationships for soil property measurements between soil horizon and method (Table 3.A3), and soil horizon and slope position (Table 3.A4) were examined under similar statistical methods (Q, P, T). GPR survey estimates collected across the hillslope (80 m lines) were sampled to evaluate means, standard deviation, and significant difference across 10 m sections (Table 3.A5, 3.A6 & 3.A7) and for the full upslope and downslope halves (40 m sections) of the hillslope (Table 3.A8) following similar analysis to the soil pit level procedure (Q, P, T).

3.3 Results.

Soil property and soil C stock estimates were collected for individual mineral soil horizons (Bf, Bfj, BC) at each of 6 excavated soil pit positions (U-1, U-2, U-3, D-1, D-2, D-3) to provide a direct comparison to GPR survey lines collected 0.5 m upslope and parallel to these pits (Figure 3.4; Table 3.A1, 3.A2, 3.A3, & 3.A4). After verifying that GPR can obtain measurements of soil horizon thickness and soil bulk density at analogous scales and locations to soil pit excavation in the boreal forest hillslope, GPR survey line data was collected along the full hillslope, roughly 80 m, for 6 separate forest hillslope lines providing continuous observations of soil properties along different hillslope positions. These continuous GPR data sections were averaged along 10 m segments to provide hillslope scale estimates of soil horizon thickness, soil bulk density, and soil C stocks across the boreal forest site (Figure 3.5). This method of investigation allowed for the comparison of different spatial soil property sampling methods through measurements completed at a common soil pit scale, as well as exploring the expanded understanding of landscape soil trends that GPR estimates utilized for hillslope scale observations can provide.

3.3.1 Ground penetrating radar estimates of horizon thickness are similar to the physical soil sampling method but are greater downslope.

Physical soil sampling measurements of soil horizon thickness across all soil pits ranged between 6 to 11 cm and exhibited little variation among mineral soil horizons, with thicker Bf horizons relative to the lower BC horizons in the upslope plots only (Figure 3.4a). The overall range in estimates of soil horizon thickness by the GPR method across all horizons and slope positions was similar to physical soil sampling measurements according to linear regression analysis between the full sets of soil pit level physical soil sampling measurements and GPR estimates (linear regression $p = 0.01$). However, GPR estimates ranged from 9 to 15 cm, showing a slightly higher and wider range in values compared to the previous sampling methods (Figure 3.4a). Overall, the difference between average soil horizon thickness between physical soil sampling and GPR estimates was about 2 cm which was relatively low despite differences in the full datasets (RMSE = 2.3 cm).

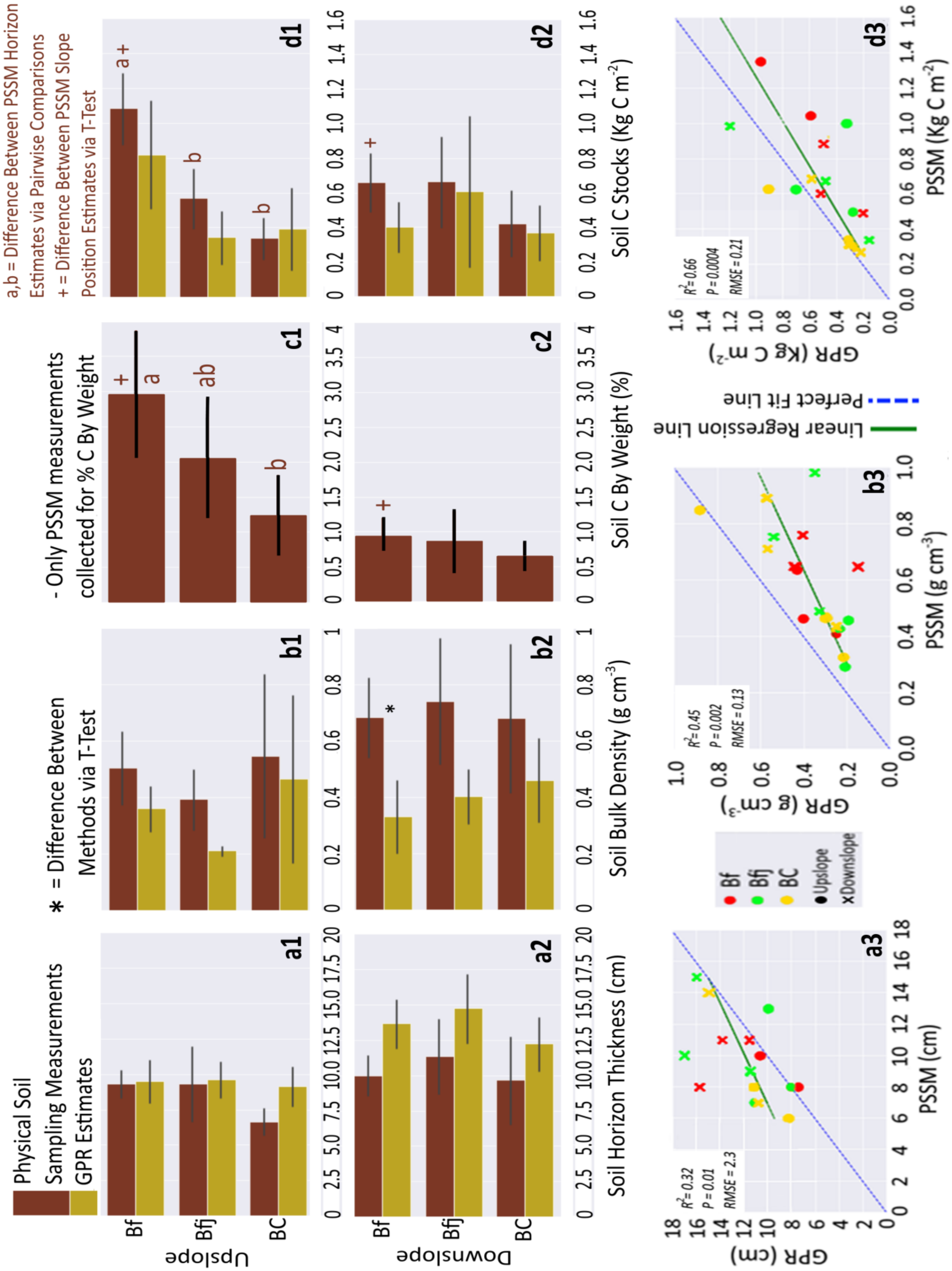

Physical Soil Sampling Measurements
GPR Estimates
* = Difference Between Methods via T-Test
- Only PSSM measurements collected for % C By Weight
a,b = Difference Between PSSM Horizon Estimates via Pairwise Comparisons
+ = Difference Between PSSM Slope Position Estimates via T-Test
Upslope
Downslope
Bf
Bfj
BC
a1
a2
a3
b1
b2
b3
c1
c2
d1
d2
d3
Soil Horizon Thickness (cm)
Soil Bulk Density (g cm^{-3})
Soil C By Weight (%)
Soil C Stocks (Kg C m^{-2})
GPR (cm)
PSSM (cm)
GPR (g cm^{-3})
PSSM (g cm^{-3})
GPR (Kg C m^{-2})
PSSM (Kg C m^{-2})
R^2= 0.32
P = 0.01
RMSE = 2.3
R^2= 0.45
P = 0.002
RMSE = 0.13
R^2= 0.66
P = 0.0004
RMSE = 0.21
Upslope
Downslope
Linear Regression Line
Perfect Fit Line

Figure 3.4. Soil horizon thickness, soil bulk density, and soil C by weight for each mineral soil horizon from the upslope (top panels) and downslope (lower panels) sites. Soil C stocks are calculated from the same soil C content (weight %) but using the soil bulk density and soil horizon thickness derived from either the physical soil sampling method (physical soil sampling method; red) or the ground penetrating radar method (GPR; yellow). All values are given as mean ± standard deviation. Three different sets of pairwise comparisons are expressed in this figure. First, differences among horizons within both slope and method are reported using lower case letters where red letters signify differences within the physical soil sampling results and yellow within the GPR results. Differences between the slope positions within individual horizons and methods are indicated using crosses (+) colour coded to the method. Comparisons by method, provided as linear regressions are given for horizon thickness (a), soil bulk density (b) and the resulting soil C stocks (c) across all sampled soil horizons and slope positions. The 1:1 line is indicated by a dashed blue line, while the linear regression line is indicated by the solid green line. Linear regression statistics of R^2, P, and root mean square error (RMSE) are indicated for each soil property.

3.3.2 Ground penetrating radar estimates of soil bulk density are lower than physical soil sampling results.

Soil bulk density as measured using physical soil sampling measurements at the excavated soil pit positions ranged from 0.4 to 0.7 g cm^{-3} and showed no significant difference across either horizon or slope, but measurements were generally higher in the downslope horizons (Figure 3.4b). Variability in the physical soil sample measurements of soil bulk density was particularly high in the deeper horizons (BC) and those in the downslope plots. The related GPR estimates of soil bulk density at the soil pit survey line positions ranged from 0.2 to 0.6 g cm^{-3} and were generally similar to analogous physical soil sampling measurements ($p = 0.002$, $R^2 = 0.41$). The linear relationship for GPR estimates of soil bulk density with physical soil sampling suggests a low variance between each method average of around 0.1 g cm^{-3} (RMSE = 0.13 g cm^{-3}).

3.3.3 Lower ground penetrating radar estimates of soil bulk density resulted in lower soil carbon stocks.

Measurements of soil C stocks for each soil horizon at upslope and downslope soil pit positions were determined using physically collected soil samples of soil C by weight in tandem with physical soil sampling and GPR estimates of soil horizon thickness and soil bulk density (Figure 3.4c). The averages of soil C by weight as a percentage value were used to calculate the soil C stock averages by both physical soil sampling and GPR, as there are no current GPR methods to make direct measures of soil C. GPR estimates of soil C stocks were generally similar to the physical soil sampling derived results across all horizons and the two slope positions as signified by the comparison of the methods via linear regression ($p = 0.0004$, $R^2 = 0.66$) (Figure 3.4d). However, the averages between both methods differed more than previous soil property comparisons of soil horizon thickness and soil bulk density, differing with an RMSE = 0.21 Kg C m^{-2} (Figure 3.4d). Downslope measurements of soil C stock means across the Bf and BC soil horizons by the GPR method were lower than their upslope counterparts (Figure 3.4c).

3.3.4 Hillslope scale ground penetrating radar reveals landscape influence on soil horizon thickness, bulk density, and C distribution.

Conducting GPR surveying along the outlined hillslope survey grid which spanned the experimental forest study site provided continuous estimates of soil horizon thickness and soil bulk density across 80 m survey lines. This landscape scale, continuous GPR surveying also revealed trends not possible to discern from the two slope positions sampled via physical methods (Figure 3.5). To summarize what this increased scale of inquiry may be able to provide, the nearly continuous dataset was averaged along 10 m sections of the hillslope and used to assess possible changes along this gradient (Figure 3.5).

GPR estimates of soil horizon thickness show general similarity in thickness across the hillslope for all horizons with soil horizons varying on average by 4.4 ± 2.3 cm across the site and largely within the range of 1 to 5 cm of that observed within slope position (7 to 15 cm) (Figure 3.5a). Organic (O) soil horizon thickness was also estimated across the hillslope using GPR measurements and showed a slight trend of increasing thickness with position downslope (Figure 3.5a).

Soil bulk density estimated by GPR across the hillslope exhibited an increasing trend downslope in the shallow mineral soil horizons (Bf, Bfj) (Figure 3.5b). However, no trends in soil bulk density were observed in the deepest BC horizon (Figure 3.5b). Like the continuous soil horizon thickness results, soil bulk density estimates demonstrated low variability amongst slope position means (0.4 to 0.7 g cm^{-3}) with variability in shallow soil samples (0.2 to 0.4 g cm^{-3} in Bf, Bfj horizons) but higher deviation in the deeper BC horizon, around 0.6 g cm^{-3}.

GPR estimates of soil horizon thickness and soil bulk density from hillslope surveying, in tandem with soil samples analyzed for percent C by weight for each horizon in the two-hillslope position, were used to make estimates of soil C stocks at each of 10 m positions along the hillslope to evaluate soil C distribution (Figure 3.5c). The GPR estimates, capturing an average stock over the entire 5725 m^2 of the hillslope suggests a full mineral soil layer (top of the Bf to the bottom of the BC horizon) C stock of 2.51 ± 2.0 Kg C m^{-2} in the upslope region and 1.35 ± 0.8 Kg C m^{-2} in the downslope (Table 3.A8). Comparatively, physical soil sampling methods completed at the soil pits with standard deviation scaled by a factor of 10 for comparison with continuous scale averages suggest a full mineral soil layer C stock of 2.25 ± 0.7 Kg C m^{-2} in the upslope region and 1.75 ± 2.0 Kg C m^{-2} in the downslope (Table 3.A8).

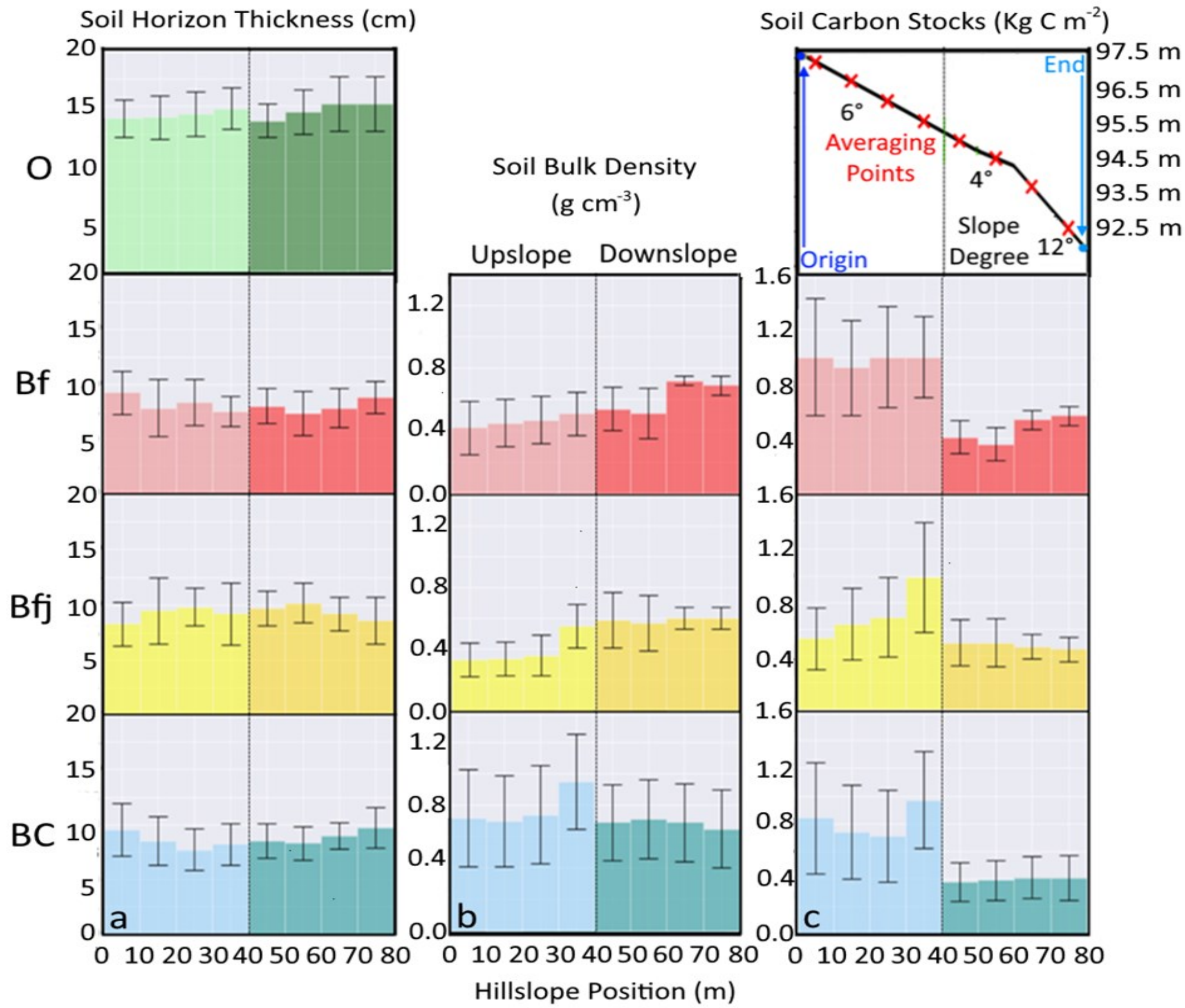

Figure 3.5. Spatial averages (10 m x 50 m area) from continuous GPR data collected from 6 survey lines for soil horizon thickness (a), and soil bulk density (b) across the 80 m hillslope surveyed utilizing GPR (see Figure 3.1 for survey layout). Continuous radargram interpretations of soil properties for each of the 6 survey lines were averaged along each 10 m segment of the hillslope to obtain a mean (± SD) value of soil horizon thickness and soil bulk density along the hillslope. Excavation sampling results for soil C content from the upslope and downslope sites were applied to soil horizon thickness and soil bulk density survey data collected from the upslope (light bars, left) and downslope (dark bars, right) regions of the hillslope, respectively, to calculate hillslope soil C stocks (c) based on GPR data.

3.4 Discussion.

3.4.1 Ground penetrating radar reveals soil horizons at depth with the potential to evaluate hillslope trends relevant to hydrogeomorphology.

Optimized GPR methods could assess soil horizon thickness at depths up to 70 cm depending on the center frequency of the antenna. This approach provides the full stratigraphy of mineral soils (Bf to BC) with continuous measurements along variable, undulating horizons. The BC mineral soil horizon was the deepest excavated soil horizon sampled (at an average depth of 34.9 ± 10.5 cm) for this study and the overlying Bfj horizons and underlying C horizons make it hard to identify the boundaries of the transitional BC layer. However, GPR estimates were generally higher (RMSE = 2.3 cm) across all horizons, especially in the downslope horizons and the upslope BC horizon (Figure 3.4a).

GPR observations of hillslope variation in the Ae horizon thickness revealed a more consistent presence and thickness in the upslope and a transition where slope gradient is lowest are consistent with greater downslope infiltration. Survey data such as this informs soil stratigraphy and hillslope hydrology which is useful in tracking soil properties including those relevant to C stores. The elevated C content of the shallow Bf soils in the upslope soils, for example, is likely the result of the increased infiltration, evidenced by the thicker Ae and the elevated water holding capacity of the soil relative to the footslope (Figure 3.2; Table 3.1).

3.4.2 Ground penetrating radar identified trends in soil bulk density consistent with hillslope transport and erosion.

GPR results were slightly lower than the physical soil sampling values, especially in the downslope locations where all GPR estimates were < 0.6 g cm^{-3} and all physical soil sampling estimates were > 0.6 g cm^{-3} (Figure 3.4b) with Bf horizon samples at downslope positions exhibiting a difference in soil bulk density estimates between the methods ($p = 0.04$; Figure 3.4b). Upslope GPR estimates of soil bulk density showed lower variability relative to the downslope and physical soil sampling values (0.3 – 0.5 g cm^{-3}) (Figure 3.4b). As well, GPR estimates of soil bulk density at the downslope position increased with depth from the Bf to the BC horizons, not observed in the more variable physical soil sampling data (Figure 3.4b).

Compared to soil bulk density measurements made using physical soil sampling methods, GPR estimates of soil bulk density across the hillslope were more variable over the smaller soil pit area excavated. Physical soil samples collected through cores or other fixed-size sampling methods can be biased in forest soils as rock and root content can routinely be larger than the cores used for sampling. This is a common issue in obtaining accurate soil bulk density, particularly in post-glaciated landscapes, where sampling likely favors high versus low soil content measurements due to the avoidance of areas of large and concentrated rocks and roots. Thus, the discrepancy between the physical soil sampling and GPR results for soil bulk density may indicate that a more reliable estimate is obtained using GPR. Further work verifying this should include applying the methods used here before excavation that provide the entire rock, root, and soil content by horizon for the entire volume surveyed. Further difference in soil bulk density interpretations between the physical soil sampling method and GPR may arise from the difference in resolution between each method's sampling procedure. GPR measurements were derived from multiple, near continuous measurements along 10 cm segments of the soil pit locations (i.e., 10 soil bulk density estimates for each horizon in a soil pit) while physical soil sampling measurements of soil bulk density were taken from 2 physical samples (4000 cm^2) for each soil horizon in each soil pit. As such, GPR averages for soil bulk density would be less influenced by isolated areas of high and low soil content, due to repeated measurements over small scales. Additionally, as GPR measurements indicated generally higher soil horizon thickness than physical soil sampling measurements, this could mean that GPR estimates for soil bulk density (which define horizons depths by the GPR estimates) would have a higher sampling volume which can result in smaller measurements of soil bulk density.

The continuous GPR data obtained here for soil bulk density follows a general trend of increasing density with position downslope in shallow soils (Bf, Bfj) consistent with transport from the upslope erosional portion, partial deposition within the downslope depositional area of the footslope (12°), and then transport and removal of these eroded particles out of the hillslope system. Where accurate, GPR surveying using similar methods as employed here has great potential to inform soil processes relevant to predicting soil and soil C content and stocks.

3.4.3 Ground penetrating radar can reliably investigate soil heterogeneity and landscape trends impacting soil carbon distribution.

While only accounting for differences in these soil property measurements between the methods, which may understate the differences in stock estimates, this examination allowed us to assess the impact of methodological differences in soil horizon thickness and soil bulk density on estimates of soil C stocks. While directly measuring soil C using GPR is not possible, strategic soil sampling along GPR survey lines could provide representative, complementary measurements of soil C and other elemental estimates to improve the resolution and coverage of soil stock calculations to validate the estimates using the GPR method. In this investigation, soil C stocks did not differ significantly by method, but overall estimates did exhibit large variations in some horizons, such as in the downslope Bfj horizon (Figure 3.4d).

The lower values of soil bulk density obtained via GPR surveying result in lower soil C stock estimates across the hillslope as well as more similarity between soil horizons in the upslope region (Figure 3.5c). Estimates of soil C stocks by GPR within the upslope (0 – 40 m) and downslope (40 – 80 m) region showed high variability in soil bulk density estimates via GPR surveying estimates because of the high variability demonstrated in GPR soil bulk density results (Figure 3.5c). Thus, discrete sampling with physical soil sampling methods may not be sufficient in representing the actual variability of soil C across the forest landscape (Figure 3.5c).

GPR estimates of soil C stocks derived from the soil bulk density and soil horizon thickness data did not show any clear hillslope trends within soil horizons but rather a clear contrast in C stock values between the upslope and downslope regions of the hillslope (40 m) (Figure 3.5c). This could be an artifact of the reliance on the physical soil sample values for C content derived from only two endmember locations along the hillslope (Figure 3.5c). Some subtle trends in the soil C stocks were observed within slope regions and congruent with increases in soil bulk density observed, for example, increased estimated stocks downslope in the Bf horizons of the downslope portion and the Bfj horizons of the upslope portion of the hillslope. Additionally, this contrast in soil C stocks at the 40 m position could also be a result of higher erosion in the downslope portion compared to the upslope in shallow soil horizons due to the steep (12°), convex slope. The upslope soil C stocks also exhibited higher variation relative to the downslope estimates in part attributed to the larger variation in C content in the upslope sample plots (Figure 3.5c). However, the continuous results for soil C stocks across the hillslope are limited by soil pit level C content data used to calculate sitewide soil C stocks.

3.5 Conclusions

Optimized, continuous GPR methods for boreal forest surveying were shown to reliably estimate soil horizon thickness and soil bulk density across a boreal forest hillslope in Pynn's Brook, Newfoundland, allowing for the examination of landscape influence and the effects of sitewide soil content distribution on soil C stock accounting. Using such methods, transport mechanics moving soil from shallow upslope soils into deeper downslope horizons were tracked along the hillslope using continuous GPR surveying, informing how erosion and deposition processes are impacting the soil stratigraphy along the hillslope and what might continue to occur over larger, temporal scales. The trends of these soil properties as observed using GPR impacted soil C stock distribution across the hillslope, with estimates indicating that soil C is being eroded from shallow, upslope soils and buried further downslope in deeper soil horizons.

As demonstrated by the analogous soil pit scale GPR estimates, the continuous data capture of soil bulk density across the hillslope better accounted for high rock and root content, and thus low soil content areas. Furthermore, plot scale GPR surveying along the forest hillslope was able to capture the variance of the measured soil properties with slope, providing insight into sitewide soil heterogeneity and landscape trends which will control soil C distribution (Figure 3.4). For example, large-scale GPR surveying in Pynn's Brook revealed consistently thicker deep (BC) soil horizons than physical soil sampling methods, which may indicate more representation of deep mineral soil layers through GPR surveying methods. Even in those locations such as the lowest relief transition zone not well represented by the soil pit locations, GPR estimates of forest soil properties appear to be consistent with expected geomorphic influences, such as relative increased infiltration expected with the lowest relief part of the hillslope coincided with the thickest Ae horizons) (Figure 3.5). Thus, there exists an opportunity to link these soil boundaries to uncover hydrogeomorphic processes and their relationship with soil properties including C content and stocks exists which can aid in developing predictive capabilities and understanding of mineral soil C stocks.

Measurements by GPR of soil C content over smaller segments of the slope may improve the resolution of soil C calculations and accounting, as has been evident with the observed hillslope morphology impacts. GPR estimates across the Pynn's Brook forest hillslope identify trends of soil content increasing continuously across the slope and at upslope and downslope positions, as well as variance in estimates with depth from physical soil sampling methods as seen in the BC horizon results for soil horizon thickness and soil bulk density averages (Figure 3.4 & 3.5). As such, through examining the variability of soil properties including soil horizon thickness and soil bulk density across the full hillslope and collecting much more sample data for each mineral soil horizon than possible through physical soil sampling methods, controls on soil C distribution could be identified such as the effects of soil bulk density distribution. Overall, this examination allowed us to assess the impact of methodological differences between physical soil sampling and GPR estimates of soil horizon thickness and soil bulk density on soil C distribution as represented through soil C stocks. Thus, we concluded that physical soil sampling method may not be sufficient for representing the realistic variability of soil C distribution across heterogeneous forest landscapes. Adoption, adaptation, and implementation of landscape scale, non-destructive, continuous methods for measuring soil property and C like GPR can further expand investigations of soil C distribution in difficult sites like boreal forests and link landscape processes and features to the heterogeneity observed in soil, rock, root, and C content.

References

Barton, C.V.M., Montagu, K.D., 2004. Detection of tree roots and determination of root diameters by ground penetrating radar under optimal conditions. *Tree Physiology*, 24(12), pp. 1323–1331. doi: 10.1093/treephys/24.12.1323.

Beaulne, J., Garneau, M., Magnan, G., Boucher, É., 2021. Peat deposits store more carbon than trees in forested peatlands of the boreal biome. *Scientific Reports*, 11(1). doi: 10.1038/s41598-021-82004-x.

Bowering, K. L., Edwards, K., Prestegaard, K., Zhu, X., Ziegler, S., 2020. Dissolved organic carbon mobilized from organic horizons of mature and harvested black spruce plots in a mesic boreal region. *Biogeosciences,* 17(3), pp. 581–595. doi: 10.5194/bg-17-581-2020.

Butnor, J. R., Doolittle, J. A., Johnsen, K. H., Samuelson, L., Stokes, T., Kress, L., 2003. Utility of ground-penetrating radar as a root biomass survey tool in forest systems. *Soil Science Society of America Journal*, 67(5), pp. 1607–1615. doi: 10.2136/sssaj2003.1607.

Collins, M. E., Doolittle, J. A., 1987. Using ground-penetrating radar to study soil microvariability. *Soil Science Society of America Journal*, 51(51), pp. 491–493.

Davis, J. L., Annan, A.P., 1989. Ground-penetrating radar for high resolution mapping of soil and rock stratigraphy. *Geophysical Prospecting*, 37(5), pp. 531–551. doi: 10.1111/j.1365-2478.1989.tb02221.x.

Dincă, L. C., Dincă, M., Vasile, D., Spârchez, G., Holonec, L., 2015. Calculating organic carbon stock from forest soils. *Notulae Botanicae Horti Agrobotanici Cluj-Napoca*, 43(2), pp. 568–575. doi: 10.15835/nbha43210041.

Doolittle, J. A., Jenkinson, B., Hopkins, D., Ulmer, M., Tuttle, W., 2006. Hydropedological investigations with ground-penetrating radar (GPR): Estimating water-table depths and local ground-water flow pattern in areas of coarse-textured soils. *Geoderma*, pp. 317–329. doi: 10.1016/j.geoderma.2005.03.027.

Doolittle, J. A., Collins, M. E., 1995. Use of soil information to determine application of ground penetrating radar. *Journal of Applied Geophysics*, 33(1–3), pp. 101–108. doi: 10.1016/0926-9851(95)90033-0.

Gerber, R., Felix-Henningsen, P., Behrens, T., Scholten, T., 2010. Applicability of ground-penetrating radar as a tool for nondestructive soil-depth mapping on pleistocene periglacial slope deposits. *Journal of Plant Nutrition and Soil Science*, 173(2), pp. 173–184. doi: 10.1002/jpln.200800163.

von Haden, A.C., Yang, W.H., DeLucia, E.H., 2020. Soils' dirty little secret: Depth-based comparisons can be inadequate for quantifying changes in soil organic carbon and other mineral soil properties. *Global Change Biology*, 26(7), pp. 3759–3770. doi: 10.1111/gcb.15124.

Hedges, J. I., Stern, J. H., 1984. Carbon and nitrogen determinations of carbonate-containing solids. *Limnology and Oceanography*, 29(3), pp. 657–663. Available at: doi: 10.4319/lo.1984.29.3.0657.

Henry, M. et al., 2015. An overview of existing and promising technologies for national forest monitoring. *Annals of Forest Science*, 72(6), pp. 779–788. doi: 10.1007/s13595-015-0463-z.

Hoffmann, U., Hoffmann, T., Johnson, E., Kuhn, N., 2014. Assessment of variability and uncertainty of soil organic carbon in a mountainous boreal forest (Canadian Rocky Mountains, Alberta). *Catena*, 113, pp. 107–121. doi: 10.1016/j.catena.2013.09.009.

Holz, M., Augustin, J., 2021. Erosion effects on soil carbon and nitrogen dynamics on cultivated slopes: A meta-analysis. *Geoderma*, 397. Available at: doi: 10.1016/j.geoderma.2021.115045.

Hu, Y., Berhe, A., Fogal, M., Heckrath, G., Kuhn, N., 2016. Transport-distance specific SOC distribution: Does it skew erosion induced C fluxes. *Biogeochemistry*, 128(3), pp. 339–351. doi: 10.1007/s10533-016-0211-y.

Hubbard, S.S. et al., 2013. Quantifying and relating land-surface and subsurface variability in permafrost environments using LiDAR and surface geophysical datasets. *Hydrogeology Journal*, 21(1), pp. 149–169. doi: 10.1007/s10040-012-0939-y.

Huisman, J. A., Hubbard, S., Redman, J., Annan, A., 2003. Measuring soil water content with ground penetrating radar: A review. *Soil Science Society of America*, 2, pp. 476–491.

Illawathure, C., Cheema, M., Kavanagh, V., Galagedara, L., 2020. Distinguishing capillary fringe reflection in a GPR profile for precise water table depth estimation in a boreal podzolic soil field. *Water* (Switzerland), 12(6). doi: 10.3390/W12061670.

Jandl, R. et al., 2014. Current status, uncertainty and future needs in soil organic carbon monitoring. *Science of the Total Environment*, 468–469, pp. 376–383. doi: 10.1016/j.scitotenv.2013.08.026.

Jobbagy, E. G., & Jackson, R. B., 2000. The vertical distribution of soil organic carbon and its relation to climate and vegetation. *Ecological Applications*, 10(2), p. 423. doi: 10.2307/2641104.

Jol, H. M., & Bristow, C. S., 2003. GPR in sediments: advice on data collection, basic processing and interpretation, a good practice guide. *Geological Society, London, Special Publications*, 211(1), pp. 9–27. doi: 10.1144/GSL.SP.2001.211.01.02.

Klotzsche, A., Jonard, F., Looms, M., van der Kruk, J., Huisman, J., 2018. Measuring soil water content with ground penetrating radar: A decade of progress. *Vadose Zone Journal*, 17(1). doi: 10.2136/vzj2018.03.0052.

Koch, J. C., Runkel, R., Striegl, R., McKnight, D., 2013. Hydrologic controls on the transport and cycling of carbon and nitrogen in a boreal catchment underlain by continuous permafrost. *Journal of Geophysical Research: Biogeosciences*, 118(2), pp. 698–712. doi: 10.1002/jgrg.20058.

Laamrani, A., Valeria, O., Cheng, L., Bergeron, Y., Camerlynck, C., 2013. The use of ground penetrating radar for remote sensing the organic layer - mineral soil interface in paludified boreal forests. *Canadian Journal of Remote Sensing*, 39(1), pp. 74–88. doi: 10.5589/m13-009.

Luo, Y., Al-Dossary, S., Marhoon, M., Alfaraj, M., 2003. Generalized Hilbert transform and its applications in geophysics. *Leading Edge* (Tulsa, OK), 22(3), pp. 198–202. doi: 10.1190/1.1564522.

Molon, M., Boyce, J. I., Arain, M. A., 2017. Quantitative, nondestructive estimates of coarse root biomass in a temperate pine forest using 3-D ground-penetrating radar (GPR). *Journal of Geophysical Research: Biogeosciences*, 122(1), pp. 80–102. doi: 10.1002/2016JG003518.

Moroni, M.T., Shaw, C. H., Otahal, P., 2010. Forest carbon stocks in newfoundland boreal forests of harvest and natural disturbance origin I: Field study. *Canadian Journal of Forest Research*, 40(11), pp. 2135–2145. doi: 10.1139/X10-154.

Munsell Color (Firm), 2010. Munsell soil color charts: with genuine Munsell color chips. Grand Rapids, MI.

Næsset, E., Gobakken, T., 2008. Estimation of above- and below-ground biomass across regions of the boreal forest zone using airborne laser. *Remote Sensing of Environment*, 112(6), pp. 3079–3090. doi: 10.1016/j.rse.2008.03.004.

Parsekian, A. D., Slater, L., Ntarlagiannis, D., Nolan, J., Sebesteyen, S., Kolka, R., Hanson, P., 2012. Uncertainty in peat volume and soil carbon estimated using ground-penetrating radar and probing. *Soil Science Society of America Journal*, 76(5), pp. 1911–1918. doi: 10.2136/sssaj2012.0040.

Pelletier, R. E., Davis, J. L., Rossiter, J. R., 1991. Peat analyses in the Hudson Bay lowlands using ground penetrating radar. *[Proceedings] IGARSS'91 Remote Sensing: Global Monitoring for Earth Management*, IEEE, pp. 2141–2144. doi: 10.1109/IGARSS.1991.575463.

Proulx-McInnis, S., St-Hilaire, A., Rosseau, A., Jutras, S., 2013. A review of ground-penetrating radar studies related to peatland stratigraphy with a case study on the determination of peat thickness in a northern boreal fen in Quebec, Canada. *Progress in Physical Geography*, SAGE Publications Ltd, pp. 767–786. doi: 10.1177/0309133313501106.

Raz-Yaseef, N., Koteen, L., Baldocchi, D. D., 2013. Coarse root distribution of a semi-arid oak savanna estimated with ground penetrating radar. *Journal of Geophysical Research: Biogeosciences*, 118(1), pp. 135–147. doi: 10.1029/2012JG002160.

Rosenbloom, N. A., Doney, S. C., Schimel, D. S., 2001. Geomorphic evolution of soil texture and organic matter in eroding landscapes. *Global Biogeochemical Cycles*, 15(2), pp. 365–381. doi: 10.1029/1999GB001251.

Scharlemann, J. P. W., Tanner, E. V. J., Hiederer, R., Kapos, V., 2014. Global soil carbon: Understanding and managing the largest terrestrial carbon pool. *Carbon Management*, pp. 81–91. doi: 10.4155/cmt.13.77.

Slessarev, E. W., Chadwick, O, Sokol, N., Nuccio, E., Pett-Ridge, J., 2022. Rock weathering controls the potential for soil carbon storage at a continental scale. *Biogeochemistry*, 157(1). doi: 10.1007/s10533-021-00859-8.

Soil Classification Working Group. 1998. The Canadian System of Soil Classification, 3rd ed. Agriculture and Agri-Food Canada Publication 1646, 187 pp.

Sothe, C., Gonsamo, A., Arabian, J., Kurz, W., Finkelstein, S., Snider, J., 2022. Large soil carbon storage in terrestrial ecosystems of Canada. *Global Biogeochemical Cycles*, 36(2). doi: 10.1029/2021GB007213.

Sucre, E. B., Tuttle, J. W., Fox, T. R., 2011. The use of ground-penetrating radar to accurately estimate soil depth in rocky forest soils. *Forest Science*, 57(1), pp. 59–66. doi: 10.1093/forestscience/57.1.59.

Throop, H. L., Archer, S. R., Monger, H. C., Waltman, S., 2012. When bulk density methods matter: Implications for estimating soil organic carbon pools in rocky soils. *Journal of Arid Environments,* 77(1), pp. 66-71. doi: 10.1016/j.jaridenv.2011.08.020.

Vadeboncoeur, M. A., Hamburg, S., Blum, J., 2012. The quantitative soil pit method for measuring belowground carbon and nitrogen stocks. *Soil Science Society of America Journal*, 76(6), pp. 2241–2255. doi: 10.2136/sssaj2012.0111.

Warner, B. G., Nobes, D .C., Theimer, B. D., 1990. An application of ground penetrating radar to peat stratigraphy of Ellice Swamp, southwestern Ontario, *Can. J. Earth Sci*.

Wei, S., Zhang, X., McLaughlin, N., Chen, X., Jia, S., Liang, A., 2017. Impact of soil water erosion processes on catchment export of soil aggregates and associated SOC. *Geoderma*, 294, pp. 63–69. doi: 10.1016/j.geoderma.2017.01.021.

Winkelbauer, J., Völkel, J., Leopold, M., Bernt, N., 2011. Methods of surveying the thickness of humous horizons using ground penetrating radar (GPR): An example from the Garmisch-Partenkirchen area of the Northern Alps. *European Journal of Forest Research*, 130(5), pp. 799–812. doi: 10.1007/s10342-010-0472-2.

Worsfold, R. D., Parashar, S. K., Perrott, T., 1986. Depth profiling of peat deposits with impulse radar, *Can. Geotech. J.*

Yoo, K., Amundson, R., Heimsath, A., Dietrich, W., 2006. Spatial patterns of soil organic carbon on hillslopes: Integrating geomorphic processes and the biological C cycle. *Geoderma*, 130(1–2), pp. 47–65. doi: 10.1016/j.geoderma.2005.01.008.

Co-author Statement

Lakshman Galagedara, Susan Ziegler, and Zachary Gates conceptualized the research topic and experiment. Zachary Gates investigated the concept and conducted data collection for this study with help from Susan Ziegler and Lakshman Galagedara. Zachary Gates conducted the literature review and writing for the original draft with direct input from Susan Ziegler, and with verification, editing and revision completed by all three authors. Additional soil property data for Al and Fe quantities were provided by Mackenzie Patrick.

Appendix

Table 3.A1. A summary table of the means and standard deviations between estimates of soil properties, including horizon thickness (cm) and soil bulk density (g cm^{-3}), and soil C stocks (Kg C m^{-2}) based on slope position (upslope vs. downslope) and within soil horizon (Bf, Bfj, BC) and method (PSSM, GPR). The means and standard deviations here are used to perform the statistical analysis found in Figure 3.4 and Table 3.A2, 3.A3 and 3.A4. Each mean of soil horizon thickness for individual soil horizons has a sample of n = 3 with df = 4. Each mean of soil bulk density and soil C stocks for individual soil horizons has a sample of n = 3 with df = 4.

Method	Slope	Horizon	Horizon Thickness Means ± (STDEV) (cm)	Soil Bulk Density Means ± (STDEV) (g cm^{-3})	Soil C Stocks Mean ± (STDEV) (Kg C m^{-2})
PSSM	Up	Bf	9.3 ± (1.3)	0.50 ± (0.01)	0.50 ± (0.01)
		Bfj	9.3 ± (3.3)	0.39 ± (0.008)	0.39 ± (0.008)
		BC	6.7 ± (1.3)	0.55 ± (0.07)	0.55 ± (0.07)
	Down	Bf	10.0 ± (3.0)	0.68 ± (0.004)	0.68 ± (0.004)
		Bfj	11.3 ± (3.3)	0.74 ± (0.06)	0.74 ± (0.06)
		BC	9.7 ± (4.3)	0.68 ± (0.05)	0.68 ± (0.05)
GPR	Up	Bf	9.5 ± (3.3)	0.36 ± (0.009)	0.36 ± (0.009)
		Bfj	9.6 ± (2.3)	0.21 ± (0.0004)	0.21 ± (0.0004)
		BC	9.2 ± (2.8)	0.46 ± (0.13)	0.46 ± (0.13)
	Down	Bf	13.7 ± (4.4)	0.33 ± (0.02)	0.33 ± (0.02)
		Bfj	14.7 ± (8.6)	0.40 ± (0.01)	0.40 ± (0.01)
		BC	12.2 ± (5.4)	0.46 ± (0.03)	0.46 ± (0.03)

Table 3.A2. A summary table of statistical analysis to determine differences between estimates of soil properties, including horizon thickness (cm) and soil bulk density (g cm^{-3}), and soil C stocks (Kg C m^{-2}) based on soil horizons (Bf, Bfj, BC) within slope position (upslope vs. downslope) and method (PSSM, GPR). The means and standard deviations used to perform this statistical analysis can be found in Figure 3.4 and Table 3.A1. To analyze the difference in estimates between slope positions, a 1-way ANOVA (factor = slope) was used to analyze the difference amongst individual, indexed mineral soil horizons ($P_{\text{Between Groups}}$) and variance within each slope-based horizon dataset ($MSE_{\text{Within Groups}}$). T-test analysis (Pairwise *P*) and post-hoc rating using a Tukey HSD test (*Q* Test Mean, Tukey *T* Value) where Q_{crit} = 4.996 were used to further evaluate the difference in horizon values with slope position. All statistical tests used to determine the difference in the data sets used an alpha value of 0.05. Indications that a test suggests a significant difference in a set are highlighted with bold text. The difference as indicated through this analysis is indicated in Figure 3.4 by lower case letters colour-coded to the method and found next to their respective bar means.

Soil Property	Method	Slope	Horizon	*P* Between Groups	MSE Within Groups	Group	*Q* test Mean	Tukey *T* Value	Pairwise *P*
Soil Horizon Thickness (cm)	PSSM	Up	Bf	0.3	4	Bf X Bfj	0	5	1
			Bfj			Bf X BC	3		**0.05**
			BC			Bfj X BC	3		0.3
		Down	Bf	0.8	9	Bf X Bfj	1	8	0.6
			Bfj			Bf X BC	0.3		0.9
			BC			Bfj X BC	2		0.6
	GPR	Up	Bf	0.9	3	Bf X Bfj	0.1	4	0.9
			Bfj			Bf X BC	0.3		0.8
			BC			Bfj X BC	0.5		0.7
		Down	Bf	0.9	3	Bf X Bfj	1	6	0.5
			Bfj			Bf X BC	1		0.3
			BC			Bfj X BC	2		0.6
Soil Bulk Density (g cm^{-3})	PSSM	Up	Bf	0.6	0.03	Bf X Bfj	0.1	0.4	0.3
			Bfj			Bf X BC	0.04		0.8
			BC			Bfj X BC	0.2		0.4
		Down	Bf	0.9	0.04	Bf X Bfj	0.06	0.5	0.7
			Bfj			Bf X BC	0.002		1
			BC			Bfj X BC	0.06		0.8
	GPR	Up	Bf	0.4	0.05	Bf X Bfj	0.2	0.5	0.1
			Bfj			Bf X BC	0.1		0.7
			BC			Bfj X BC	0.3		0.3
		Down	Bf	0.6	0.02	Bf X Bfj	0.07	0.4	0.5
			Bfj			Bf X BC	0.1		0.4
			BC			Bfj X BC	0.06		0.7
Soil C Stocks (Kg C m^{-2})	PSSM	Up	Bf	0.003	0.03	Bf X Bfj	**0.6**	0.4	**0.01**
			Bfj			Bf X BC	**0.8**		**0.005**
			BC			Bfj X BC	0.2		0.2
		Down	Bf	0.5	0.06	Bf X Bfj	0.007	0.6	1
			Bfj			Bf X BC	0.2		0.3
			BC			Bfj X BC	0.2		0.4
	GPR	Up	Bf	0.2	0.09	Bf X Bfj	**0.5**	0.5	0.09
			Bfj			Bf X BC	0.4		0.2
			BC			Bfj X BC	0.08		0.8
		Down	Bf	0.7	0.1	Bf X Bfj	0.2	0.9	0.8
			Bfj			Bf X BC	0.04		0.5
			BC			Bfj X BC	0.2		0.6

Table 3.A3. A summary table of statistical analysis to determine differences between estimates of soil properties, including horizon thickness (cm) and soil bulk density (g cm^{-3}), and soil C stocks (Kg C m^{-2}) based on slope position (upslope vs. downslope) and within soil horizon (Bf, Bfj, BC) and method (Physical soil sampling methods = PSSM, GPR). The means and standard deviations used to perform this statistical analysis can be found in Figure 3.4 and Table 3.A1. To analyze the difference in estimates between slope positions, a 1-way ANOVA (factor = slope) was used to analyze the difference amongst individual, indexed mineral soil horizons ($P_{\text{Between Groups}}$) and variance within each slope-based horizon dataset ($MSE_{\text{Within Groups}}$). *T*-test analysis (Pairwise *P*) and post-hoc rating using a Tukey HSD test (*Q* Test Mean, Tukey *T* Value) where Q_{crit} = 3.926 were used to further evaluate the difference in horizon values with slope position. All statistical tests used to determine the difference in the data sets used an alpha value of 0.05. Indications that a test suggests a significant difference in a set are highlighted with bold text. The difference as indicated through this analysis is indicated in Figure 3.4 by + symbols colour-coded to the method and found next to the respective bar means.

Soil Property	Method	Horizon	*P* Between Groups	MSE Within Groups	*Q* test Mean	Tukey *T* Value	Pairwise *P*
Soil Horizon Thickness (cm)	PSSM	Bf	0.6	2	0.7	3	0.6
	PSSM	Bfj	0.5	10	2	7	0.5
	PSSM	BC	0.3	8	3	6	0.3
	GPR	Bf	0.06	4	4	5	0.06
	GPR	Bfj	0.06	5	**5**	5	0.07
	GPR	BC	0.1	4	3	5	0.1
Soil Bulk Density (g cm^{-3})	PSSM	Bf	0.08	0.009	0.2	0.2	0.1
	PSSM	Bfj	0.08	0.03	0.3	0.4	0.1
	PSSM	BC	0.6	0.06	0.1	0.6	0.5
	GPR	Bf	0.8	0.02	0.03	0.3	0.8
	GPR	Bfj	**0.04**	0.007	**0.2**	0.2	0.1
	GPR	BC	1	0.08	0.004	0.6	1
Soil C Stocks (Kg C m^{-2})	**PSSM**	**Bf**	**0.02**	0.03	**0.5**	0.4	**0.03**
	PSSM	Bfj	0.9	0.06	0.02	0.6	0.9
	PSSM	BC	1	0.04	0.0009	0.5	1
	GPR	Bf	0.05	0.04	0.4	0.5	0.07
	GPR	Bfj	0.6	0.2	0.2	0.9	0.6
	GPR	BC	0.6	0.08	0.1	0.6	0.6

Table 3.A4. A summary table of statistical analysis to determine differences between estimates of soil properties, including horizon thickness (cm) and soil bulk density (g cm^{-3}), and soil C stocks (Kg C m^{-2}) based on the sample collection method (Physical Soil Sampling Methods, or PSSM vs. GPR) and within soil horizon (Bf, Bfj, BC) and slope position (upslope, downslope). The means and standard deviations used to perform this statistical analysis can be found in Figure 3.4 and Table 3.A1. To analyze the difference in estimates between methods, a 1-way ANOVA (factor = slope) was used to analyze the difference amongst individual, indexed mineral soil horizons ($P_{\text{Between Groups}}$) and variance within each method dataset ($MSE_{\text{Within Groups}}$). *T*-test analysis (Pairwise *P*) and post-hoc rating using a Tukey HSD test (*Q* Test Mean, Tukey *T* Value) where Q_{crit} = 3.926 were used to further evaluate the difference in horizon values with the method. All statistical tests used to determine the difference in the data sets used an alpha value of 0.05. Indications that a test suggests a significant difference in a set are highlighted with bold text. The difference as indicated through this analysis is indicated in Figure 3.4 by * symbols and found next to their respective bar means.

Soil Property	Slope	Horizon	*P* Between Groups	MSE Within Groups	*Q* Test Mean	Tukey *T* Value	Pairwise *P*
Soil Horizon Thickness (cm)	Up	Bf	0.9	2	0.2	3.5	0.9
	Up	Bfj	0.9	6	0.3	5.7	0.9
	Up	BC	0.1	2	2	3	0.1
	Down	Bf	0.08	4	**4**	4	0.08
	Down	Bfj	0.2	9	3	7	0.2
	Down	BC	0.4	10	3	7	0.4
Soil Bulk Density (g cm^{-3})	Up	Bf	0.2	0.01	0.1	0.2	0.2
	Up	Bfj	**0.03**	0.004	**0.2**	0.1	0.06
	Up	BC	0.8	0.1	0.08	0.7	0.8
	Down	**Bf**	**0.02**	0.01	**0.4**	0.3	**0.04**
	Down	Bfj	0.1	0.04	0.3	0.4	0.1
	Down	BC	0.3	0.04	0.2	0.5	0.3
Soil C Stocks (Kg C m^{-2})	Up	Bf	0.1	0.04	0.3	0.5	0.2
	Up	Bfj	0.2	0.04	0.2	0.5	0.3
	Up	BC	0.8	0.08	0.07	0.6	0.8
	Down	Bf	0.2	0.03	0.2	0.4	0.2
	Down	Bfj	0.9	0.2	0.06	1	0.9
	Down	BC	0.8	0.04	0.06	0.5	0.8

Table 3.A5. Means and standard deviations (STDEV) of soil horizon thickness estimates (cm) collected by GPR over the 80 m hillslope site, averaged along 10 m segments. Additional averaging for horizon thickness means across slope positions (0 - 40 m upslope, 40 - 80 m downslope) are calculated from the 10 m segment data.

Slope (m)	Horizon	Soil Horizon Thickness Means ± (STDEV) (cm)	Slope Mean	Horizon	Soil Horizon Thickness Means ± (STDEV) (cm)	Slope Mean	Horizon	Soil Horizon Thickness Means ± (STDEV) (cm)	Slope Mean
0 - 10	Bf	9.2 ± (2.0)		Bfj	8.3 ± (2.0)		BC	9.5 ± (2.4)	
10 - 20	Bf	7.8 ± (2.1)	8.2 ± (3.0)	Bfj	9.5 ± (2.9)	9.2 ± (3.0)	BC	8.5 ± (2.2)	8.5 ± (2.9)
20 - 30	Bf	8.3 ± (2.9)		Bfj	9.8 ± (1.7)		BC	7.7 ± (1.9)	
30 – 40	Bf	7.5 ± (2.2)		Bfj	9.2 ± (2.8)		BC	8.2 ± (1.9)	
40 – 50	Bf	8.0 ± (1.6)		Bfj	9.7 ± (1.6)		BC	8.5 ± (1.5)	
50 – 60	Bf	7.3 ± (2.0)	8.0 ± (2.9)	Bfj	10 ± (1.8)	9.4 ± (2.4)	BC	8.3 ± (1.6)	8.9 ± (2.4)
60 – 70	Bf	7.8 ± (1.8)		Bfj	9.2 ± (1.5)		BC	9.0 ± (1.9)	
70 - 80	Bf	8.8 ± (1.5)		Bfj	8.6 ± (2.1)		BC	9.7 ± (2.0)	

Table 3.A6. Means and standard deviations (STDEV) of soil bulk density estimates (g cm^{-3}) collected by GPR over the 80 m hillslope site, averaged along 10 m segments. Additional averaging for soil bulk density means across slope positions (0 - 40 m upslope, 40 - 80 m downslope) are calculated from the 10 m segment data.

Slope (m)	Horizon	Soil Bulk Density Means ± (STDEV) (g cm^{-3})	Slope Mean	Horizon	Soil Bulk Density Means ± (STDEV) (g cm^{-3})	Slope Mean	Horizon	Soil Bulk Density Means ± (STDEV) (g cm^{-3})	Slope Mean
0 - 10	Bf	0.42 ± (0.34)	0.46 ± (0.34)	Bfj	0.33 ± (0.23)	0.40 ± (0.36)	BC	0.72 ± (0.62)	0.78 ± (0.60)
10 - 20	Bf	0.45 ± (0.30)		Bfj	0.34 ± (0.22)		BC	0.70 ± (0.58)	
20 - 30	Bf	0.47 ± (0.31)		Bfj	0.36 ± (0.26)		BC	0.74 ± (0.63)	
30 – 40	Bf	0.51 ± (0.28)		Bfj	0.55 ± (0.34)		BC	0.95 ± (0.59)	
40 – 50	Bf	0.54 ± (0.29)	0.62 ± (0.30)	Bfj	0.59 ± (0.37)	0.59 ± (0.26)	BC	0.69 ± (0.48)	0.69 ± (0.51)
50 – 60	Bf	0.51 ± (0.32)		Bfj	0.57 ± (0.37)		BC	0.71 ± (0.49)	
60 – 70	Bf	0.72 ± (0.06)		Bfj	0.60 ± (0.13)		BC	0.69 ± (0.49)	
70 - 80	Bf	0.69 ± (0.12)		Bfj	0.60 ± (0.13)		BC	0.66 ± (0.50)	

Table 3.A7. Means and standard deviations (STDEV) of soil C stock estimates (Kg C m -2) collected by GPR over the 80 m hillslope site, averaged along 10 m segments. Additional averaging for soil C stock means across slope positions (0 - 40 m upslope, 40 - 80 m downslope) are calculated from the 10 m segment data.

Slope (m)	Horizon	Soil C Stocks Means ± (STDEV) (Kg C m^{-2})	Slope Mean	Horizon	Soil C Stocks Means ± (STDEV) (Kg C m^{-2})	Slope Mean	Horizon	Soil C Stocks Means ± (STDEV) (Kg C m^{-2})	Slope Mean
0 - 10	Bf	1.01 ± (0.85)	0.99 ± (0.77)	Bfj	0.53 ± (0.47)	0.71 ± (0.66)	BC	0.85 ± (0.80)	0.81 ± (0.78)
10 - 20	Bf	0.92 ± (0.70)		Bfj	0.64 ± (0.54)		BC	0.74 ± (0.68)	
20 - 30	Bf	1.01 ± (0.74)		Bfj	0.69 ± (0.60)		BC	0.71 ± (0.66)	
30 – 40	Bf	1.00 ± (0.60)		Bfj	0.99 ± (0.81)		BC	0.97 ± (0.70)	
40 – 50	Bf	0.41 ± (0.24)	0.47 ± (0.29)	Bfj	0.50 ± (0.34)	0.48 ± (0.29)	BC	0.38 ± (0.28)	0.40 ± (0.31)
50 – 60	Bf	0.36 ± (0.24)		Bfj	0.51 ± (0.36)		BC	0.39 ± (0.28)	
60 – 70	Bf	0.54 ± (0.13)		Bfj	0.47 ± (0.17)		BC	0.41 ± (0.29)	
70 - 80	Bf	0.57 ± (0.14)		Bfj	0.45 ± (0.19)		BC	0.42 ± (0.32)	

Table 3.A8. Means and standard deviations (STDEV) of soil horizon thickness, bulk density, and C stock estimates for 40 m slope regions (upslope, downslope) as collected by pit scale (1 m sampling position) physical soil sampling method (PSSM) and GPR methods as well as plot scale GPR surveying averaged from 80 hillslope sampling lines averaged along.

Soil Property	Horizon	Slope	Soil Pit Scale PSSM Region Means	Soil Pit Scale GPR Region Means	Hillslope Scale GPR Region Means
Soil Horizon Thickness (cm)	Bf	Up	9.3 ± (1.3)	9.5 ± (3.3)	8.2 ± (3.0)
	Bf	Down	10.0 ± (3.0)	13.7 ± (4.4)	8.0 ± (2.9)
	Bfj	Up	9.3 ± (3.3)	9.6 ± (2.3)	9.2 ± (3.0)
	Bfj	Down	11.3 ± (3.3)	14.7 ± (8.6)	9.4 ± (2.4)
	BC	Up	6.7 ± (1.3)	9.2 ± (2.8)	8.5 ± (2.9)
	BC	Down	9.7 ± (4.3)	12.2 ± (5.4)	8.9 ± (2.4)
Soil Bulk Density (g cm^{-3})	Bf	Up	0.50 ± (0.01)	0.36 ± (0.009)	0.46 ± (0.34)
	Bf	Down	0.68 ± (0.004)	0.33 ± (0.02)	0.62 ± (0.30)
	Bfj	Up	0.39 ± (0.008)	0.21 ± (0.0004)	0.40 ± (0.36)
	Bfj	Down	0.74 ± (0.06)	0.40 ± (0.01)	0.59 ± (0.26)
	BC	Up	0.55 ± (0.07)	0.46 ± (0.13)	0.78 ± (0.60)
	BC	Down	0.68 ± (0.05)	0.46 ± (0.03)	0.69 ± (0.51)
Soil C Stocks (Kg C m^{-2})	Bf	Up	1.19 ± (0.02)	0.87 ± (0.06)	0.99 ± (0.77)
	Bf	Down	0.66 ± (0.04)	0.41 ± (0.03)	0.47 ± (0.29)
	Bfj	Up	0.64 ± (0.02)	0.41 ± (0.06)	0.71 ± (0.66)
	Bfj	Down	0.67 ± (0.10)	0.61 ± (0.28)	0.48 ± (0.29)
	BC	Up	0.42 ± (0.03)	0.49 ± (0.13)	0.81 ± (0.78)
	BC	Down	0.42 ± (0.05)	0.37 ± (0.04)	0.40 ± (0.31)

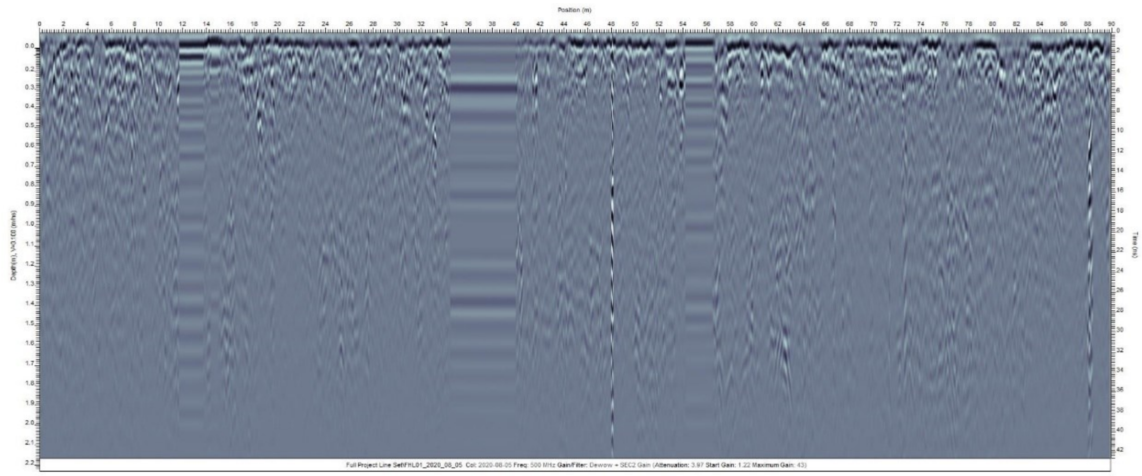
Position (m)

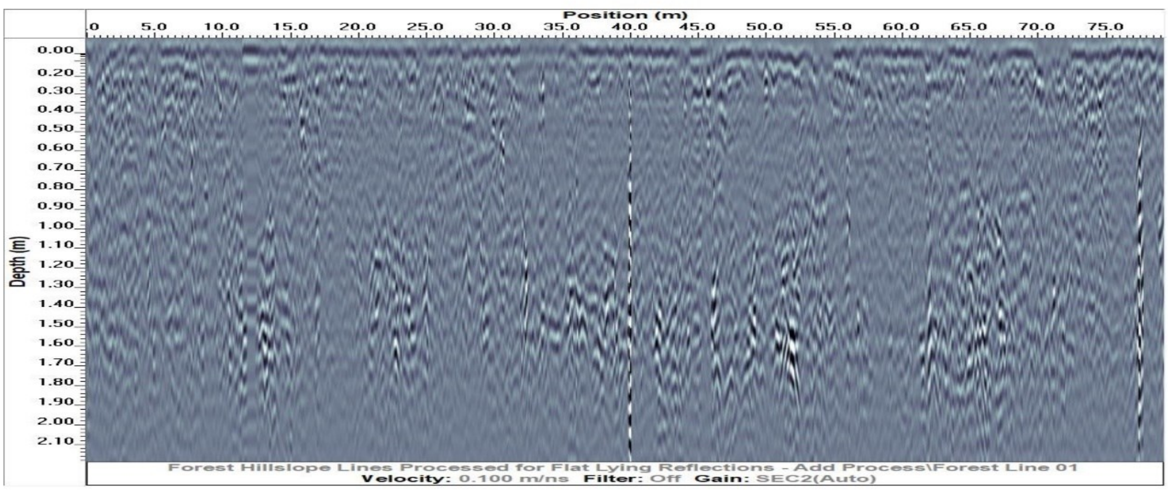
Position (m)
Depth (m)
Forest Hillslope Lines Processed for Flat Lying Reflections - Add Process\Forest Line 01
Velocity: 0.100 m/ns Filter: Off Gain: SEC2(Auto)

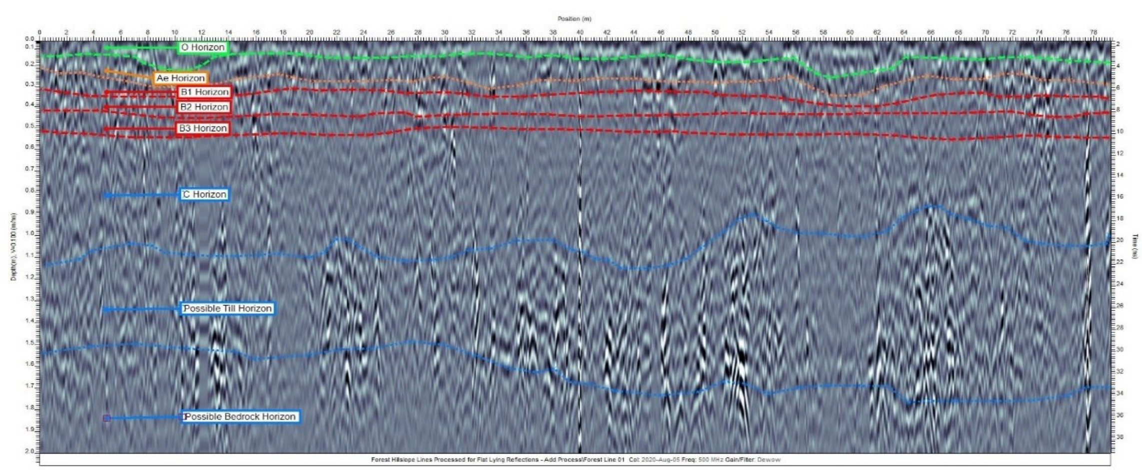
Position (m)
O Horizon
Ae Horizon
B1 Horizon
B2 Horizon
B3 Horizon
C Horizon
Possible Till Horizon
Possible Bedrock Horizon

Figure 3.A1. Radargrams collected by Zachary Gates and Lakshman Galagedara along forest hillslope survey line 1 in the Pynn's Brook Experimental Watershed Area, Newfoundland, Canada, using a 500 MHz Sensors & Software PulseEkko GPR system. The GPR survey line was roughly 80 m long and parallel to the hillslope. The radargram data collected is presented in its unprocessed form (top) and after it has undergone processing for soil horizon thickness measurements as outlined Section 3.2.6 (middle). Interpretations made by Zachary Gates for soil horizon boundary positions (bottom) based on the processed radargram data were used for the evaluation of GPR estimates for forest soil thickness in this study.

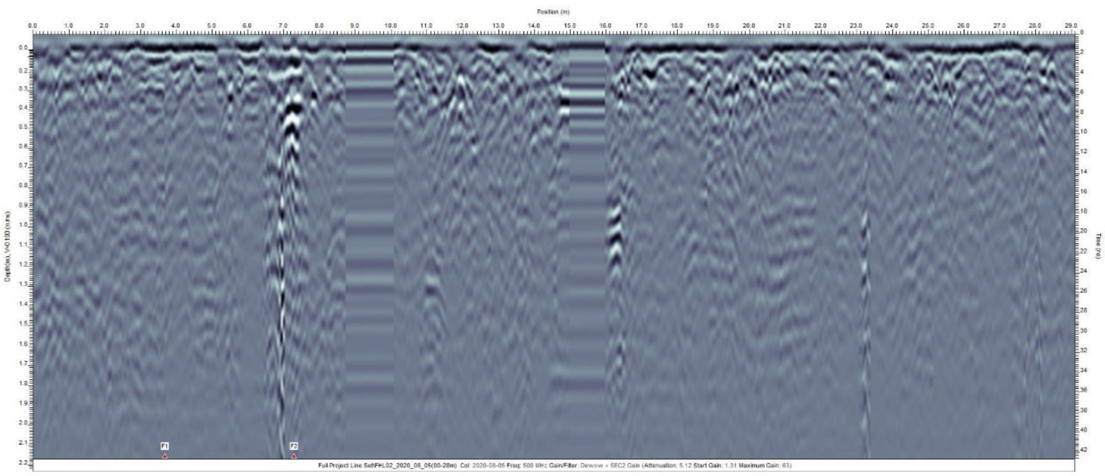
Position (m)
F1
F2

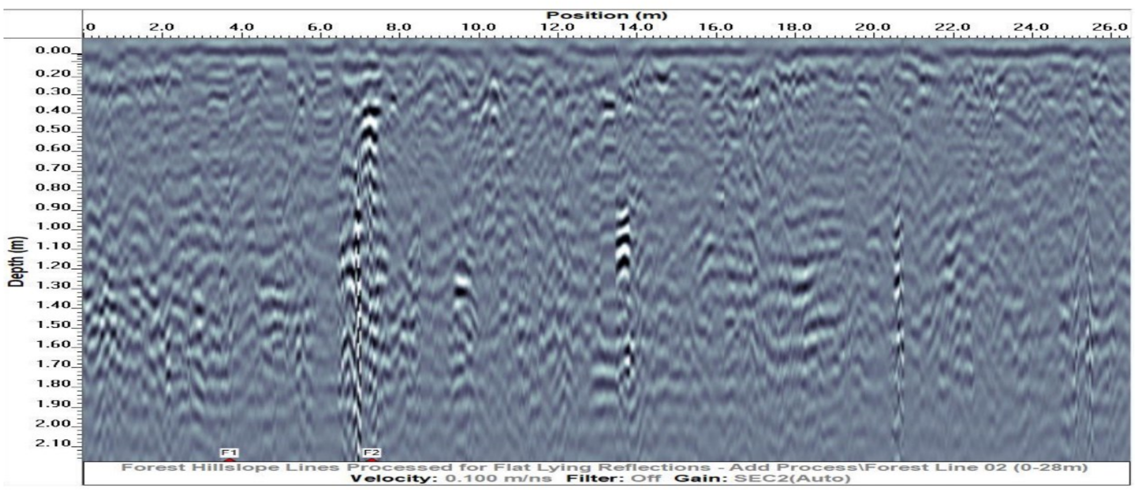
Position (m)
Depth (m)
F1
F2
Forest Hillslope Lines Processed for Flat Lying Reflections - Add Process\Forest Line 02 (0-28m)
Velocity: 0.100 m/ns Filter: Off Gain: SEC2(Auto)

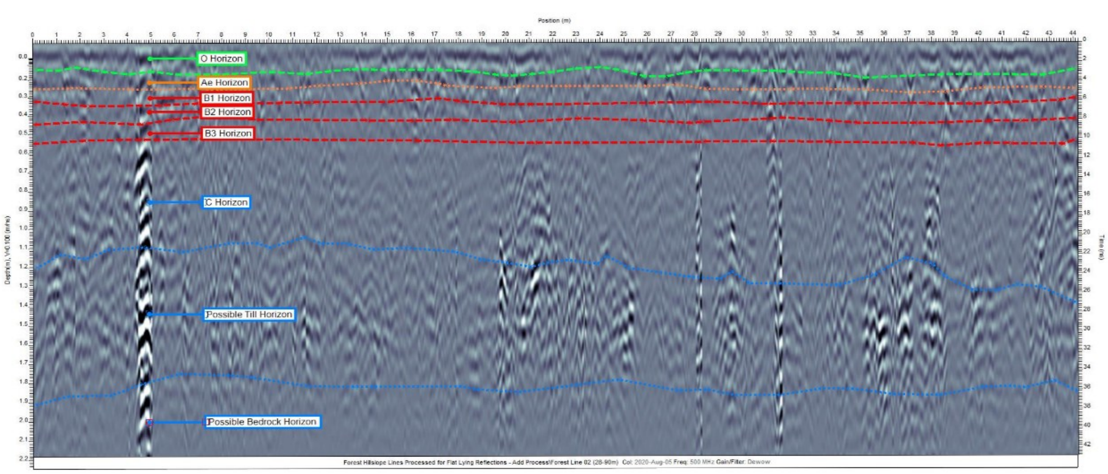
O Horizon
Ae Horizon
B1 Horizon
B2 Horizon
B3 Horizon
C Horizon
Possible Till Horizon
Possible Bedrock Horizon

Figure 3.A2. Radargrams collected by Zachary Gates and Lakshman Galagedara along a section of the forest hillslope survey line 2 in the Pynn's Brook Experimental Watershed Area, Newfoundland, Canada, using a 500 MHz Sensors & Software PulseEkko GPR system. The GPR survey line was roughly 28 m long (radargram data collected from the top of the hillslope to 28 m downslope) and parallel to the hillslope. The radargram data collected is presented in its unprocessed form (top) and after it has undergone processing for soil horizon thickness measurements as outlined Section 3.2.6 (middle). Interpretations made by Zachary Gates for soil horizon boundary positions (bottom) based on the processed radargram data were used for the evaluation of GPR estimates for forest soil thickness in this study.

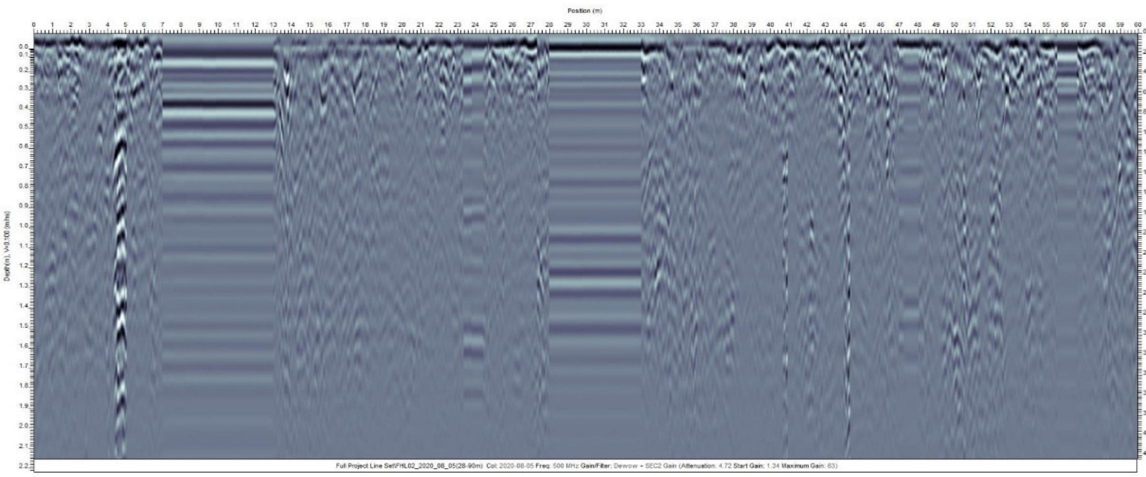
Position (m)

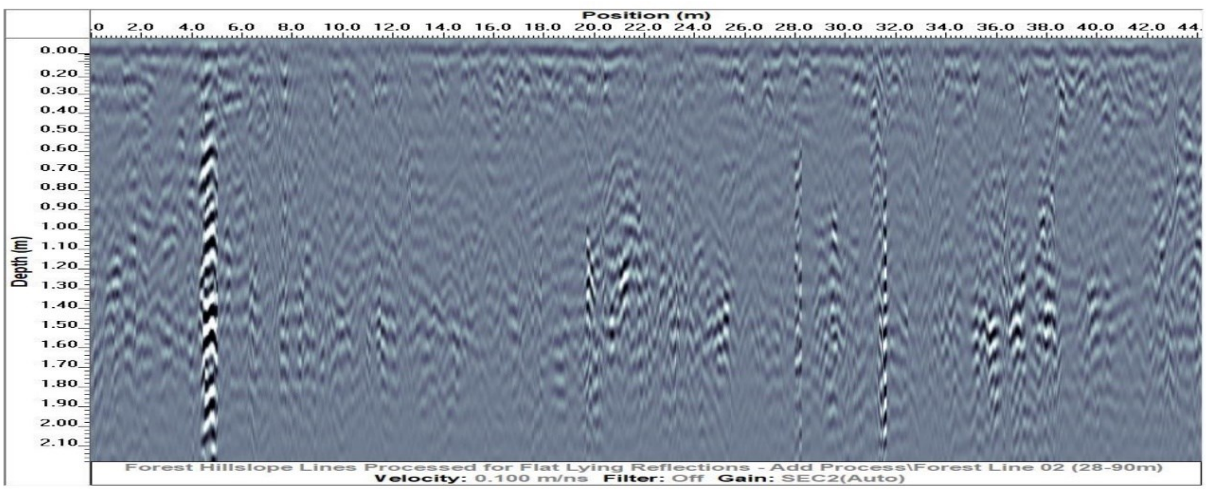
Position (m)
Depth (m)
Forest Hillslope Lines Processed for Flat Lying Reflections - Add Process\Forest Line 02 (28-90m)
Velocity: 0.100 m/ns Filter: Off Gain: SEC2(Auto)

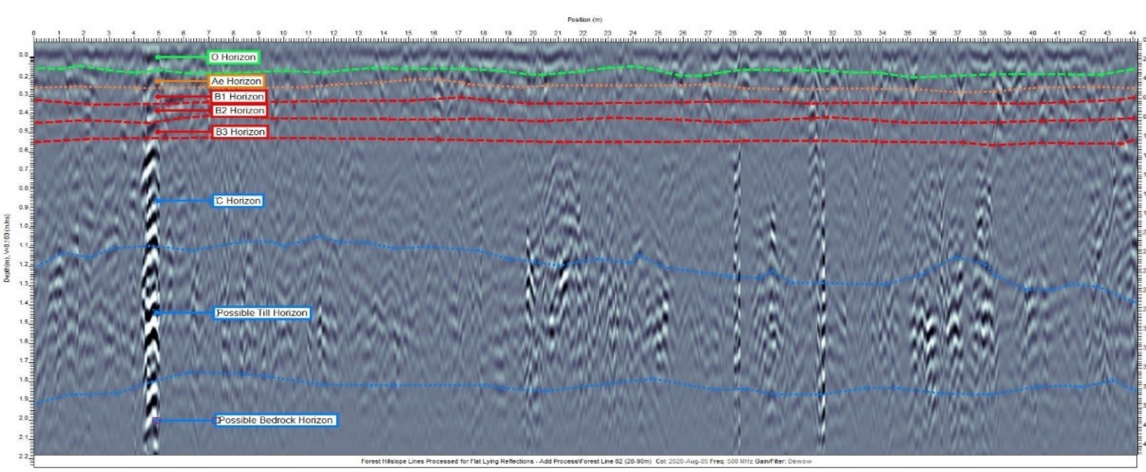
Position (m)
O Horizon
Ae Horizon
B1 Horizon
B2 Horizon
B3 Horizon
C Horizon
Possible Till Horizon
Possible Bedrock Horizon

Figure 3.A3. Radargrams collected by Zachary Gates and Lakshman Galagedara along a section of the forest hillslope survey line 2 in the Pynn's Brook Experimental Watershed Area, Newfoundland, Canada, using a 500 MHz Sensors & Software PulseEkko GPR system. The GPR survey line was roughly 60 m long (radargram data collected from 29 m downslope from the top of the hillslope to the bottom of the slope) and parallel to the hillslope. The radargram data collected is presented in its unprocessed form (top) and after it has undergone processing for soil horizon thickness measurements as outlined Section 3.2.6 (middle). Interpretations made by Zachary Gates for soil horizon boundary positions (bottom) based on the processed radargram data were used for the evaluation of GPR estimates for forest soil thickness in this study.

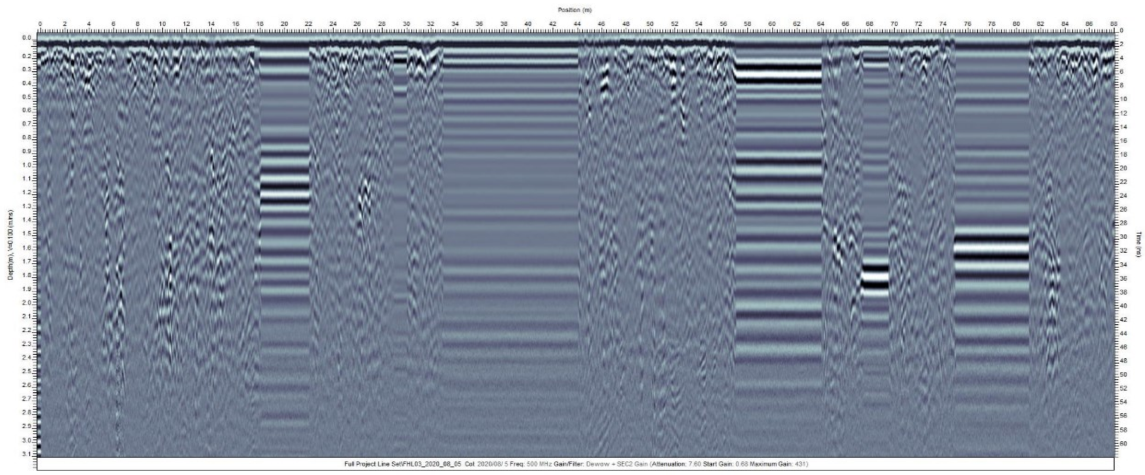

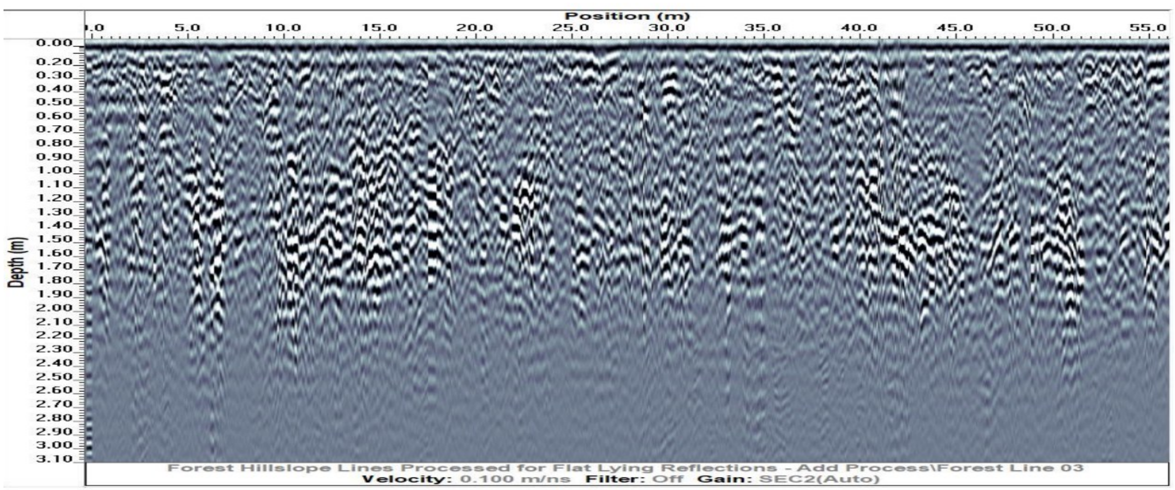
Position (m)
Depth (m)
Forest Hillslope Lines Processed for Flat Lying Reflections - Add Process\Forest Line 03
Velocity: 0.100 m/ns Filter: Off Gain: SEC2(Auto)

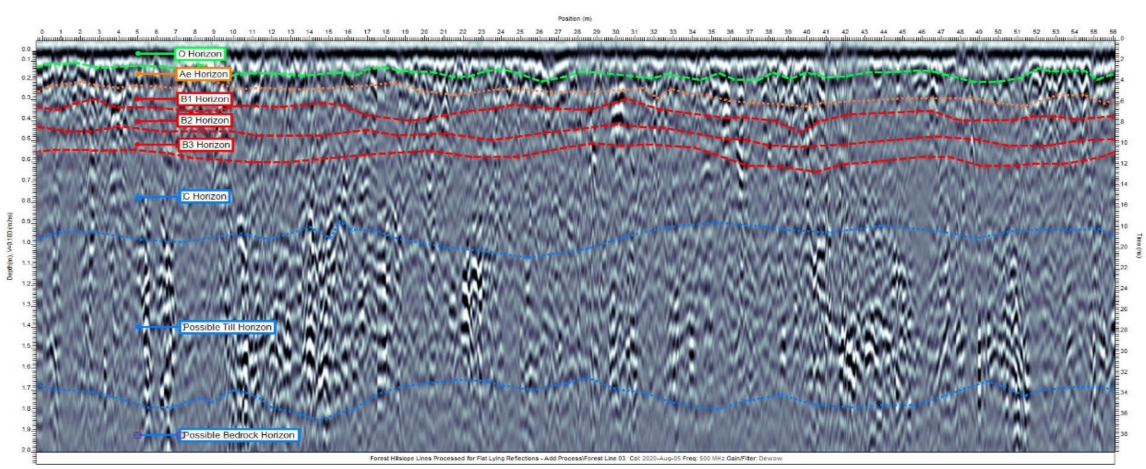
O Horizon
Ae Horizon
B1 Horizon
B2 Horizon
B3 Horizon
C Horizon
Possible Till Horizon
Possible Bedrock Horizon

Figure 3.A4. Radargrams collected by Zachary Gates and Lakshman Galagedara along forest hillslope survey line 3 in the Pynn's Brook Experimental Watershed Area, Newfoundland, Canada, using a 500 MHz Sensors & Software PulseEkko GPR system. The GPR survey line was roughly 80 m long and parallel to the hillslope. The radargram data collected is presented in its unprocessed form (top) and after it has undergone processing for soil horizon thickness measurements as outlined Section 3.2.6 (middle). Interpretations made by Zachary Gates for soil horizon boundary positions (bottom) based on the processed radargram data were used for the evaluation of GPR estimates for forest soil thickness in this study.

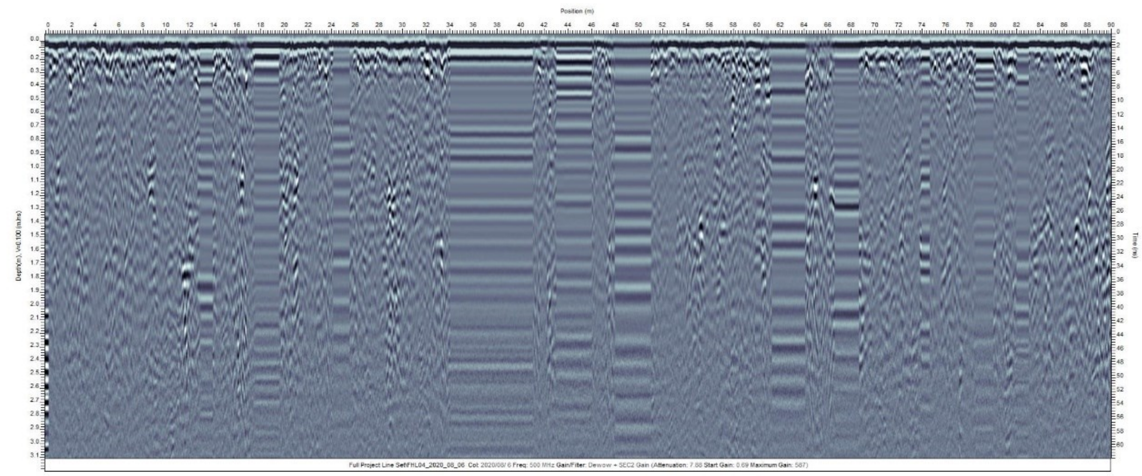
Position (m)
Full Project Line Set\FHL04_2020_08_06 Col: 2020/08/ 6 Freq: 500 MHz Gain/Filter: Dewow + SEC2 Gain (Attenuation: 7.88 Start Gain: 0.69 Maximum Gain: 587)

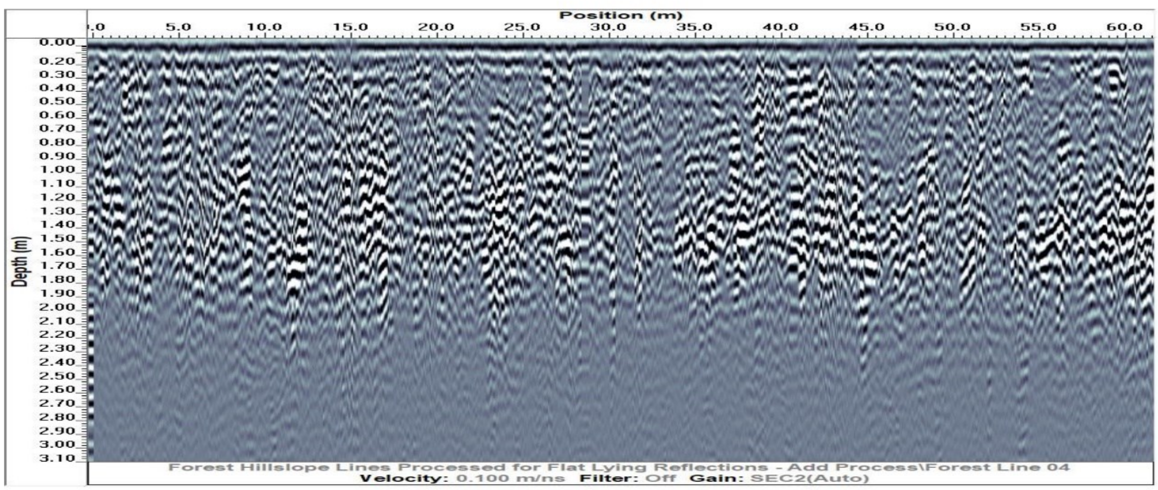
Position (m)
Depth (m)
Forest Hillslope Lines Processed for Flat Lying Reflections - Add Process\Forest Line 04
Velocity: 0.100 m/ns Filter: Off Gain: SEC2(Auto)

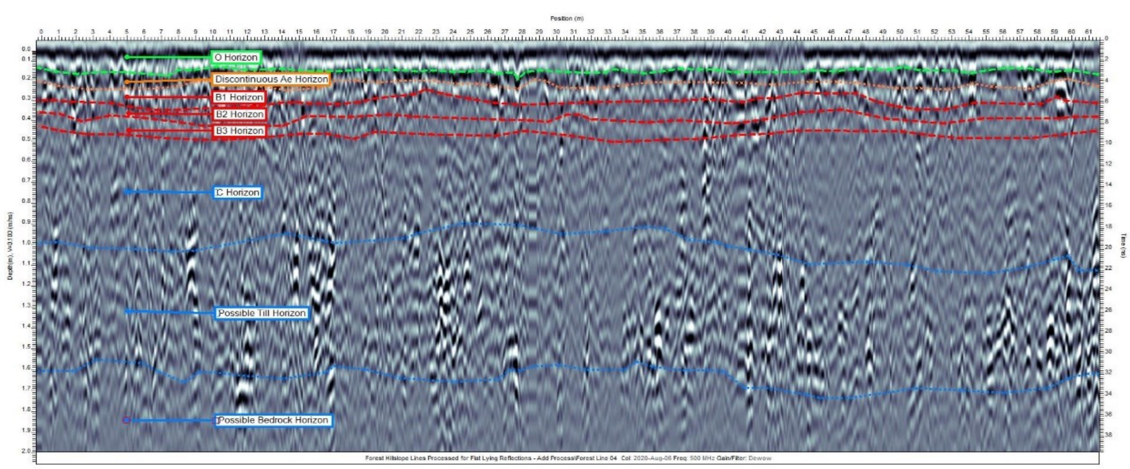
Position (m)
O Horizon
Discontinuous Ae Horizon
B1 Horizon
B2 Horizon
B3 Horizon
C Horizon
Possible Till Horizon
Possible Bedrock Horizon
Forest Hillslope Lines Processed for Flat Lying Reflections - Add Process\Forest Line 04 Col: 2020-Aug-06 Freq: 500 MHz Gain/Filter: Dewow

Figure 3.A5. Radargrams collected by Zachary Gates and Lakshman Galagedara along forest hillslope survey line 4 in the Pynn's Brook Experimental Watershed Area, Newfoundland, Canada, using a 500 MHz Sensors & Software PulseEkko GPR system. The GPR survey line was roughly 80 m long and parallel to the hillslope. The radargram data collected is presented in its unprocessed form (top) and after it has undergone processing for soil horizon thickness measurements as outlined Section 3.2.6 (middle). Interpretations made by Zachary Gates for soil horizon boundary positions (bottom) based on the processed radargram data were used for the evaluation of GPR estimates for forest soil thickness in this study.

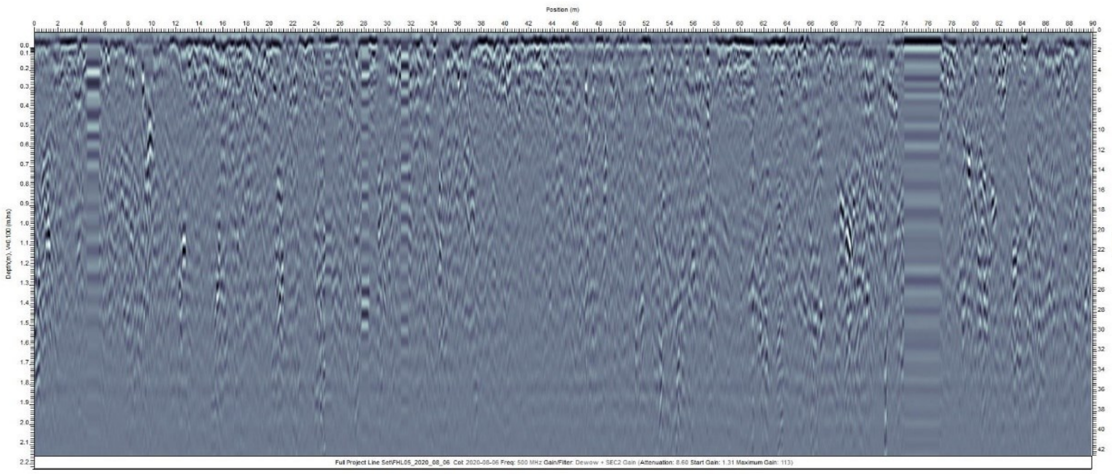
Position (m)

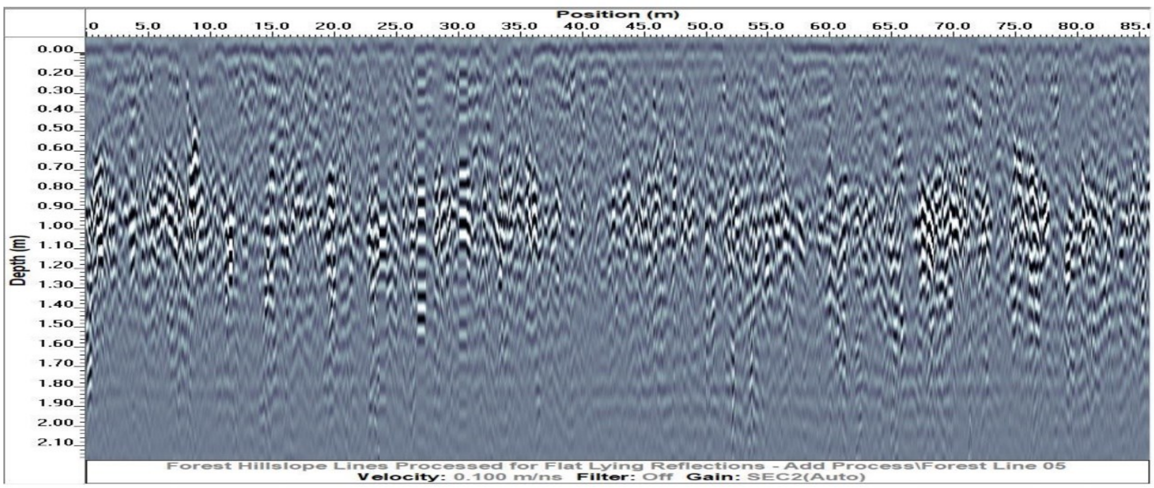
Position (m)
Depth (m)
Forest Hillslope Lines Processed for Flat Lying Reflections - Add Process\Forest Line 05
Velocity: 0.100 m/ns Filter: Off Gain: SEC2(Auto)

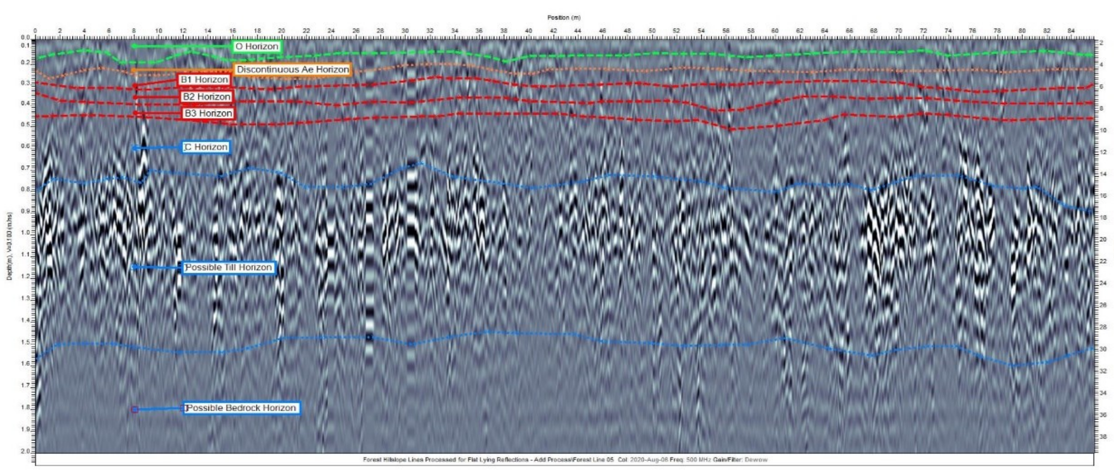
Position (m)
O Horizon
Discontinuous Ae Horizon
B1 Horizon
B2 Horizon
B3 Horizon
C Horizon
Possible Till Horizon
Possible Bedrock Horizon

Figure 3.A6. Radargrams collected by Zachary Gates and Lakshman Galagedara along forest hillslope survey line 5 in the Pynn's Brook Experimental Watershed Area, Newfoundland, Canada, using a 500 MHz Sensors & Software PulseEkko GPR system. The GPR survey line was roughly 80 m long and parallel to the hillslope. The radargram data collected is presented in its unprocessed form (top) and after it has undergone processing for soil horizon thickness measurements as outlined Section 3.2.6 (middle). Interpretations made by Zachary Gates for soil horizon boundary positions (bottom) based on the processed radargram data were used for the evaluation of GPR estimates for forest soil thickness in this study.

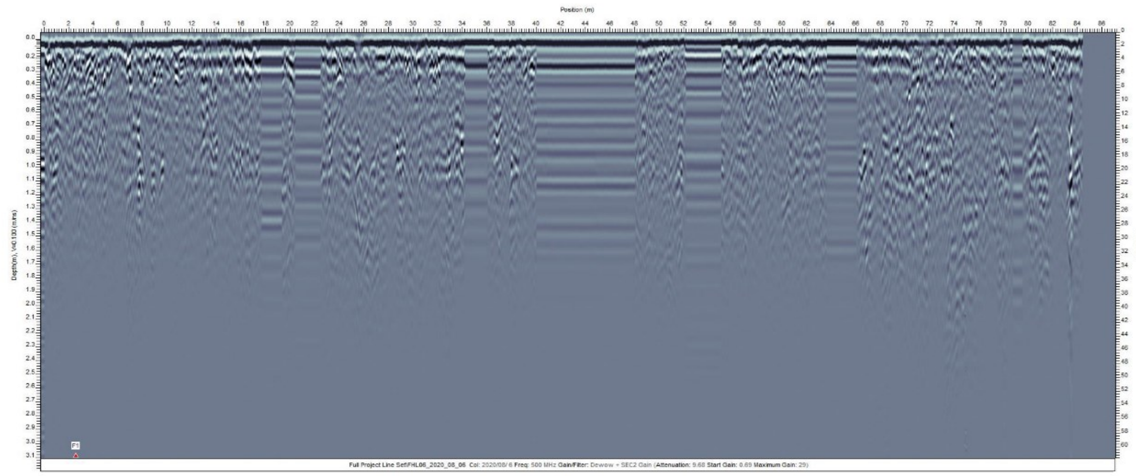
Position (m)
Depth(m), V=0.100 (m/ns)
Time (ns)
F1
Full Project Line Set\FHL06_2020_08_06 Col: 2020/08/ 6 Freq: 500 MHz Gain/Filter: Dewow + SEC2 Gain (Attenuation: 9.68 Start Gain: 0.69 Maximum Gain: 29)

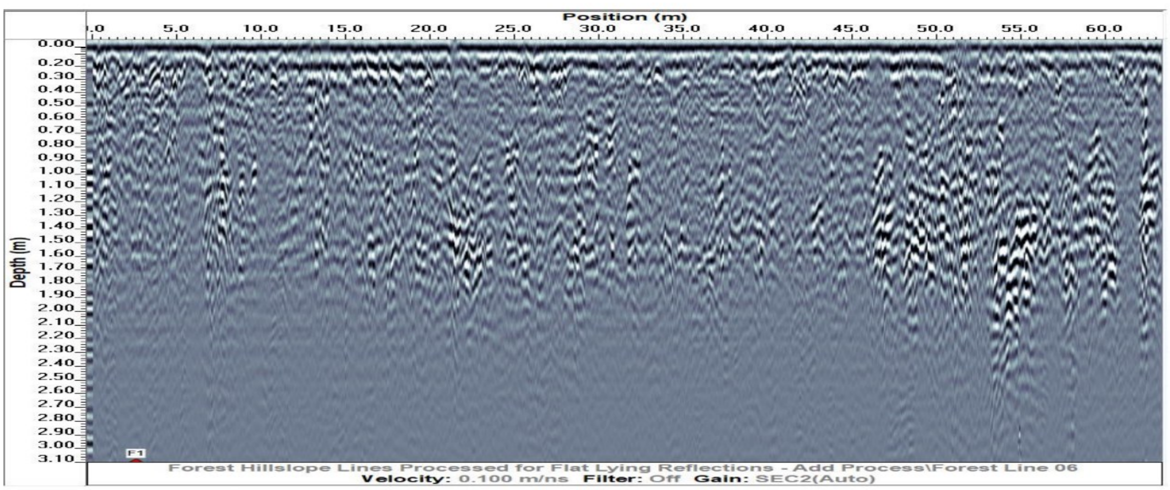
Position (m)
Depth (m)
F1
Forest Hillslope Lines Processed for Flat Lying Reflections - Add Process\Forest Line 06
Velocity: 0.100 m/ns Filter: Off Gain: SEC2(Auto)

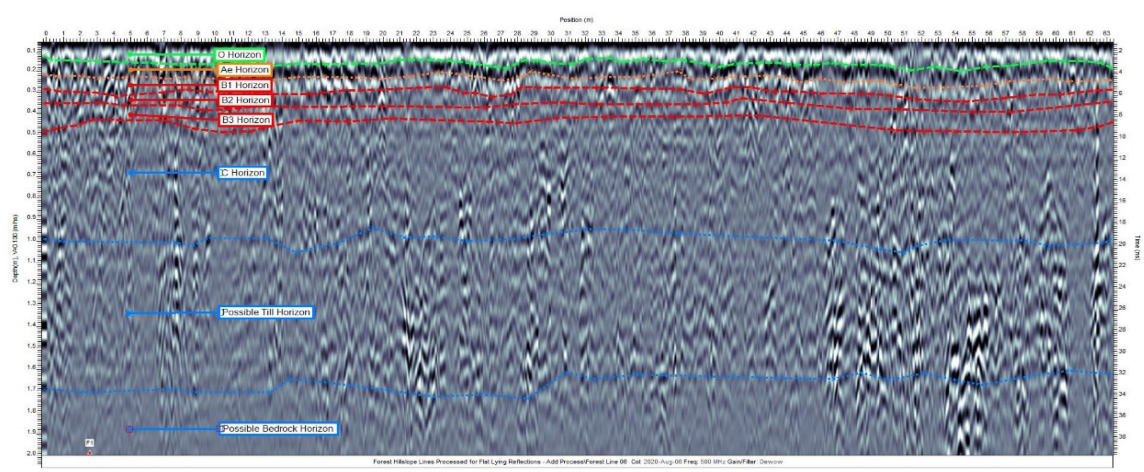
Position (m)
O Horizon
Ae Horizon
B1 Horizon
B2 Horizon
B3 Horizon
C Horizon
Possible Till Horizon
Possible Bedrock Horizon
Time (ns)
F1
Forest Hillslope Lines Processed for Flat Lying Reflections - Add Process\Forest Line 06 Col: 2020-Aug-06 Freq: 500 MHz Gain/Filter: Dewow

Figure 3.A7. Radargrams collected by Zachary Gates and Lakshman Galagedara along forest hillslope survey line 7 in the Pynn's Brook Experimental Watershed Area, Newfoundland, Canada, using a 500 MHz Sensors & Software PulseEkko GPR system. The GPR survey line was roughly 80 m long and parallel to the hillslope. The radargram data collected is presented in its unprocessed form (top) and after it has undergone processing for soil horizon thickness measurements as outlined Section 3.2.6 (middle). Interpretations made by Zachary Gates for soil horizon boundary positions (bottom) based on the processed radargram data were used for the evaluation of GPR estimates for forest soil thickness in this study.

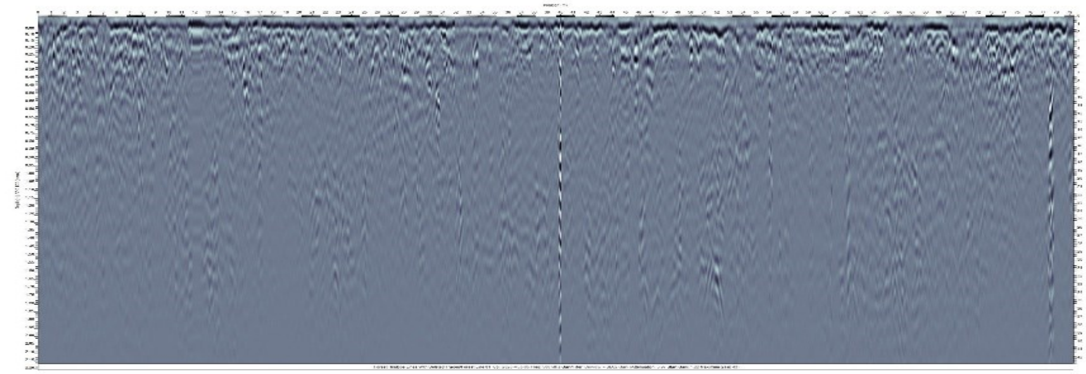

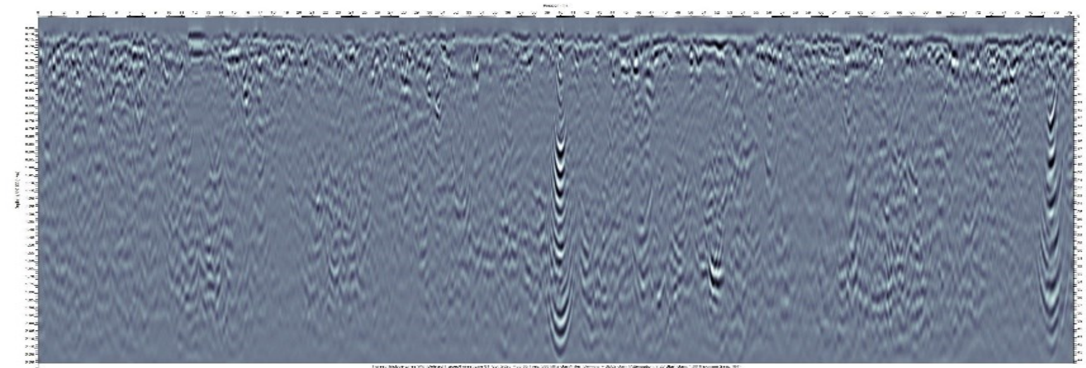

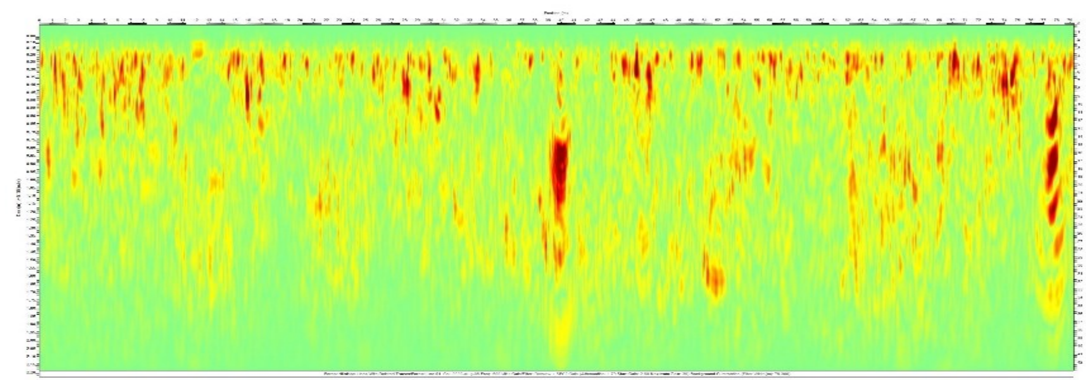

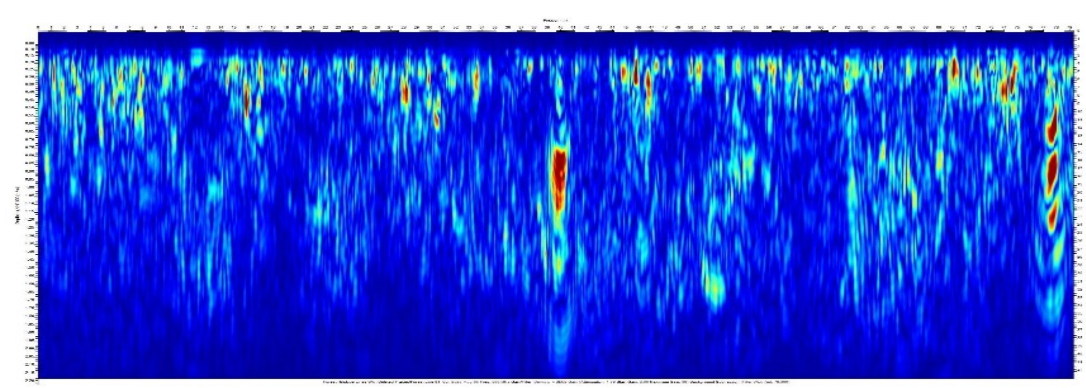

Figure 3.A8. Radargrams collected by Zachary Gates and Lakshman along forest hillslope survey line 1 in the Pynn's Brook Experimental Watershed Area, Newfoundland, Canada, using a 500 MHz Sensors & Software PulseEkko GPR system. The GPR survey line was roughly 80 m long and parallel to the hillslope. The radargram data collected is presented in its unprocessed form (top) and after it has undergone processing for soil bulk density measurements as outlined Section 3.2.7 (middle). The processed radargram data underwent Hilbert Transformation, processed By Zachary Gates, using EkkoProject 5's Assisted Pick Processing tool. The transformed radargram data is displayed under polarized (c) and nonpolarized (d) scaling and used to assess soil, rock, and root distribution for estimates of forest soil bulk density.

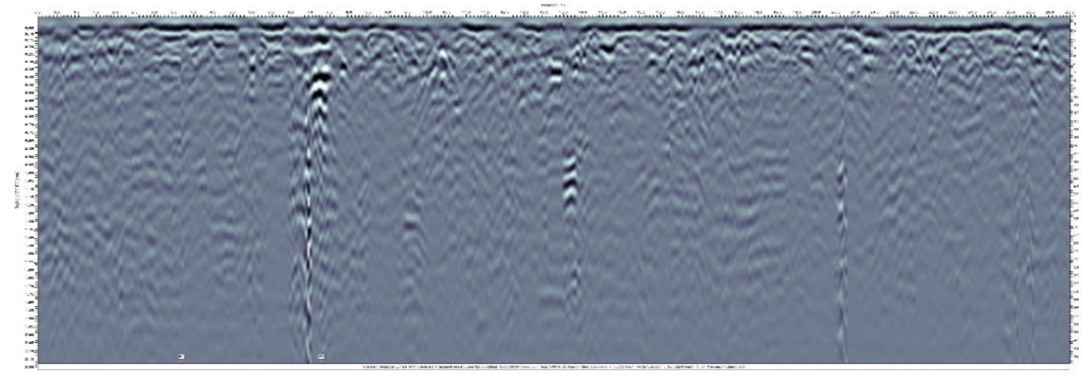

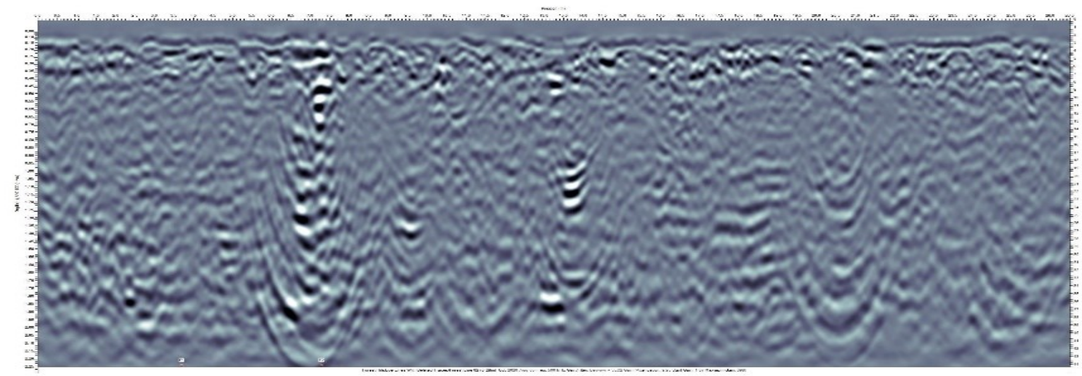

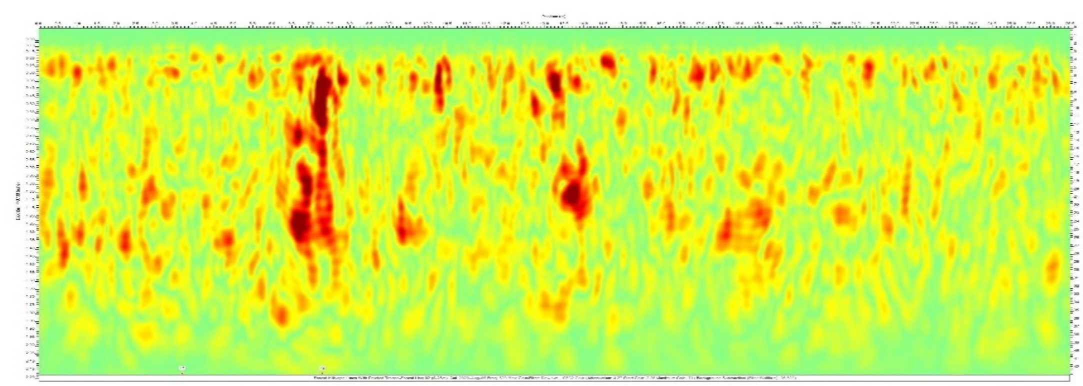

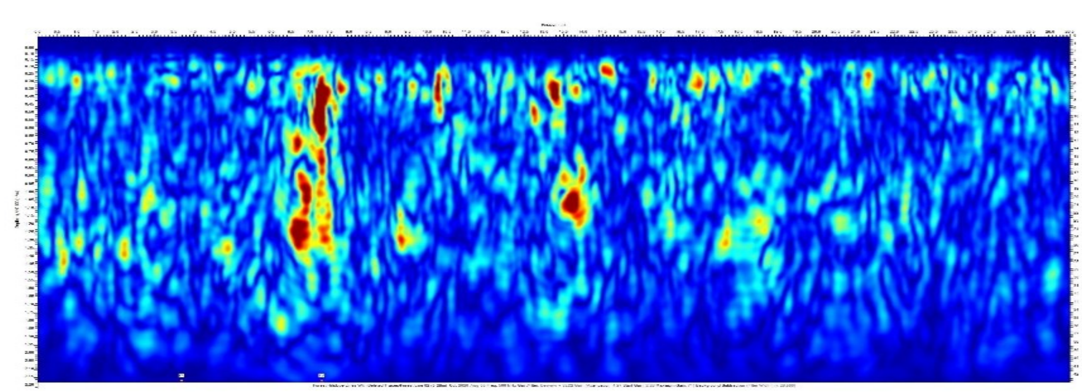

Figure 3.A9. Radargrams collected by Zachary Gates and Lakshman Galagedara along a section of the forest hillslope survey line 2 in the Pynn's Brook Experimental Watershed Area, Newfoundland, Canada, using a 500 MHz Sensors & Software PulseEkko GPR system. The GPR survey line was roughly 28 m long (radargram data collected from the top of the hillslope to 28 m downslope) and parallel to the hillslope. The radargram data collected is presented in its unprocessed form (top) and after it has undergone processing for soil bulk density measurements as outlined Section 3.2.7 (middle). The processed radargram data underwent Hilbert Transformation, processed By Zachary Gates, using EkkoProject 5's Assisted Pick Processing tool. The transformed radargram data is displayed under polarized (c) and nonpolarized (d) scaling and used to assess soil, rock, and root distribution for estimates of forest soil bulk density.

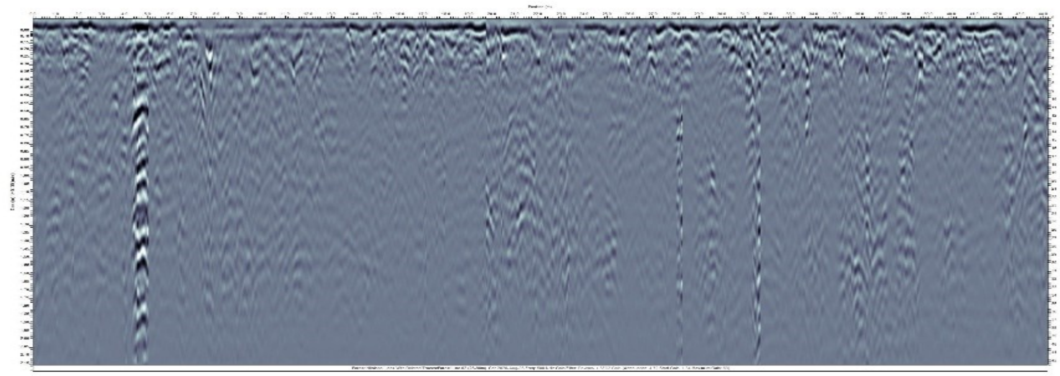

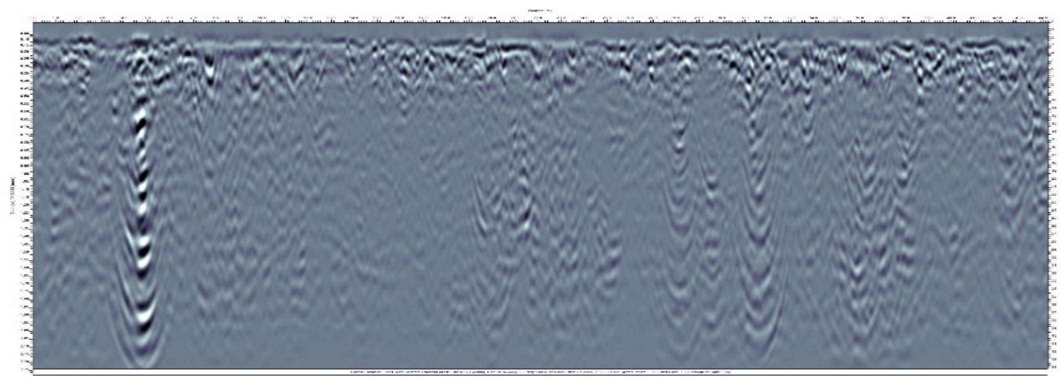

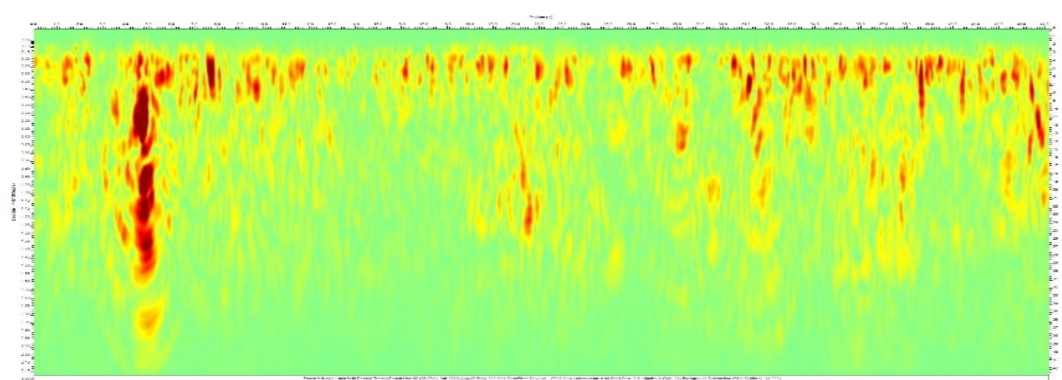

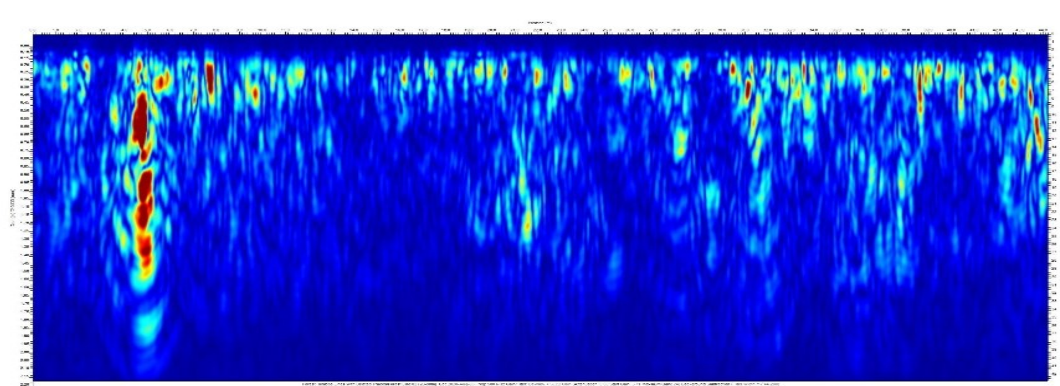

Figure 3.A10. Radargrams collected by Zachary Gates and Lakshman Galagedara along a section of the forest hillslope survey line 2 in the Pynn's Brook Experimental Watershed Area, Newfoundland, Canada, using a 500 MHz Sensors & Software PulseEkko GPR system. The GPR survey line was roughly 60 m long (radargram data collected from 29 m downslope from the top of the hillslope to the bottom of the slope) and parallel to the hillslope. The radargram data collected is presented in its unprocessed form (top) and after it has undergone processing for soil bulk density measurements as outlined Section 3.2.7 (middle). The processed radargram data underwent Hilbert Transformation, processed By Zachary Gates, using EkkoProject 5's Assisted Pick Processing tool. The transformed radargram data is displayed under polarized (c) and nonpolarized (d) scaling and used to assess soil, rock, and root distribution for estimates of forest soil bulk density.

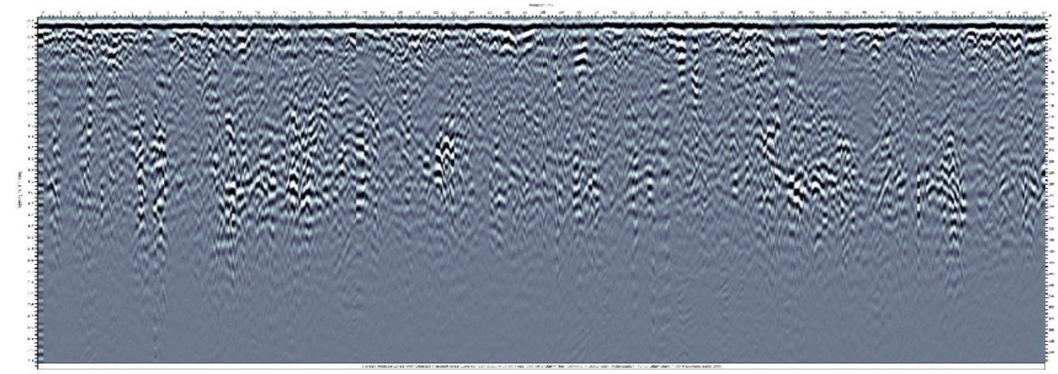

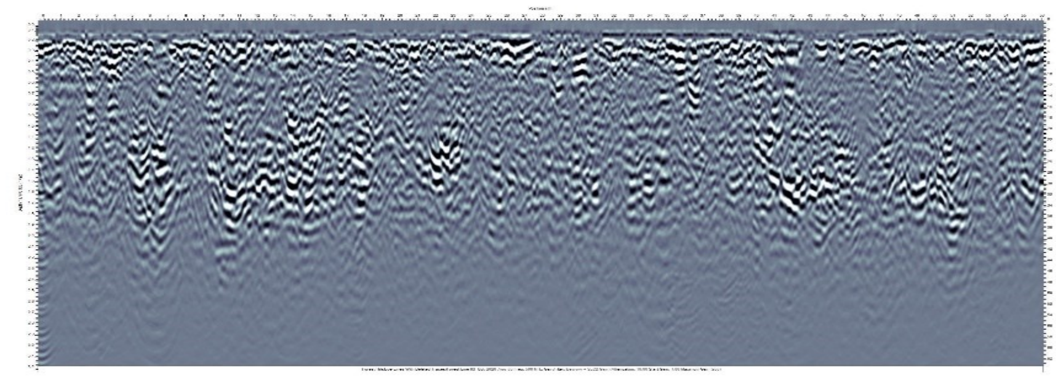

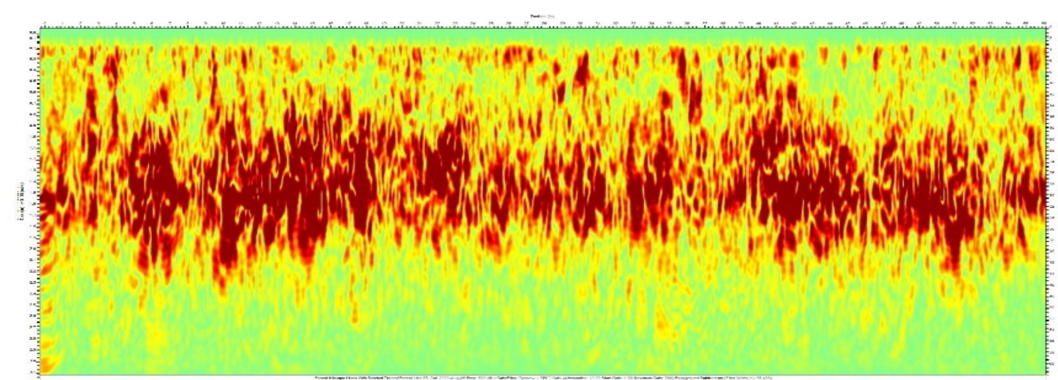

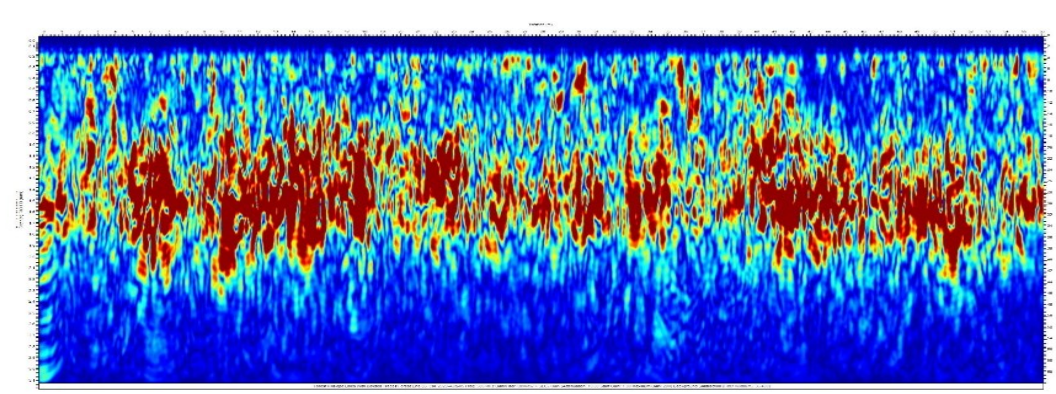

Figure 3.A11. Radargrams collected by Zachary Gates and Lakshman along forest hillslope survey line 3 in the Pynn's Brook Experimental Watershed Area, Newfoundland, Canada, using a 500 MHz Sensors & Software PulseEkko GPR system. The GPR survey line was roughly 80 m long and parallel to the hillslope. The radargram data collected is presented in its unprocessed form (top) and after it has undergone processing for soil bulk density measurements as outlined Section 3.2.7 (middle). The processed radargram data underwent Hilbert Transformation, processed By Zachary Gates, using EkkoProject 5's Assisted Pick Processing tool. The transformed radargram data is displayed under polarized (c) and nonpolarized (d) scaling and used to assess soil, rock, and root distribution for estimates of forest soil bulk density.

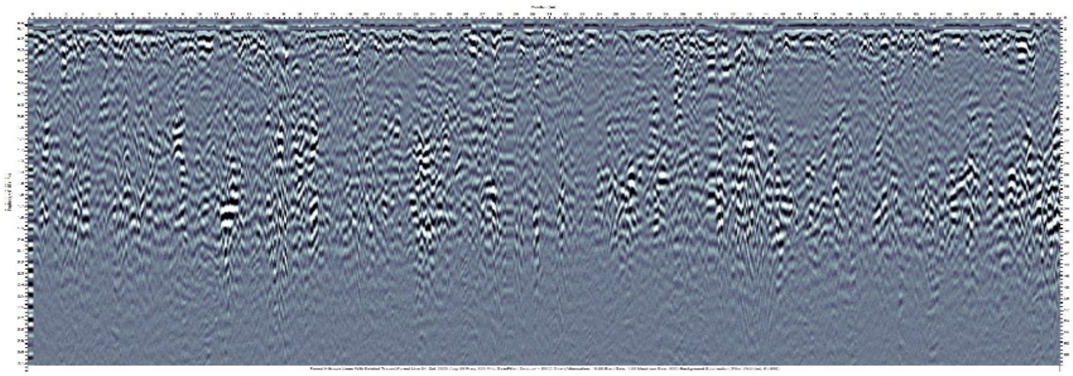

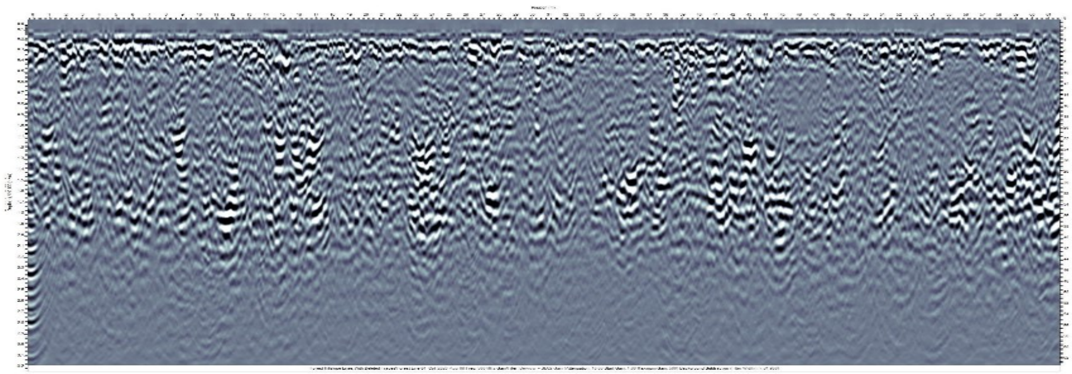

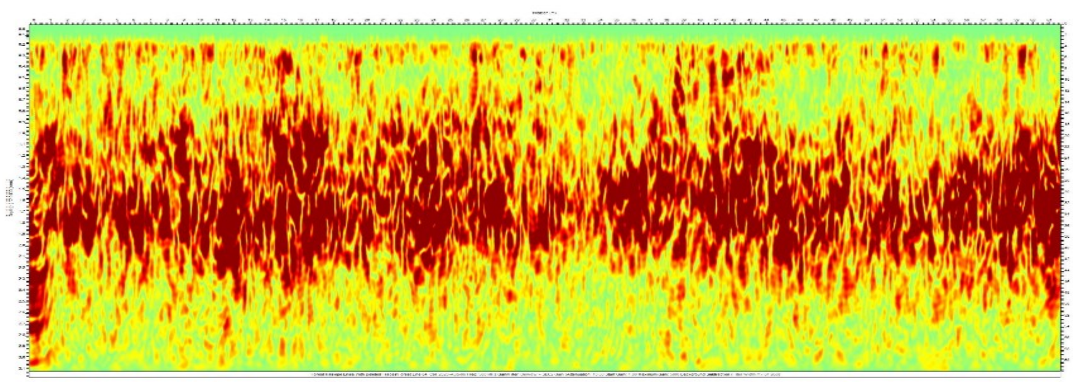

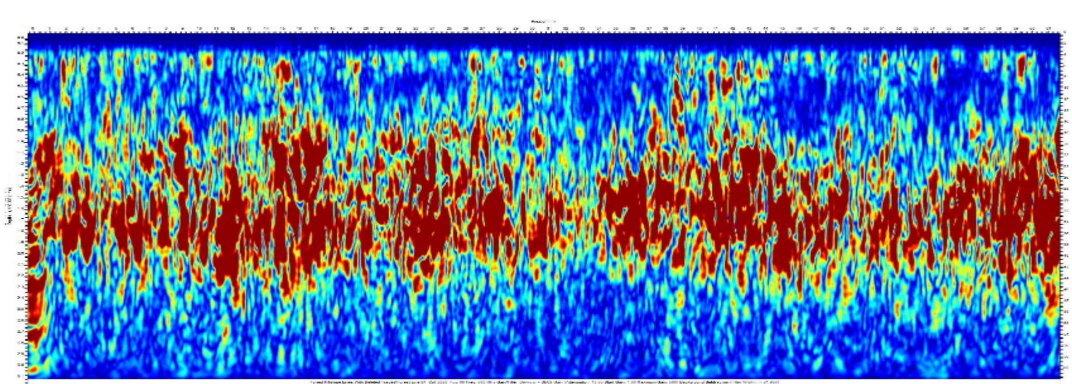

Figure 3.A12. Radargrams collected by Zachary Gates and Lakshman along forest hillslope survey line 4 in the Pynn's Brook Experimental Watershed Area, Newfoundland, Canada, using a 500 MHz Sensors & Software PulseEkko GPR system. The GPR survey line was roughly 80 m long and parallel to the hillslope. The radargram data collected is presented in its unprocessed form (top) and after it has undergone processing for soil bulk density measurements as outlined Section 3.2.7 (middle). The processed radargram data underwent Hilbert Transformation, processed By Zachary Gates, using EkkoProject 5's Assisted Pick Processing tool. The transformed radargram data is displayed under polarized (c) and nonpolarized (d) scaling and used to assess soil, rock, and root distribution for estimates of forest soil bulk density.

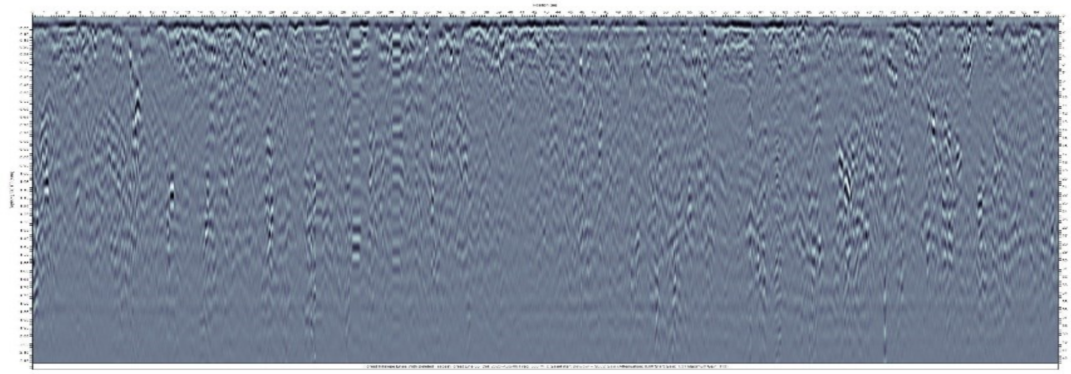

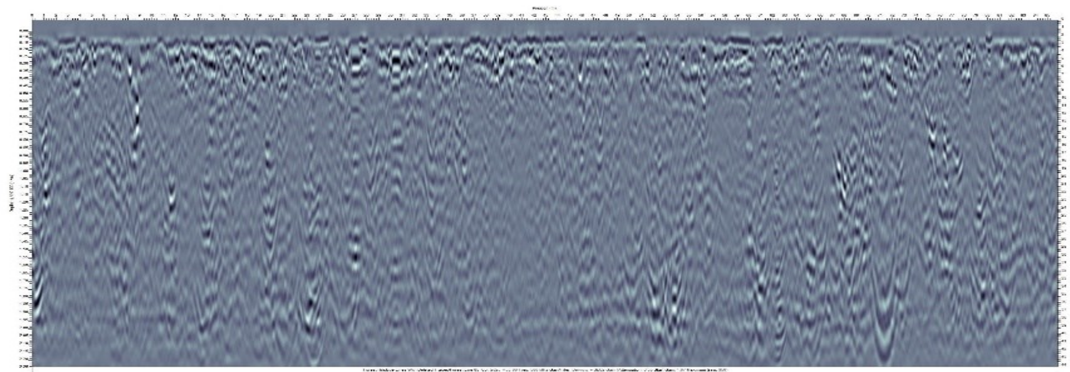

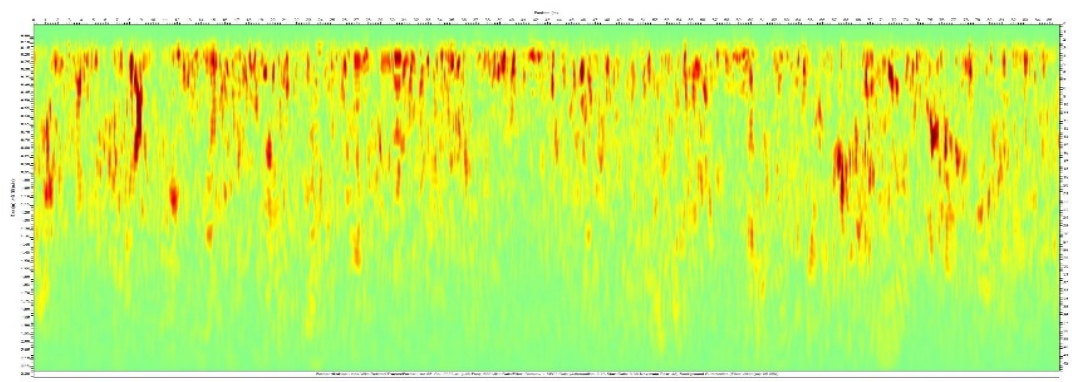

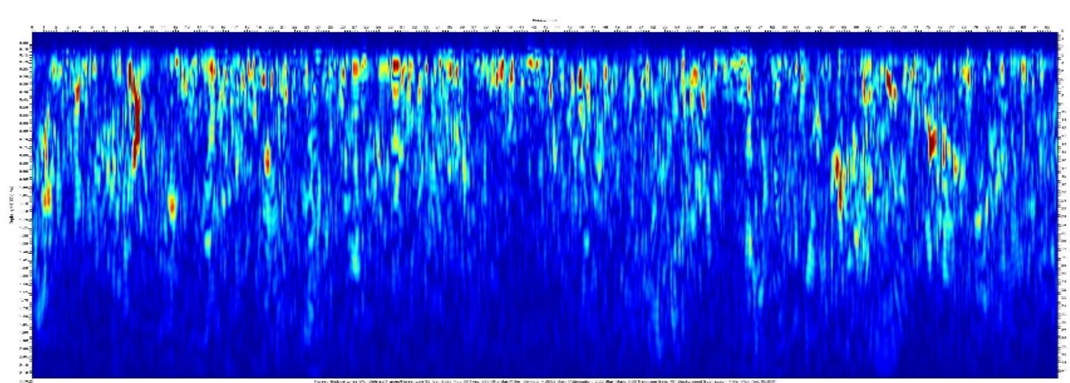

Figure 3.A13. Radargrams collected by Zachary Gates and Lakshman along forest hillslope survey line 5 in the Pynn's Brook Experimental Watershed Area, Newfoundland, Canada, using a 500 MHz Sensors & Software PulseEkko GPR system. The GPR survey line was roughly 80 m long and parallel to the hillslope. The radargram data collected is presented in its unprocessed form (top) and after it has undergone processing for soil bulk density measurements as outlined Section 3.2.7 (middle). The processed radargram data underwent Hilbert Transformation, processed by Zachary Gates, using EkkoProject 5's Assisted Pick Processing tool. The transformed radargram data is displayed under polarized (c) and nonpolarized (d) scaling and used to assess soil, rock, and root distribution for estimates of forest soil bulk density.

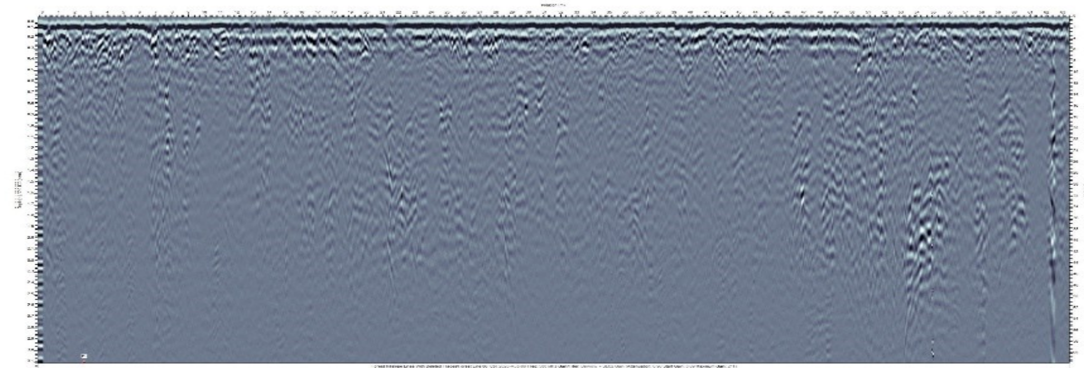

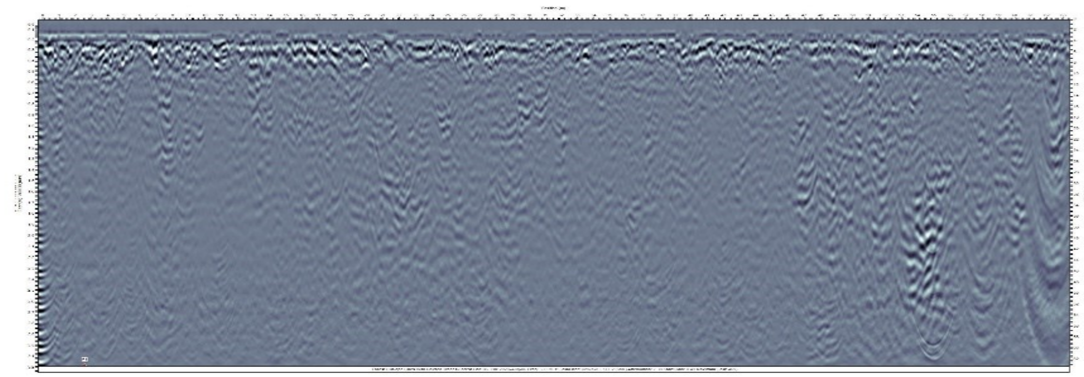

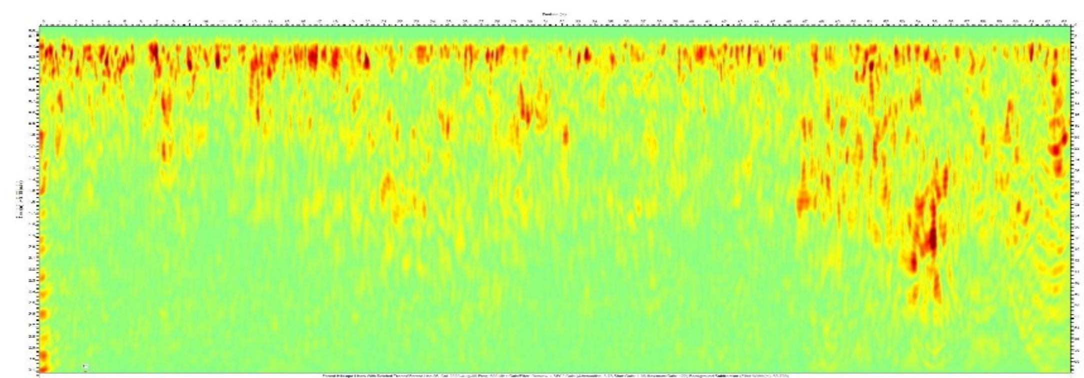

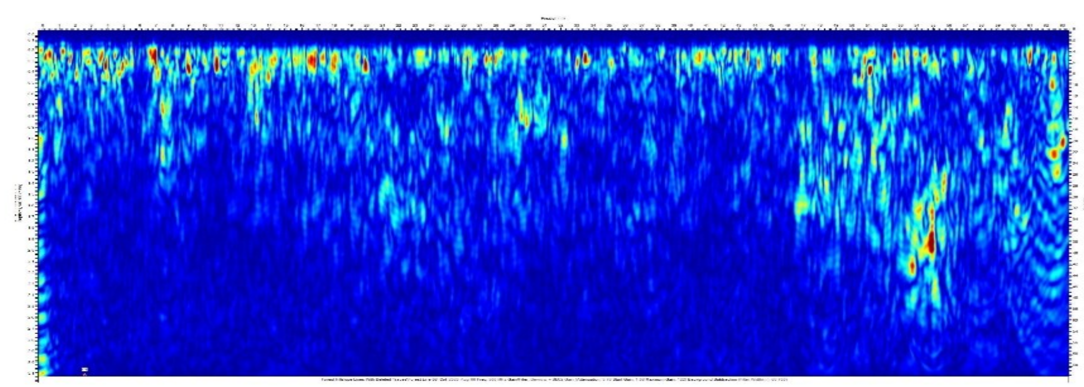

Figure 3.A14. Radargrams collected by Zachary Gates and Lakshman along forest hillslope survey line 6 in the Pynn's Brook Experimental Watershed Area, Newfoundland, Canada, using a 500 MHz Sensors & Software PulseEkko GPR system. The GPR survey line was roughly 80 m long and parallel to the hillslope. The radargram data collected is presented in its unprocessed form (top) and after it has undergone processing for soil bulk density measurements as outlined Section 3.2.7 (middle). The processed radargram data underwent Hilbert Transformation, processed by Zachary Gates, using EkkoProject 5's Assisted Pick Processing tool. The transformed radargram data is displayed under polarized (c) and nonpolarized (d) scaling and used to assess soil, rock, and root distribution for estimates of forest soil bulk density.

CHAPTER 4

Conclusions

4.1 Goals and achievements of this study

The research completed for this study aimed to fill the gaps of knowledge in forest soil C distribution that arise due to a lack of continuous, deep, large spatial scale soil property data. The means to obtain this soil property data at larger scales were identified in Chapter 2. By reviewing published literature on forest GPR surveys we were able to compile these findings into an optimized GPR method for obtaining estimates of soil horizon thickness and soil bulk density in difficult forest environments. Furthermore, this study verified the usefulness of these optimized GPR methods in Chapter 3 through comparison with physical soil sampling methods at small spatial scales and by applying the developed optimized methodology to a large-scale investigation of soil C distribution across a boreal forest hillslope in Pynn's Brook, Newfoundland.

The larger scale, higher resolution soil property sampling possible through this optimized GPR method allowed for a better understanding of soil C distribution across the boreal forest hillslope. This was accomplished through large-scale data collection across a higher range of soil horizon thickness and soil bulk density samples which provided more expansive soil property datasets that account for larger volumes of soil both laterally and with depth than physical soil sampling methods. Furthermore, continuous data collection across the landscape possible by optimized GPR methods allowed for the identification of linkages between observed trends in soil property measurements and controls on soil C distribution, such as the control on soil C exerted by soil bulk density distribution. Thus, optimized GPR methods were able to identify landscape distribution and trends as sources for variability in GPR estimates of soil horizon thickness and soil bulk density estimates as well as soil C distribution as represented through soil C stocks. As such, the goals of this research were addressed as the optimized GPR methods from Chapter 2 were able to assess soil heterogeneity and landscape trends for soil horizon thickness and soil bulk density in Chapter with depth and slope position at small and large scales and observe trends in these soil properties within horizons at specific hillslope positions as well as across the slope, for mineral soil horizons layer.

4.2 Ground penetrating radar optimization recommendations for forest soil property investigations.

To constrain variability related to spatial sampling and limitations of physical sampling, allowing for a better understanding of realistic variance in soil C distribution, our review of previous geophysical forest studies in Chapter 2 and field testing in Chapter 3 recommended specific optimization steps and settings to provide the highest degree of interpretability possible for complex forest GPR data. These optimization practices included adopting large-scale GPR methods to collect soil property measurements at least 1-2 m deep at a high-resolution (resolve targets ≥ 10 cm) using GPR system settings including a high-frequency antenna (≥ 500 MHz), high stacking rate (> 32), and low trace spacing (≤ 5 cm for 10 cm resolution). These methods were both tested and optimized to be viable for small scale (1 m^2) and larger, landscape scales (> 1000 m^2), allowing for comparison of the new GPR method with previous PSSM data on the expansion of forest site soil data collection.

Following data collection under these settings, optimized data processing steps for specific soil property estimates of soil horizon thickness and soil bulk density were found to greatly improve the interpretation quality of forest GPR radargrams. To measure soil horizon thickness from radargrams, data processing steps including a dewow filter for noise removal, zero-time static correction for correct initial signal interpretations, a bandpass filter to remove low and high-frequency noise, and gain control to enhance weaker reflections were taken. To measure for soil bulk density using GPR methods required additional, specific processing including additional background noise removal, application of an F-K migration filter to correct the positioning of reflections associated with rock and root reflections, and using a Hilbert transform filter was applied, as detailed in Chapter 2, to allow for interpretations of rock and soil content as a percentage of amplitude.

4.3 Large-scale ground penetrating radar measurements of soil horizon thickness and bulk density allow for the assessment of landscape trends.

The experiment in Chapter 3 aimed to assess the optimized GPR methods across a boreal forest hillslope site to investigate soil heterogeneity and landscape trends in soil horizon thickness and soil bulk density with slope position and depth to identify potential associations between soil properties and hillslope morphology relevant to understanding boreal forest soil C stocks. Continuous GPR collection of soil properties across the entire forest hillslope was able to provide more landscape representation of morphological processes, such as particle transport, ground and surface water flow, and erosion in hillslope soil property data. Thus, linkages between the soil property results demonstrated in this study with soil content and C distribution across a forest landscape can aid in identifying the hydrogeomorphic processes responsible for such alterations, allowing for better predictive capabilities in measurements of soil C such as through soil C stocks.

The results gathered via GPR help confirm that landscape processes can exert influence on forest soil properties and thus C stock distribution. Such sediment transport mechanics can result in thicker soil horizons which the riparian zone, dependent on hillslope dip, curvature, erosional rates, and relief (Pacific et al., 2011; Patton et al., 2018). Smaller size soil particles such as clay and silt may be transported with less force resulting deposition of these particles at the bottom of forested hillslopes (Rosenbloom et al., 2001) Furthermore, increased soil erosion across a forested hillslope can lead to the transport of fine soil content from shallow horizons into deeper layers

(Haden et al., 2020; Jobbágy & Jackson, 2000; Rosenbloom et al., 2001; Yoo et al., 2006). As soil C storage has been shown to correlate with soil particle size, the impacts of landscape trends in soil texture across a study site can be associated with soil C distribution and thus requires dense spatial data collection to properly represent C stock totals (Jobbágy & Jackson, 2000). Furthermore, differences in soil property estimates between physical and GPR methods, as was present for soil bulk density measurements in Chapter 3, can arise from the difference in resolution as the number of samples in each method dataset between the sampling procedures of both methods. These kinds of discrepancies between the physical soil sampling and GPR method results of soil properties and C seem to show that GPR can provide similarly reliable estimates to PSSM at larger spatial scales, but further work in verifying these approaches and methods over a diverse set of forest sites is required to fully evaluate the usefulness, capabilities, and limitations of GPR as a tool for investigating soil C distribution.

Continuous datasets of key soil properties for investigating soil C distribution, like soil horizon thickness and soil bulk density may be coupled with spatially explicit datasets in future investigations, like LiDAR, for the potential to aid in monitoring efforts to assess mitigation efforts associated with forestry management practices. As physical soil sampling methods can easily bias estimates of forest soil content, in particular soil bulk density, an expansion of spatial data collection is necessary to improve the site representation of such investigations. Such physical sampling bias can likely result in overestimates of soil bulk density, and thus the quantity of soil, especially at depth. These circumstances were demonstrated through the results and analysis contained in Chapter 3. The reliability of GPR data in this study was further supported by the landscape trends which are in line with hillslope processes expected in these soils. As such, the application of these optimized GPR methods across large scales in the forest in Chapter 3 demonstrated the potential of continuous data collection to not only provide information on landscape-scale soil property variations but also the opportunity for integration with other relevant surface and above-ground spatial data methods, such as airborne and LiDAR surveys.

References

von Haden, A.C., Yang, W.H., DeLucia, E.H., 2020. Soils' dirty little secret: Depth-based comparisons can be inadequate for quantifying changes in soil organic carbon and other mineral soil properties. *Global Change Biology*, 26(7), pp. 3759–3770. doi: 10.1111/gcb.15124.

Jobbagy, E. G., & Jackson, R. B., 2000. The vertical distribution of soil organic carbon and its relation to climate and vegetation. *Ecological Applications*, 10(2), p. 423. doi: 10.2307/2641104.

Pacific, V. J., McGlynn, B., Riveros-Iregui, D., Welsch, D., Epstien, H., 2011. Landscape structure, groundwater dynamics, and soil water content influence soil respiration across riparian-hillslope transitions in the Tenderfoot Creek Experimental Forest, Montana. *Hydrological Processes*, 25(5), pp. 811–827. doi: 10.1002/hyp.7870.

Patton, N. R., Lohse, K., Godsey, S., 2018. Predicting soil thickness on soil mantled hillslopes. *Nature Communications*, 9(1). doi: 10.1038/s41467-018-05743-y.

Rosenbloom, N. A., Doney, S. C., Schimel, D. S., 2001. Geomorphic evolution of soil texture and organic matter in eroding landscapes. *Global Biogeochemical Cycles*, 15(2), pp. 365–381. doi: 10.1029/1999GB001251.

Yoo, K., Amundson, R., Heimsath, A., Dietrich, W., 2006. Spatial patterns of soil organic carbon on hillslopes: Integrating geomorphic processes and the biological C cycle. *Geoderma*, 130(1–2), pp. 47–65. doi: 10.1016/j.geoderma.2005.01.008.